CSIRO Environmental Modelling Suite: Scientific description of the optical, carbon chemistry and biogeochemical models (B3p0).

Mark E. Baird[1], Matthew P. Adams[2], John Andrewartha[1], Nagur Cherukuru[1], Malin Gustafsson[3], Scott Hadley[1], Mike Herzfeld[1], Emlyn Jones[1], Nugzar Margvelashvili[1], Mathieu Mongin[1], John Parslow[1], Peter J. Ralph[3], Farhan Rizwi[1], Barbara Robson[5], Uwe Rosebrock[1], Pavel Sakov[6], Thomas Schroeder[1], Jenny Skerratt[1], Andrew D. L. Steven[1], Karen A. Wild-Allen[1], and Monika Soja-Wozniak[1]

[1]CSIRO, Oceans and Atmosphere, Hobart, Australia
[2]School of Chemical Engineering, The University of Queensland, Brisbane, Australia
[3]Plant Functional Biology and Climate Change Cluster, Faculty of Science, University of Technology Sydney, Sydney, Australia
[4]CSIRO, Land and Water, Canberra, Australia
[5]Australian Institute of Marine Science
[6]Bureau of Meteorology

March 27, 2019

Contents

List of Tables

List of Figures

1 Abstract

Over 20 years, Australia's Commonwealth Science Industry and Research Organisation (CSIRO) has developed a biogeochemical model for coupling with a hydrodynamic and sediment model for application in shallow and shelf seas, and applied this model around the Australian continent. With the focus on shallow seas, the model includes more detailed representations of benthic plants such as seagrass, macroalgae and corals than other marine biogeochemical models, and a detailed spectrally-resolved optical model. A second focus has been on, where possible, the geometric derivation of ecological rates. Thus nutrient uptake by microalgae considers the divergence of the gradient of the nutrient field in the vicinity of the cell, zooplankton grazing considers encounter rates based on summing relative motion, chlorophyll synthesis includes a geometrically-derived self-shading term, and the bottom coverage of benthic plants is generically-related to their biomass using a form derived from geometric arguments. This approach has led to an algebraically-complicated, and unfamiliar, set of equations, when compared to other biogeochemical models. But while being algebraically-complicated, the model has fewer unconstrained parameters and is therefore numerically simpler than it would otherwise be. Thus at this mature point in the model's developed, a full mathematical description of the model, including the rationale for many of the geometric derivations used, is required. The model is now being applied on the Great Barrier Reef, northeast Australia in a near real time capacity.

2 Overview

The CSIRO Environmental Modelling Suite (EMS) has been developed over 20 years to model coupled physical, sediment, chemical and biogeochemical processes in marine and estuarine environments. Recently the biogeochemical model has been significantly improved through the addition of a spectrally-resolved optical model and a number of new biogeochemical processes (carbon chemistry, coral processes, multiple seagrass species etc). This document provides a summary of the science used for the optical and biogeochemical models in the eReefs project, and a precise description of the equations used in the simulations.

2.1 Spectrally-resolved optical model

The optical model undertakes calculations at distinct wavelengths of light (say 395, 405, 415, 705 nm) representative of individual wavebands (say 400-410, 410-420 nm etc.), and can be modified for the particular application. First the spectrally-resolved Inherent Optical Properties (IOPs) of the water column are calculated from the model biogeochemical state (phytoplankton biomass,

particulate concentrations etc). These include the absorption and scattering properties of clear water, colour dissolved organic matter, suspended solids and each microalgal population.

Using the calculated IOPs, as a well as sun angle, surface albedo and refraction, the spectrally-resolved light field (downwelling and scalar irradiance) is calculated for each grid cell in the model. From this light field phytoplankton absorption is calculated. The light that reaches the bottom is absorbed by epibenthic flora as a function of wavelength, depending on the absorbance of each individual flora. From the calculation of the light field other apparent optical properties (AOPs), such as remote-sensing reflectance, can be determined, and compared to remotely-sensed products. As AOPs can be recalculated from IOPs post-simulation, the model can be run for one set of wavelengths to optimise the integration speed and accuracy, and the AOPs re-calculated at another set of wavelengths for comparison with hyperspectral observations such as those used to calculate chlorophyll from the MODIS ocean color sensors.

The use of remote-sensing reflectance introduces a novel means of model assessment - simulated true colour. The model output can be processed to produce simulated true colour images of the water surface, with features such as bottom reflectance, river plumes and microalgal blooms easily characterised by their colour.

2.2 Biogeochemical model

The ecological model is organised into 3 zones: pelagic, epibenthic and sediment. Depending on the grid formulation the pelagic zone may have one or several layers of similar or varying thickness. The epibenthic zone overlaps with the lowest pelagic layer and the top sediment layer and shares the same dissolved and suspended particulate material fields. The sediment is modelled in multiple layers with a thin layer of easily resuspendable material overlying thicker layers of more consolidated sediment.

Dissolved and particulate biogeochemical tracers are advected and diffused throughout the model domain in an identical fashion to temperature and salinity. Additionally, biogeochemical particulate substances sink and are resuspended in the same way as sediment particles. Biogeochemical processes are organized into pelagic processes of phytoplankton and zooplankton growth and mortality, detritus remineralisation and fluxes of dissolved oxygen, nitrogen and phosphorus; epibenthic processes of growth and mortality of macroalgae, seagrass and corals, and sediment based processes of plankton mortality, microphytobenthos growth, detrital remineralisation and fluxes of dissolved substances (Fig. 1).

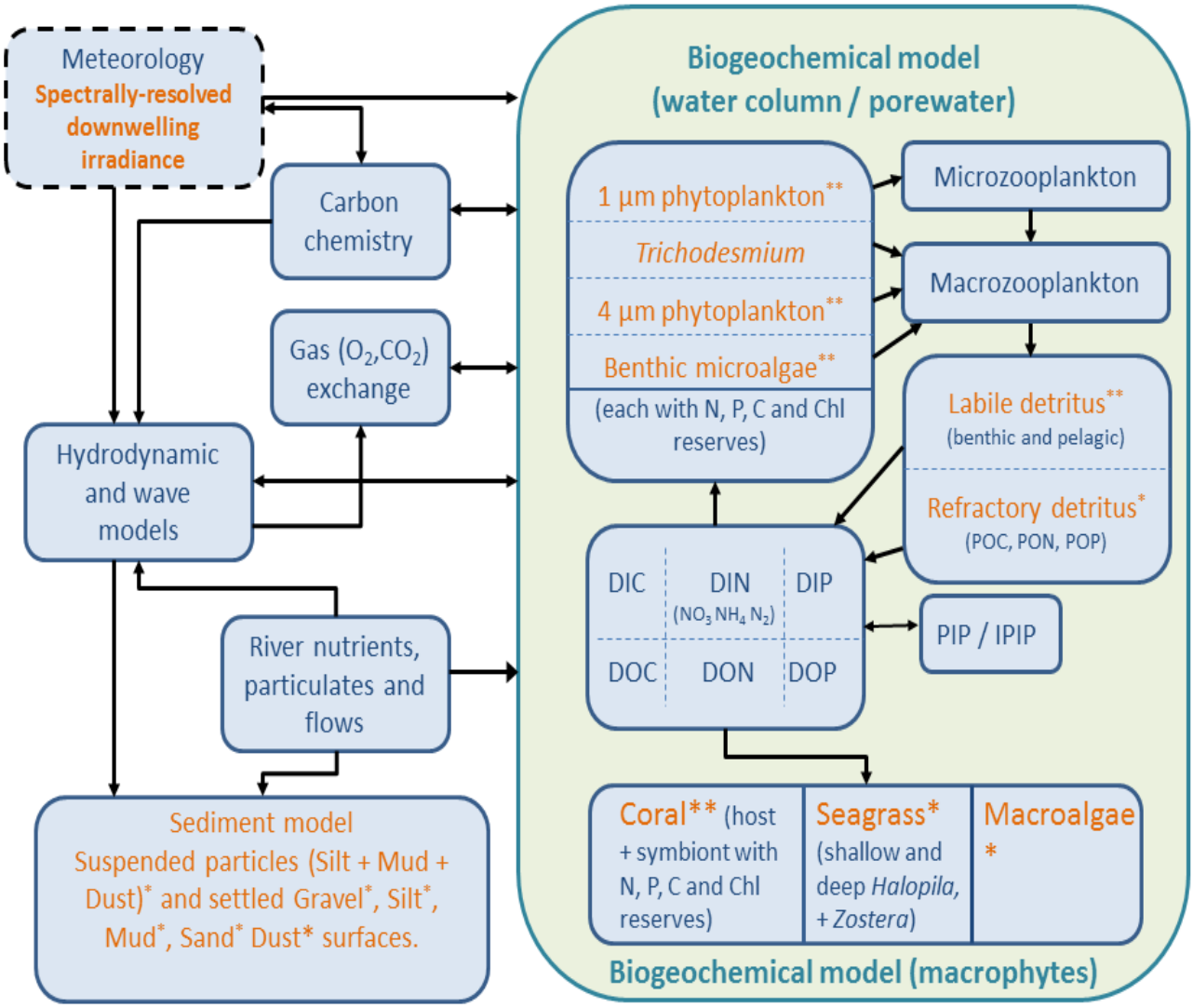

Figure 1: Schematic of CSIRO Environmental Modelling Suite. This document describes the biogeochemical processes in the water column, epipelagic and sediment zones. The orange colours represent optically-active components.

The biogeochemical model considers four groups of microalgae (small and large phytoplankton, microphytobenthos and *Trichodesmium*), four macrophytes types (seagrass types corresponding to *Zostera*, *Halophila* and a deep *Halophila*, macroalgae) and coral polyps. Photosynthetic growth is determined by concentrations of dissolved nutrients (nitrogen and phosphate) and photosynthetically active radiation. Autotrophs take up dissolved ammonium, nitrate, phosphate and inorganic carbon. Microalgae incorporate carbon (C), nitrogen (N) and phosphorus (P) at the Redfield ratio (106C:16N:1P) while macrophytes do so at the Atkinson ratio (550C:30N:1P). Microalgae contain chlorophyll *a* and accessory pigments, and have variable carbon:pigment ratios determined using a photoadaptation model.

Micro- and meso-zooplankton graze on small and large phytoplankton respectively, at rates determined by particle encounter rates and maximum ingestion rates. Additionally large zooplankton consume small zooplankton. Of the grazed material that is not incorporated into zooplankton biomass, half is released as dissolved and particulate carbon, nitrogen and phosphate, with the remainder forming detritus. Additional detritus accumulates by mortality. Detritus and dissolved organic substances are remineralised into inorganic carbon, nitrogen and phosphate with labile detritus transformed most rapidly (days), refractory detritus slower (months) and dissolved organic material transformed over the longest timescales (years). The production (by photosynthesis) and consumption (by respiration and remineralisation) of dissolved oxygen is also included in the model and depending on prevailing concentrations, facilitates or inhibits the oxidation of ammonia to nitrate and its subsequent denitrification to di-nitrogen gas which is then lost from the system.

Additional water column chemistry calculations are undertaken to solve for the equilibrium carbon chemistry ion concentrations necessary to undertake ocean acidification (OA) studies, and to consider sea-air fluxes of oxygen and carbon dioxide. The adsorption and desorption of phosphorus onto inorganic particles as a function of the oxic state of the water is also considered.

In the sediment porewaters, similar remineralisation processes occur as found in the water column (Fig. 2). Additionally, nitrogen is denitrified and lost as N_2 gas while phosphorus can become adsorbed onto inorganic particles, and become permanently immobilised in sediments.

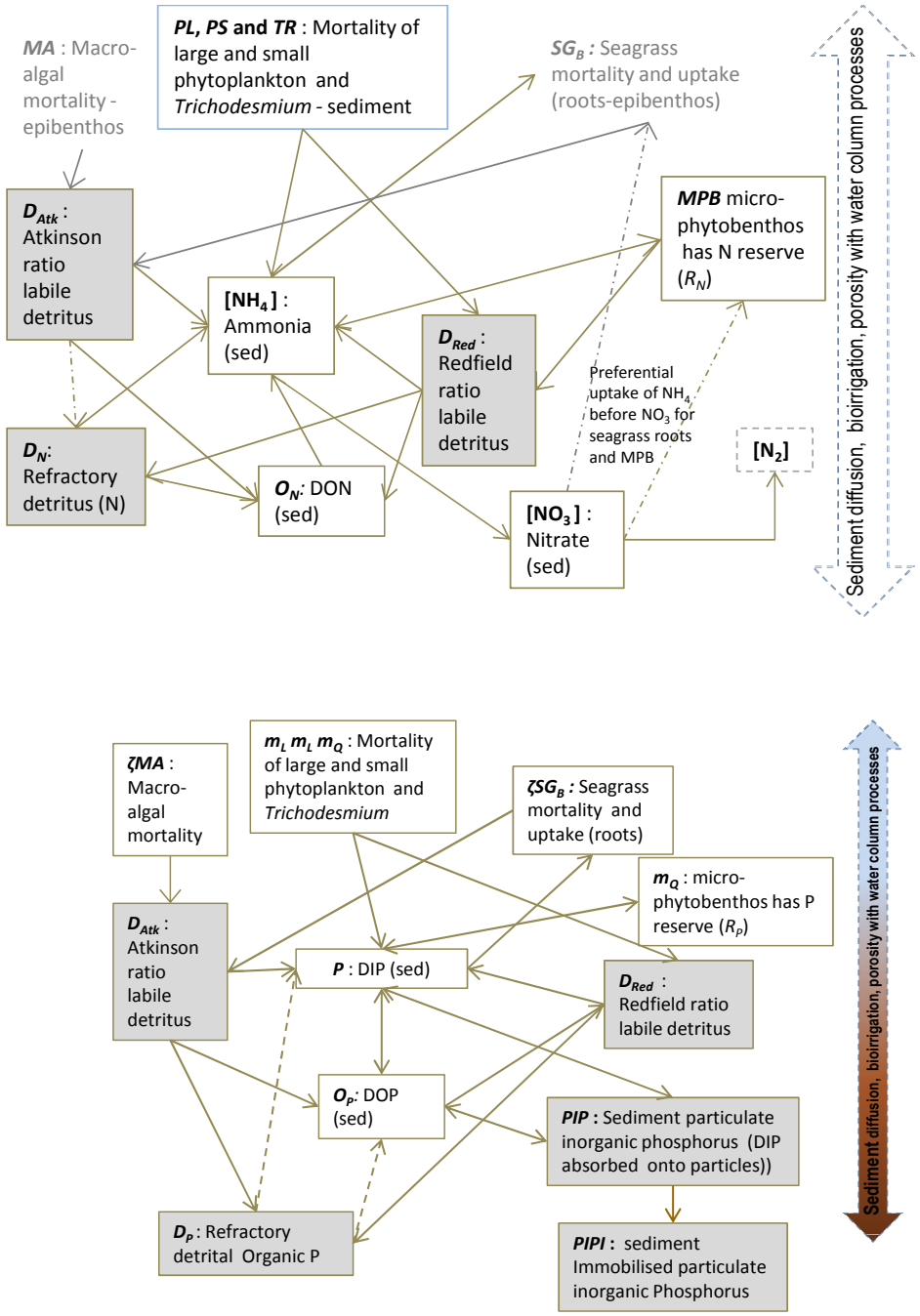

Figure 2: Schematic of sediment nitrogen and phosphorus pools and fluxes. Processes represented include phytoplankton mortality, detrital decomposition, denitification (nitrogen only), phosphorus adsorption (phosphorus only) and microphytobenthic growth.

2.3 Code structure and availability

The entire Environmental Modelling Suite (EMS) C code is available on GitHub at:

https://github.com/csiro-coasts/EMS/

This paper is a scientific description of the EMS ecological library (/EMS/model/lib/ecology). The code consists of some initialisation routines in the top directory (such as bio_opt.c). The model equations are primarily derivatives of the ecological state variables, and have been split in this paper into separate processes (such as a phytoplankton growth). The code for these derivatives are also split into files for individual processes (such as phytoplankton_spectral_grow_wc.c). This object-based approach allows individual processes to be included / excluded in a configuration file without re-writing the model code.

Within a process file, the routine containing the ecological derivatives is <process_name>_calc, and within that routine the ecological derivatives are stored within the array y1. Each element in the array y1 stores the derivatives of a state variable. The index to the array for each state variable is determined within each process initialisation routine, <process_name>_init, and stored in the processes' workspace ws. In the case of nitrate, for example, the derivative held in y1 will be the sum of the derivatives calculated in multiple processes (such as each autotrophic growth process, nitrification, denitrification, and each grazing and mortality process). The array of derivatives is then used by the model's adaptive integrator to update the model's state, y.

Some components of the ecological model are updated only once every time step without the derivatives being calculated. These include the optical and carbon chemistry model state variables. In these cases, the state variables, which are stored in the array y, are updated directly and this is done in either the routine <process_name>_precalc or <process_name>_postcalc.

The list of processes that this paper describes are for version B3p0, which is invoked with a configuration file listing the processes in each of the domains water, sediment and epibenthic:

```
water
{
tfactor
viscosity
moldiff
values_common
remineralization
microphytobenthos_spectral_grow_wc
phytoplankton_spectral_grow_wc(small)
phytoplankton_spectral_grow_wc(large)
```

```
trichodesmium_mortality_wc
trichodesmium_spectral_grow_wc
phytoplankton_spectral_mortality_wc(small)
phytoplankton_spectral_mortality_wc(large)
zooplankton_mortality_wc(small)
zooplankton_mortality_wc(large)
zooplankton_large_carnivore_spectral_grow_wc
zooplankton_small_spectral_grow_wc
nitrification_wc
p_adsorption_wc
carbon_chemistry_wc
gas_exchange_wc(carbon,oxygen)
light_spectral_wc(H,HPLC)
massbalance_wc
}
epibenthos
{
tfactor_epi()
values_common_epi()
macroalgae_spectral_grow_epi()
seagrass_spectral_grow_epi(Zostera)
seagrass_spectral_grow_epi(Halophila)
seagrass_spectral_grow_epi(Deep)
coral_spectral_grow_bleach_epi()
coral_spectral_carb_epi(H)
macroalgae_mortality_epi()
seagrass_spectral_mortality_proto_epi(Zostera)
seagrass_spectral_mortality_proto_epi(Halophila)
seagrass_spectral_mortality_proto_epi(Deep)
massbalance_epi()
light_spectral_uq_epi(H)
diffusion_epi()
}
sediment
{
tfactor
viscosity
moldiff
values_common
remineralization
light_spectral_sed(HPLC)
```

```
microphytobenthos_spectral_grow_sed
carbon_chemistry_wc()
microphytobenthos_spectral_mortality_sed
phytoplankton_spectral_mortality_sed(small)
phytoplankton_spectral_mortality_sed(large)
zooplankton_mortality_sed(small)
zooplankton_mortality_sed(large)
trichodesmium_mortality_sed
nitrification_denitrification_sed
p_adsorption_sed
massbalance_sed()
}
```

or alternatively with a call in the configuration file: `PROCESSFNAME B3p0`.

Other processes in the `process_library` can be validly called, but their scientific description is not given in this paper. The header for each process file gives detail about it use within the code, such as any arguments that it requires (for example `seagrass_spectral_grow_epi` requires the seagrass type as an argument). More documentation of the EMS code can be found at:

`https://research.csiro.au/cem/software/ems/`

There is an extensive User Guide for the entire EMS package, which contains any information that is generic across the hydrodynamic, sediment, transport and ecological models, such as input/output formats. A much smaller Biogeochemical User Guide documents details relevant only to the biogeochemical and optical models (such as how to specify wavelengths for the optical model), and a Developer's Guide describes how to add additional processes to the code.

2.4 Outline of document

The description of the optical and biogeochemical models is divided into the primary environmental zones: pelagic, epibenthic and sediment. Within these zones, descriptions are sorted by processes, such as microalgae growth, coral processes, food web interactions etc. This organisation allows the model to be explained, with notation, in self-contained chunks. For each process the complete set of model equations, parameter values and state variables are given. As the code itself allows the inclusion / exclusion of processes at runtime, the process-based structuring of this document aligns with the structure of the code. To investigate the complete equation for a single state variable, such as nitrate concentration, the reader will need to combine the individual terms affecting the variable from all processes.

Section 8 gives some of the details of the numerical methods that solve the model equations, and Section 9 lists peer-reviewed publications from the CSIRO EMS modelling suite.

The appendices gives a listing of all the state (App. A), diagnostic variables (App. A) and parameter values (App. C), and a description of their interpretation. This metadata will be most useful for those using the model outputs.

Enjoy.

3 Changes from B2p0 to B3p0

The following changes in the model equations were made between versions B2p0 and B3p0:

- Optical properties of carbonate particles (absorption, scattering and backscattering coefficients) are introduced using observations from the Lucinda Jetty Coastal Observatory.
- Spectrally-resolved phytoplankton backscattering replaces a wavelength-independent value.
- Coral bleaching processes added using new variables (Coral N, P, C reserves, xanthophyll photosynthetic and heat dissipating pigments, oxidised, reduced and inhibited reaction centres, reactive oxygen species), parameter values (ROS_threshold) and diagnostics (Rubisco activity, bleaching rate) following (Baird et al., 2018).
- Coral heterotrophic feeding fixed: reserves from grazed phytoplankton now returned to water column.
- New diagnostic variables included in optical model: simulated fluorescence, simulated turbidity, simulated normalised fluorescence line height, simulated Secchi depth, downwelling light on z-level interfaces, SWR_bot_abs (the PAR weighted bottom absorption calculated by the model), OC4Me - chlorophyll algorithm for MERIS and Sentinel satellites.
- Optical code now has options of spectral absorption coefficients calculated from mass-specific absorption laboratory experiments.
- Apply a relationship between aragonite saturation and sediment carbonate dissolution (Eyre et al., 2018).
- Spectrally-resolved light absorption by microphytobenthos in the sediment porewaters.
- Mass balance for oxygen includes oxygen atoms in nitrate, with stoichiometry changed for photosynthesis / respiration.
- In the model description, energy reserves are more correctly referred to as carbon reserves.
- Quadratic term for seagrass mortality.
- Remineralisation rate of phosphorus has a separate rate to that of C and N, requiring 2 new parameters (Φ_{RD_P}, Φ_{DOM_P}).
- Introduced new sediment-water exchange rate diagnostic variables for C, N, P, and O.

4 Pelagic processes

4.1 Transport

The local rate of change of concentration of each dissolved and particulate constituent, C, contains sink/source terms, S_C, which are described in length in this document, and the advection, diffusion and sinking terms:

$$\frac{\partial C}{\partial t} + \mathbf{v} \cdot \nabla^2 C = \nabla \cdot (K \nabla C) + w_{sink} \frac{\partial C}{\partial z} + S_C \tag{1}$$

where the symbol $\nabla = \left(\frac{\partial}{\partial x}, \frac{\partial}{\partial y}, \frac{\partial}{\partial z}\right)$, $\mathbf{v}$ is the velocity field, K is the eddy diffusion coefficient which varies in space and time, and w_C is the local sinking rate (positive downwards) and the z co-ordinate is positive upwards. The calculation of $\mathbf{v}$ and K is described in the hydrodynamic model (Herzfeld, 2006; Gillibrand and Herzfeld, 2016).

The microalgae are particulates that contain internal concentrations of dissolved nutrients (C, N, P) and pigments that are specified on a per cell basis. To conserve mass, the local rate of change of the concentration of microalgae, B, multiplied by the content of the cell, R, is given by:

$$\frac{\partial (BR)}{\partial t} + \mathbf{v} \cdot \nabla^2 (BR) = \nabla \cdot (K \nabla (BR)) + w_C \frac{\partial (BR)}{\partial z} + S_{BR} \tag{2}$$

For more information see Sec. 4.3.5 and Sec. 3.1 of Baird et al. (2004a).

4.2 Optical model

The optical model considers the processes of absorption and scattering by clear water, coloured dissolved organic matter (CDOM), non-algal particulates (NAP) and phytoplankton cells. First the inherent optical properties (IOPs), such as spectrally-resolved total phytoplankton absorption, are calculated from the model state variables (e.g. phytoplankton chlorophyll biomass) and model parameters (e.g. cell radius). The optical model then solves for the apparent optical properties (AOPs), such as the spectrally-resolved scalar irradiance, from the surface downwelling light field and the IOPs. Finally, the AOPs can be directly compared to remotely-sensed products such as remote-sensing reflectance and simulated true colour images.

4.2.1 Inherent optical properties (IOPs)

Phytoplankton absorption. The model contains 4 phytoplankton types (small and large phytoplankton, benthic mircoalgae and *Trichodesmium*), each with a unique ratio of internal concentration

of accessory photosynthetic pigments to chlorophyll-a. To calculate the absorption due to each pigment, we use a database of spectrally-resolved mass-specific absorption coefficients (Clementson and Wojtasiewicz, sub. 9th Jan 2019). As it can be assumed that accessory pigments stay in a constant ratio to chlorophyll-a, the model needs only a state variable for chlorophyll-a for each phytoplankton type. The model then calculates the chlorophyll-a specific absorption coefficient due to all pigments by using the Chl-a state variable, the ratio of concentration of the accessory pigment to chlorophyll-a, and the mass-specific absorption coefficient of each of the accessory pigments. Thus the chlorophyll-a specific absorption coefficient due to all photosynthetic pigments for small phytoplankton at wavelength λ, $\gamma_{small,\lambda}$, is given by:

$$\gamma_{small,\lambda} = 1.0\gamma_{Chla,\lambda} + 0.35\gamma_{Zea,\lambda} + 0.05\gamma_{Echi,\lambda} + 0.1\gamma_{\beta-car,\lambda} + 2\gamma_{PE,\lambda} + 1.72\gamma_{PC,\lambda} \tag{3}$$

where Chla is the pigment chlorophyll-a, Zea is zeaxanthin, Echi is echinenone, β-car is beta-carotene, PE is phycoerithin, and PC is phycocyanin, and the ratios of chlorophyll-a to accessory pigment concentration are determined from Wojtasiewicz and Stoń-Egiert (2016). Note that the coefficient in Eq. 3 for Chla is 1.0 because the ratio of chlorophyll-a to chlorophyll-a is 1. The resulting chlorophyll-a specific absorption coefficient is shown in Fig. 3.

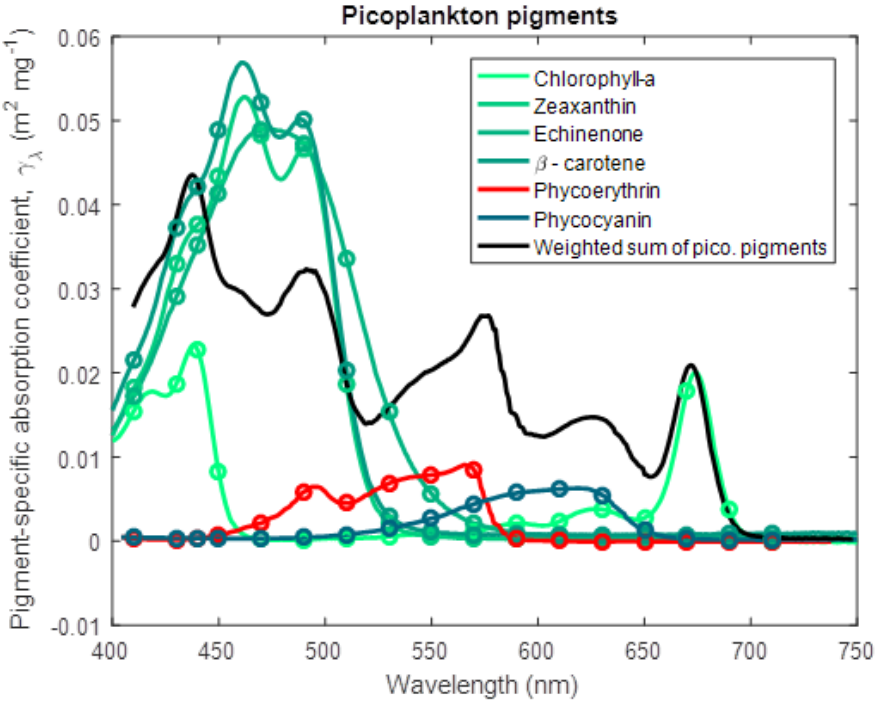

Figure 3: Pigment-specific absorption coefficients for the dominant pigments found in small phytoplankton determined using laboratory standards in solvent in a 1 cm vial. Green and red lines are photosynthetic pigments constructed from 563 measured wavelengths. Circles represent the wavelengths at which the optical properties are calculated in the simulations. The black line represents the weighted sum of the photosynthetic pigments (Eq. 3), with the weighting calculated from the ratio of each pigment concentration to chlorophyll *a*. The spectra are wavelength-shifted from their raw measurement by the ratio of the refractive index of the solvent to the refractive index of water (1.352 for acetone used with chlorophyll *a* and β-carotene; 1.361 for ethanol used with zeaxanthin, echinenone; 1.330 for water used with phycoerythrin, phycocyanin).

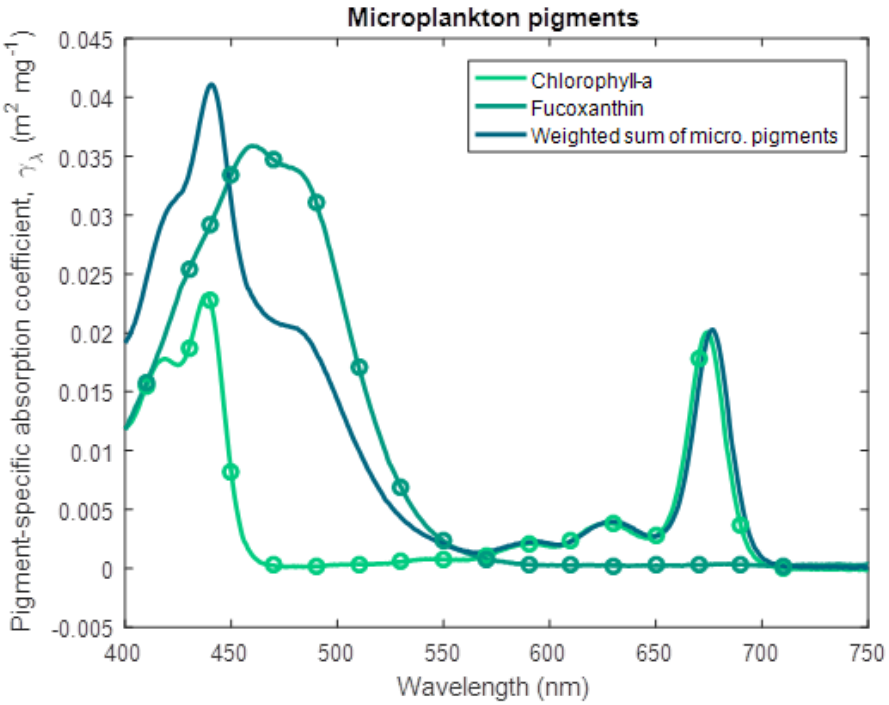

Figure 4: Pigment-specific absorption coefficients for the dominant pigments found in large phytoplankton and microphytobenthos determined using laboratory standards in solvent in a 1 cm vial. The aqua line represents the weighted sum of the photosynthetic pigments (Eq. 4), with the weighting calculated from the ratio of each pigment concentration to chlorophyll *a*. See Fig. 3 for more details. Fucoxanthin was dissolved in ethanol.

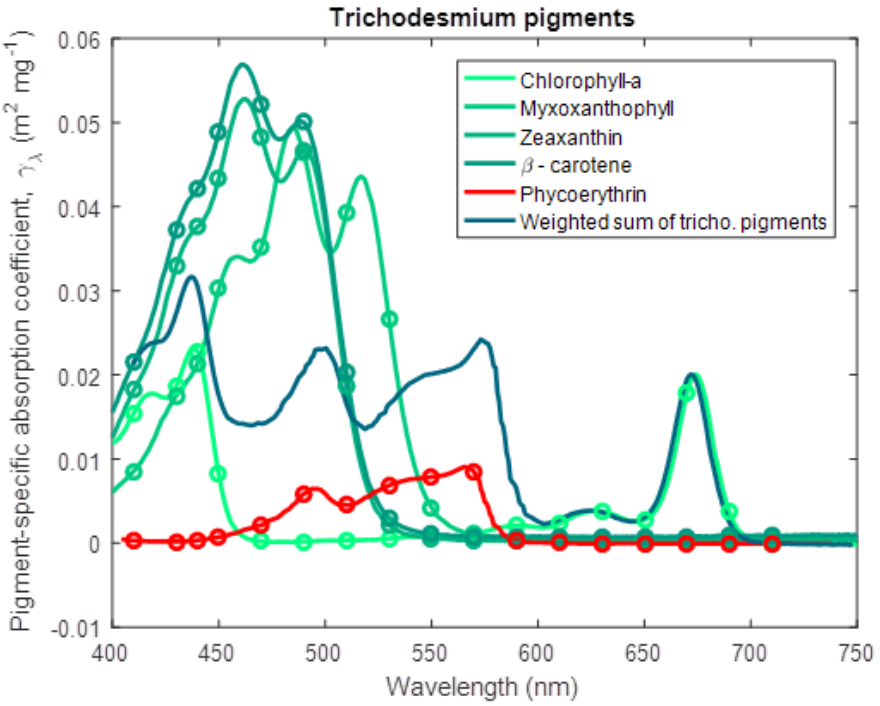

Figure 5: Pigment-specific absorption coefficients for the dominant pigments found in *Trichodesmium* determined using laboratory standards in solvent in a 1 cm vial. The aqua line represents the weighted sum of the photosynthetic pigments (Eq. 5), with the weighting calculated from the ratio of each pigment concentration to chlorophyll *a*. See Fig. 3 for more details. Myxoxanthophyll was dissolved in acetone.

Similarly for large phytoplankton and microphytobenthos (Wright et al., 1996):

$$\gamma_{large,\lambda} = 1.0\gamma_{Chla,\lambda} + 0.6\gamma_{Fuco,\lambda} \tag{4}$$

where Fuco is fucoxanthin. And for *Trichodesmium* (Carpenter et al., 1993) :

$$\gamma_{Tricho,\lambda} = 1.0\gamma_{Chla,\lambda} + 0.1\gamma_{Zea,\lambda} + 0.02\gamma_{Myxo,\lambda} + 0.09\gamma_{\beta-car,\lambda} + 2.5\gamma_{PE,\lambda} \tag{5}$$

where Myxo is myxoxanthophyll.

The absorption cross-section at wavelength λ (α_λ) of a spherical cell of radius (r), chla-specific absorption coefficient (γ_λ), and homogeneous intracellular chlorophyll-a concentration (c_i) can be calculated using geometric optics (i.e., ray tracing without considering internal scattering) and is given by (Duysens, 1956; Kirk, 1975):

$$\alpha_\lambda = \pi r^2 \left(1 - \frac{2(1 - (1 + 2\gamma_\lambda c_i r)e^{-2\gamma_\lambda c_i r})}{(2\gamma_\lambda c_i r)^2}\right) \tag{6}$$

where πr^2 is the projected area of a sphere, and the bracketed term is 0 for no absorption ($\gamma c_i r = 0$) and approaches 1 as the cell becomes fully opaque ($\gamma c_i r \to \infty$). Note that the bracketed term in Eq. 6 is mathematically equivalent to the dimensionless efficiency factor for absorption, Q_a (used in Morel and Bricaud (1981), Finkel (2001) and Bohren and Huffman (1983)), of homogeneous spherical cells with an index of refraction close to that of the surrounding water.

The use of an absorption cross-section of an individual cell has two significant advantages. Firstly, the same model parameters used here to calculated absorption in the water column are used to determine photosynthesis by individual cells, including the effect of packaging of pigments within cells. Secondly, the dynamic chlorophyll concentration determined later can be explicitly included in the calculation of phytoplankton absorption. Thus the absorption of a population of n cell m^{-3} is given by $n\alpha$ m^{-1}, while an individual cell absorbs αE_o light, where E_o is the scalar irradiance.

Coloured Dissolved Organic Matter (CDOM) absorption. Two equations for CDOM absorption are presently being trialled. The two schemes are:

Scheme 1. The absorption of CDOM, $a_{CDOM,\lambda}$, is determined from a relationship with salinity in the region (Schroeder et al., 2012):

$$a_{CDOM,443} = -0.0332S + 1.2336 \tag{7}$$

where S is the salinity. In order to avoid unrealistic extrapolation, the salinity used in this relationship is the minimum of the model salinity and 36. In some cases coastal salinities exceed 36 due to evaporation. The absorption due to CDOM at other wavelengths is calculated using a CDOM spectral slope for the region (Blondeau-Patissier et al., 2009):

$$a_{CDOM,\lambda} = a_{CDOM,443} \exp\left(-S_{CDOM}\left(\lambda - 443.0\right)\right) \tag{8}$$

	Symbol	Value
Constants		
Speed of light	c	2.998×10^8 m s^{-1}
Planck constant	h	6.626×10^{-34} J s^{-1}
Avogadro constant	A_V	6.02×10^{23} mol^{-1}
[a]Total scattering coefficient of phytoplankton	b_{phy}	0.2 (mg Chl a m^{-2})$^{-1}$
[b]Azimuth-independent scattering coefficient	g_i	0.402
[b]Azimuth-dependent scattering coefficient	g_{ii}	0.180
[c]CDOM-specific absorption coefficient at 443 nm	$k^*_{CDOM,443}$	0.02 m^2 mg C^{-1}
[c]Spectral slope of CDOM absorption	S_{CDOM}	0.012 nm^{-1}
[d]Linear remote-sensing reflectance coefficient	g_0	0.0895
[d]Quadratic remote-sensing reflectance coefficient	g_1	0.1247

Table 1: Constants and parameter values used in the optical model.[a] Kirk (1994).[b] Kirk (1991) using an average cosine of scattering of 0.924 (Mobley, 1994). [c] Blondeau-Patissier et al. (2009). [d] Brando et al. (2012). [e] Vaillancourt et al. (2004).

where S_{CDOM} is an approximate spectral slope for CDOM, with observations ranging from 0.01 to 0.02 nm^{-1} for significant concentrations of CDOM. Lower magnitudes of the spectral slope generally occur at lower concentrations of CDOM (Blondeau-Patissier et al., 2009).

Scheme 2. The absorption of CDOM, $a_{CDOM,\lambda}$, is directly related to the concentration of dissolved organic carbon, D_C.

$$a_{CDOM,\lambda} = k^*_{CDOM,443} D_C \exp\left(-S_{CDOM}\left(\lambda - 443.0\right)\right) \tag{9}$$

where $k^*_{CDOM,443}$ is the dissolved organic carbon-specific CDOM absorption coefficient at 443 nm.

Both schemes have drawbacks. Scheme 2, using the concentration of dissolved organic carbon, is closer to reality, but is likely to be sensitive to poorly-known parameters such as remineralisation rates and initial detritial concentrations. Scheme 1, a function of salinity, will be more stable, but perhaps less accurate, especially in estuaries where hypersaline waters may have large estuarine loads of coloured dissolved organic matter.

Absorption due to non-algal particulate material. The waters of the Great Barrier Reef contain suspended sediments originating from various marine sources, such as the white calcium carbonate fragments generated by coral erosion, and sediments derived from terrestrial sources such as granite (Soja-Woźniak et al., submitted). The model uses spectrally-resolved mass-specific absorption coefficients (and also total scattering measurements) from a database of laboratory measurements conducted on either pure mineral suspensions, or mineral mixtures, at two ranges of size distribu-

	Symbol	Units
Downwelling irradiance at depth z, wavelength λ	$E_{d,z,\lambda}$	W m^{-2}
Scalar irradiance at depth z, wavelength λ	$E_{o,z,\lambda}$	W m^{-2}
In water azimuth angle	θ	rad
Fractional backscattering	u_λ	-
Below-surface remote-sensing reflectance	$r_{rs,\lambda}$	sr^{-1}
Above-surface remote-sensing reflectance	$R_{rs,\lambda}$	sr^{-1}
Thickness of model layer	h	m
Optical depth weighting function	$w_{z,\lambda}$	
Vertical attenuation coefficient	K_λ	m^{-1}
Total absorption coefficient	$a_{T,\lambda}$	m^{-1}
Total scattering coefficient	$b_{T,\lambda}$	m^{-1}
Absorption cross-section	α_λ	m^2 cell^{-1}
Concentration of cells	n	cell m^{-3}

Table 2: State and derived variables in the water column optical model.

tions (Fig. 6, Stramski et al. (2007)). In this model version we use the calcium carbonate sample CAL1 for $CaCO_3$-based particles

For the terrestrially-sourced particles we used observations from Gladstone Harbour in the central GBR (Fig. 7). These IOPs gave a realistic surface colour for the Queensland river sediment plumes (Baird et al., 2016b). In the model, optically-active non-algal particulates (NAPs) includes the inorganic particulates (such as sand and mud, see Sec. 6.1) and detritus. We assumed the optical properties of the detritus was the same as the optical properties in Gladstone Harbour, although open ocean studies have used a detritial absorption that is more like CDOM (Dutkiewicz et al., 2015).

The absorption due to calcite-based NAP is given by:

$$a_{NAP_{\mathrm{CaCO_3},\lambda}} = c_1 NAP_{\mathrm{CaCO_3}} \tag{10}$$

where c_1 is the mass-specific, spectrally-resolved absorption coefficient determine from laboratory experiments (Fig. 6). The absorption due to non-calcite NAPs, $NAP_{\mathrm{non-CaCO_3}}$, combined with detritus, is given by:

$$a_{NAP_{\mathrm{non-CaCO_3},\lambda}} = c_2 NAP_{\mathrm{non-CaCO_3}} + \left(\frac{550}{30}\frac{12}{14} D_{Atk} + \frac{106}{16}\frac{12}{14} D_{Red} + D_C \right) / 10^6 \tag{11}$$

where c_2 is the mass-specific, spectrally-resolved absorption coefficient determine from field measurements (Fig. 7), $NAP_{\mathrm{non-CaCO_3}}$ is quantified in kg m^{-3}, D_{Atk} and D_{Red} are quantified in mg N m^{-3} and D_C is quantified in mg C m^{-3}.

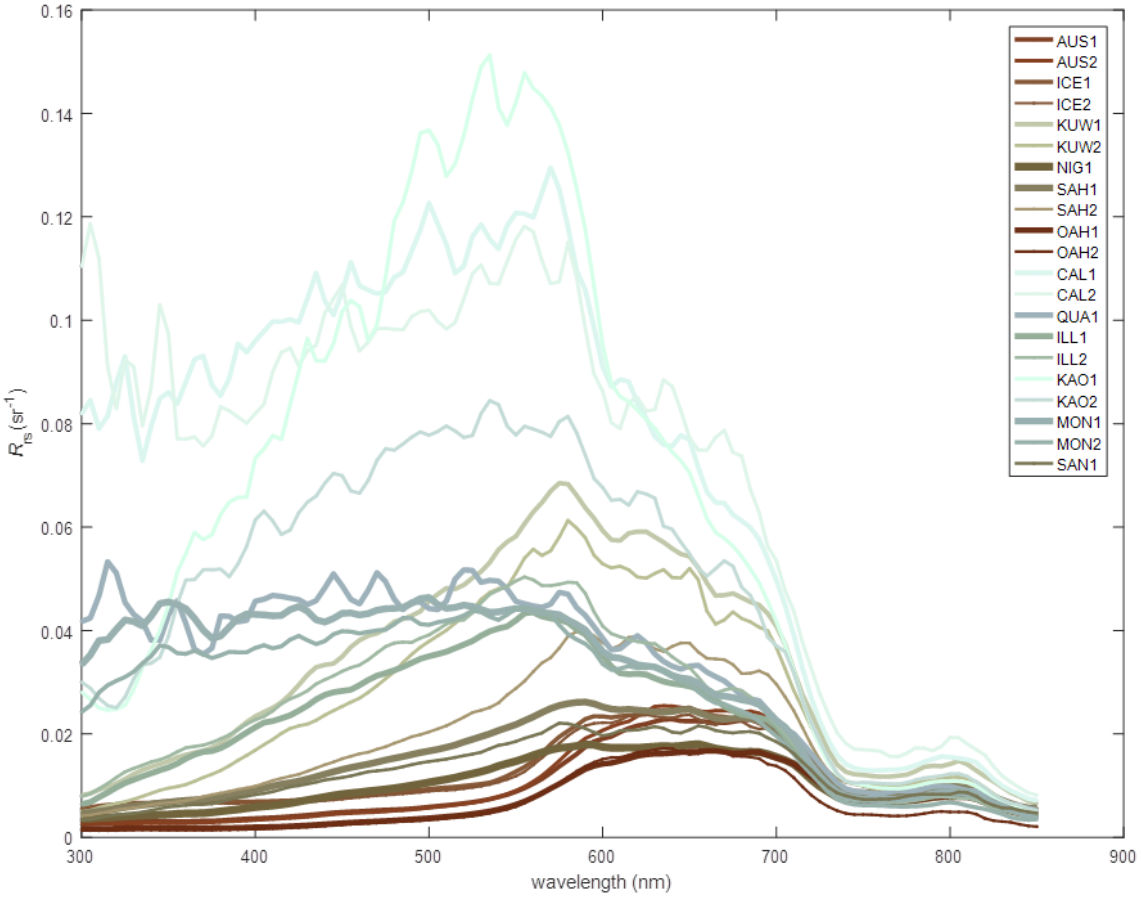

Figure 6: The remote-sensing reflectance of the 21 mineral mixtures suspended in water as measured by Stramski et al. (2007). Laboratory measurements of absorption and scattering properties are used to calculated u (Eq. 24). The remote-sensing reflectance is then calculated using Eq. 28, with the line colouring corresponding to that produced by the mineral suspended in clear water as calculated using the MODIS true color algorithm (Sec. B.2). CAL1, with a median particle diameter of 2 μm, is used for $\text{Mud}_{\text{CaCO}_3}$.

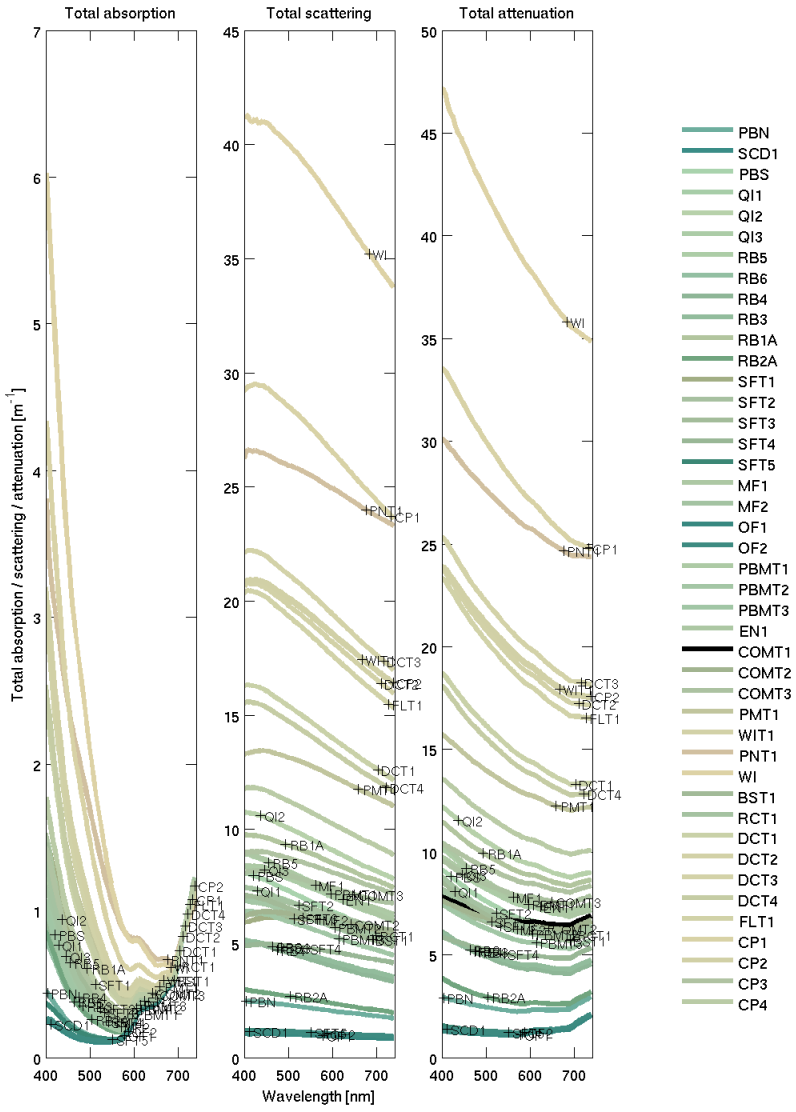

Figure 7: Inherent optical properties (total absorption and total scattering) at sample sites in Gladstone Harbour on 13-19 September 2013 (Babcock et al., 2015). The line colour is rendered like Fig. 6. The site labelling is ordered in time, from the first sample collected during neap tides at the top, to the last sample collected at spring tides on the bottom. The IOPs used for the $\text{Mud}_{\text{non}-\text{CaCO}_3}$ end-member is from the WIT site at the centre of the harbour, was dominated by inorganic particles. The measured concentration of NAP at the site was 33.042 mg L^{-1}, and is used to calculate mass-specific IOPs.

Total absorption. The total absorption, $a_{T,\lambda}$, is given by:

$$a_{T,\lambda} = a_{w,\lambda} + a_{NAP_{\text{non-CaCO}_3},\lambda} + a_{NAP_{\text{CaCO}_3},\lambda} + a_{CDOM,\lambda} + \sum_{x=1}^{N} n_x \alpha_{x,\lambda} \tag{12}$$

where $a_{w,\lambda}$ is clear water absorption (Fig. 8) and N is the number of phytoplankton classes (see Table 4).

Scattering. The total scattering coefficient is given by

$$b_{T,\lambda} = b_{w,\lambda} + c_1 NAP_{\text{non-CaCO}_3} + c_2 NAP_{\text{CaCO}_3} + b_{phy,\lambda} \sum_{x=1}^{N} n_x c_{i,x} V_x \tag{13}$$

where NAP is the concentration of non-algal particulates, $b_{w,\lambda}$ is the scattering coefficient due to clear water (Fig. 8), c_1 and c_2 are the spectrally-resolved, mass-specific coefficients (Figs. 6 & 7) and phytoplankton scattering is the product of the chlorophyll-specific phytoplankton scattering coefficient, $b_{phy,\lambda}$, and the water column chlorophyll concentration of all classes, $\sum n_x c_{i,x} V_x$ (where c_i is the chlorophyll concentration in the cell, and V is the cell volume). The value for $b_{phy,\lambda}$ is set to 0.2 (mg Chl a m^{-2})$^{-1}$ for all wavelengths, a typical value for marine phytoplankton (Kirk, 1994). For more details see Baird et al. (2007).

Backscattering In addition to the IOPs calculated above, the calculation of remote-sensing reflectance uses a backscattering coefficient, b_b, which has a component due to pure seawater, and a component due to algal and non-algal particulates. The backscattering ratio is a coarse resolution representation of the volume scattering function, and is the ratio of the forward and backward scattering.

The backscattering coefficient for clear water is 0.5, a result of isotropic scattering of the water molecule.

The particulate component of backscattering for phytoplankton is strongly related to cell carbon (and therefore cell size) and the number of cells (Vaillancourt et al., 2004):

$$b^*_{bphy,\lambda} = 5 \times 10^{-15} m_C^{1.002} \quad (R^2 = 0.97) \tag{14}$$

where m_C is the carbon content of the cells, here in pg cell^{-1}.

For inorganic particles, backscattering can vary between particle mineralogies, size, shape, and at different wavelengths, resulting, with spectrally-varying absorption, in the variety of colours that we see from suspended sediments. Splitting sediment types by mineralogy only, the backscattering ratio for carbonate and non-carbonate particles is given in Table 3.

The backscatter due to phytoplankton is approximately 0.02. To account for a greater backscattering ratio, and therefore backscatter, at low wavelengths (Fig. 4 of Vaillancourt et al. (2004)), we

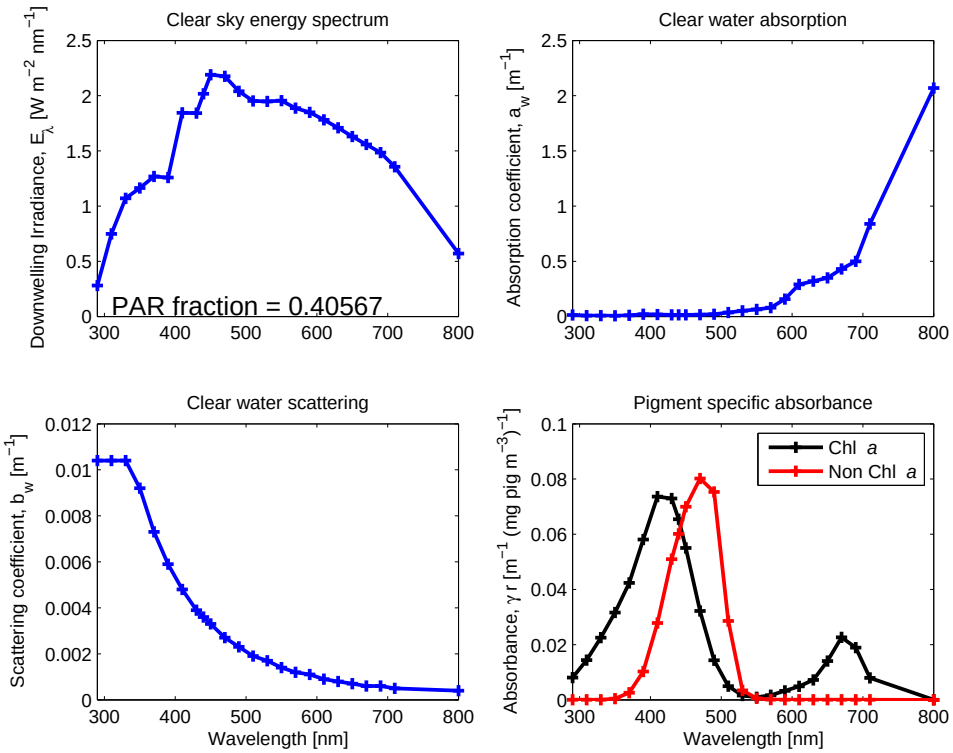

Figure 8: Spectrally-resolved energy distribution of sunlight, clear water absorption, and clear water scattering (Smith and Baker, 1981). The fraction of solar radiation between 400 and 700 nm for clear sky irradiance at the particular spectral resolution is given in the top left panel. The centre of each waveband used in the model simulations is identified by a cross on each curve. The bottom right panel shows the pigment-specific absorbance of Chl *a* and generic photosynthetic carotenoids (Ficek et al., 2004) that were used in earlier versions of this model (Baird et al., 2016b) before the mass-specific absorption coefficients of multiple accessory pigments was implemented (Figs. 3, 4 & 5).

	Wavelength [nm]								
	412.0	440.0	488.0	510.0	532.0	595.0	650.0	676.0	715.0
Carbonate	0.0209	0.0214	0.0224	0.0244	0.0216	0.0201	0.0181	0.0170	0.0164
Terrestrial	0.0028	0.0119	0.0175	0.0138	0.0128	0.0134	0.0048	0.0076	0.0113

Table 3: Particulate backscattering ratio for carbonate and non-carbonate minerals based on samples at Lucinda Jetty Coastal Observatory, a site at the interface on carbonate and terrestrial bottom sediment (Soja-Woźniak et al., submitted).

linearly increased the backscatter ratio from 0.02 at 555 nm to 0.04 at 470 nm. Above and below 555 nm and 470 nm respectively the backscatter ratio remained constant.

The total backscatter then becomes:

$$b_{b,\lambda} = \tilde{b}_w b_{w,\lambda} + b^*_{bphy,\lambda} n + \tilde{b}_{b,NAP_{non-CaCO_3},\lambda} c_1 NAP_{\text{non-CaCO}_3} + \tilde{b}_{b,NAP_{CaCO_3},\lambda} c_2 NAP_{\text{non-CaCO}_3} NAP_{\text{CaCO}_3} \quad (15)$$

where the backscatter ratio of pure seawater, $\tilde{b}_w$, is 0.5, n is the concentration of cells, and for particulate matter (NAP and detritus), $\tilde{b}_{b,NAP,\lambda}$, is variable (Table 3) and the coefficients c_1 and c_2 come from the total scattering equations above.

4.2.2 Apparent optical properties (AOPs)

The optical model is forced with the downwelling short wave radiation just above the sea surface, based on remotely-sensed cloud fraction observations and calculations of top-of-the-atmosphere clear sky irradiance and solar angle. The calculation of downwelling radiation and surface albedo (a function of solar elevation and cloud cover) is detailed in the hydrodynamic scientific description (`https://research.csiro.au/cem/software/ems/ems-documentation/`, Sec 9.1.1).

The downwelling irradiance just above the water interface is split into wavebands using the weighting for clear sky irradiance (Fig. 8). Snell's law is used to calculate the azimuth angle of the mean light path through the water, θ_{sw}, as calculated from the atmospheric azimuth angle, θ_{air}, and the refraction of light at the air/water interface (Kirk, 1994):

$$\frac{\sin\theta_{air}}{\sin\theta_{sw}} = 1.33 \quad (16)$$

Calculation of in-water light field. Given the IOPs determined above, the exact solution for AOPs would require a radiative transfer model (Mobley, 1994), which is too computationally-expensive for a complex ecosystem model such as developed here. Instead, the in-water light field is solved for

using empirical approximations of the relationship between IOPs and AOPs (Kirk, 1991; Mobley, 1994).

The vertical attenuation coefficient at wavelength λ when considering absorption and scattering, K_λ, is given by:

$$K_\lambda = \frac{a_{T,\lambda}}{\cos\theta_{sw}}\sqrt{1 + (g_i \cos\theta_{sw} - g_{ii})\frac{b_{T,\lambda}}{a_{T,\lambda}}} \tag{17}$$

The term outside the square root quantifies the effect of absorption, where $a_{T,\lambda}$ is the total absorption. The term within the square root of Eq. 17 represents scattering as an extended pathlength through the water column, where g_i and g_{ii} are empirical constants and take values of 0.402 and 0.180 respectively. The values of g_i and g_{ii} depend on the average cosine of scattering. For filtered water with scattering only due to water molecules, the values of g_i and g_{ii} are quite different to natural waters. But for waters ranging from coastal to open ocean, the average cosine of scattering varies by only a small amount (0.86 - 0.95, Kirk (1991)), and thus uncertainties in g_i and g_{ii} do not strongly affect K_λ.

The downwelling irradiance at wavelength λ at the bottom of a layer h thick, $E_{d,\lambda,bot}$, is given by:

$$E_{d,bot,\lambda} = E_{d,top,\lambda}e^{-K_\lambda h} \tag{18}$$

where $E_{d,top,\lambda}$ is the downwelling irradiance at wavelength λ at the top of the layer and K_λ is the vertical attenuation coefficient at wavelength λ, a result of both absorption and scattering processes.

Assuming a constant attenuation rate within the layer, the average downwelling irradiance at wavelength λ, $E_{d,\lambda}$, is given by:

$$E_{d,\lambda} = \frac{1}{h}\int_{bot}^{top} E_{d,z,\lambda}e^{-K_\lambda z}dz = \frac{E_{d,top,\lambda} - E_{d,bot,\lambda}}{K_\lambda h} \tag{19}$$

We can now calculate the scalar irradiance, E_o, for the calculation of absorbing components, from downwelling irradiance, E_d. The light absorbed within a layer must balance the difference in downwelling irradiance from the top and bottom of the layer (since scattering in this model only increases the pathlength of light), thus:

$$E_{o,\lambda}a_{T,\lambda}h = E_{d,top,\lambda} - E_{d,bot,\lambda} = E_{d,\lambda}K_\lambda h \tag{20}$$

Canceling h, and using Eq. 17, the scalar irradiance as a function of downwelling irradiance is given by:

$$E_{o,\lambda} = \frac{E_{d,\lambda}}{\cos\theta_{sw}}\sqrt{1 + (g_i \cos\theta_{sw} - g_{ii})\frac{b_{T,\lambda}}{a_{T,\lambda}}} \tag{21}$$

This correction conserves photons within the layer, although it is only as a good as the original approximation of the impact of scattering and azimuth angle on vertical attenuation (Eq. 17).

Vertical attenuation of heat. The vertical attenuation of heat is given by:

$$K_{heat} = -\int \frac{1}{E_{d,z,\lambda}} \frac{\partial E_{d,z,\lambda}}{\partial z} d\lambda \tag{22}$$

and the local heating by:

$$\frac{\partial T}{\partial t} = -\frac{1}{\rho c_p} \int \frac{\partial E_{d,\lambda}}{\partial z} d\lambda \tag{23}$$

where T is temperature, ρ is the density of water, and $c_p = 4.1876$ J m^{-3} K^{-1} is the specific heat of water. This calculation does not feed back to the hydrodynamic model.

4.2.3 Remote-sensing reflectance

The ratio of the backscattering coefficient to the sum of backscattering and absorption coefficients for the water column, u_λ, is:

$$u_\lambda = \sum_{z'=1}^{N} \frac{w_{\lambda,z'} b_{b,\lambda,z'}}{a_{\lambda,z'} + b_{b,\lambda,z'}} \tag{24}$$

where $w_{\lambda,z'}$ is a weighting representing the component of the remote-sensing reflectance due to the absorption and scattering in layer number z', and N is the number of layers.

The weighting fraction in layer z' is given by:

$$w_{\lambda,z'} = \frac{1}{z_1 - z_0} \left(\int_0^{z_1} \exp\left(-2K_{\lambda,z}\right) dz - \int_0^{z_0} \exp\left(-2K_{\lambda,z}\right) dz \right) \tag{25}$$

$$= \frac{1}{z_1 - z_0} \int_{z_0}^{z_1} \exp\left(-2K_{\lambda,z}\right) dz \tag{26}$$

where K_λ is the vertical attenuation coefficient at wavelength λ described above, and the factor of 2 accounts for the pathlength of both downwelling and upwelling light. The integral of $w_{\lambda,z}$ to infinite depth is 1. In areas where light reaches the bottom, the integral of $w_{\lambda,z}$ to the bottom is less than one, and bottom reflectance is important (see Sec. 6.2.2).

The below-surface remote-sensing reflectance, r_{rs}, is given by:

$$r_{rs,\lambda} = g_0 u_\lambda + g_1 u_\lambda^2 \tag{27}$$

where $g_0 = 0.0895$ (close to $1/4\pi$) and $g_1 = 0.1247$ are empirical constants for the nadir-view in oceanic waters (Lee et al., 2002; Brando et al., 2012), and these constants result in a change of units from the unitless u to a per unit of solid angle, sr^{-1}, quantity $r_{rs,\lambda}$.

The above-surface remote-sensing reflectance, through rearranging Lee et al. (2002), is given by:

$$R_{rs,\lambda} = \frac{0.52 r_{rs,\lambda}}{1 - 1.7 r_{rs,\lambda}} \tag{28}$$

At open ocean values, $R_{rs} \sim 0.06u$ sr^{-1}. Thus if total scattering and absorption are approximately equal, $u = 0.5$ and $R_{rs} \sim 0.03$ sr^{-1}.

4.3 Microalgae

The model contains four function groups of suspended microalgae: small and large phytoplankton, microphytobenthos and *Trichodesmium*. The growth model for each of the functional groups is identical and explained below. The differences in the ecological interactions of the four functional groups are summarised in Table 4.

	small phyto.	large phyto.	benthic phyto.	*Trichodesmium*
Radius (μm)	1	4	10	5
[a]Maximum growth rate (d^{-1})	1.6	1.4	0.839	0.2
Sink rate (m d^{-1})				variable
Surface sediment growth	×	×	√	×
Nitrogen fixation	×	×	×	√
Water column mort.	√	√	×	√
Sediment mort.	√	√	√	√
[b]Ratio of xanthophyll to Chl *a*	0.51	0.81	0.81	0.50

Table 4: Traits of suspended microalgae cells.[a] At $T_{ref} = 20°C$. [b] Values for *Trichodesmium* from Subramaniam et al. (1999), other values from CSIRO parameter library.

4.3.1 Growth

The model considers the diffusion-limited supply of dissolved inorganic nutrients (N and P) and the absorption of light, delivering N, P and fixed C to the internal reserves of the cell (see Fig. 3 in Baird et al. (2018)). Nitrogen and phosphorus are taken directly into the reserves, but carbon is first fixed through photosynthesis (Kirk, 1994):

$$106CO_2 + 212H_2O \xrightarrow{1060 \text{ photons}} 106CH_2O + 106H_2O + 106O_2 \tag{29}$$

The internal reserves of C, N, and P are consumed to form structural material at the Redfield ratio (Redfield et al., 1963):

$$\begin{aligned} 106CH_2O + 16NH_4^+ + PO_4^{3-} + 16H_2O & \\ \longrightarrow \quad (CH_2O)_{106}(NH_3)_{16}H_3PO_4 + 13H^+ & \end{aligned} \tag{30}$$

where we have represented nitrogen as ammonia (NH_4) in Eq. 30. When the nitrogen source to the cell is nitrate, NO_3, it is assumed to lose its oxygen at the cell wall (Sec. 7.1). The growth rate of

Variable	Symbol	Units
Scalar irradiance	E_o	W m^{-2}
Dissolved inorganic nitrogen (DIN)	N	mg N m^{-3}
Dissolved inorganic phosphorus (DIP)	P	mg P m^{-3}
Dissolved inorganic carbon (DIC)	DIC	mg C m^{-3}
Dissolved oxygen	$[O_2]$	mg O m^{-3}
Reserves of nitrogen	R_N	mg N cell^{-1}
Reserves of phosphorus	R_P	mg P cell^{-1}
Reserves of carbon	R_C	mg C cell^{-1}
Maximum reserves of nitrogen	$R_N^{\max}$	mg N cell^{-1}
Maximum reserves of phosphorus	$R_P^{\max}$	mg P cell^{-1}
Maximum reserves of carbon	$R_C^{\max}$	mg C cell^{-1}
Normalised reserves of nitrogen	$R_N^* \equiv R_N/R_N^{\max}$	-
Normalised reserves of phosphorus	$R_P^* \equiv R_P/R_P^{\max}$	-
Normalised reserves of carbon	$R_C^* \equiv R_C/R_C^{\max}$	-
Intracellular Chl a concentration	c_i	mg m^{-3}
Structural phytoplankton biomass	B	mg N m^{-3}
Absorption cross-section	α	m^2 cell^{-1}
Diffusion shape factor	ψ	m cell^{-1}
Wavelength	λ	nm
Maximum Chl a synthesis rate	$k_{\text{Chl}}^{\max}$	mg Chl m^{-3} d^{-1}
Photon absorption-weighted opaqueness	$\overline{\Theta}$	-
Non-dimensional absorbance	$\rho_\lambda = \gamma_\lambda c_i r$	-

Table 5: State and derived variables for the microalgae growth model. DIN is given by the sum of nitrate and ammonia concentrations, $[NO_3]$+$[NH_4]$.

microalgae is given by the maximum growth rate, μ^{max}, multiplied by the normalised reserves, R^*, of each of N, P and C:

$$\mu = \mu^{max} R_N^* R_P^* R_C^* \tag{31}$$

The mass of the reserves (and therefore the total C:N:P:Chl a ratio) of the cell depends on the interaction of the supply and consumption rates (Fig. 9). When consumption exceeds supply, and the supply rates are non-Redfield, the normalised internal reserves of the non-limiting nutrients approach 1 while the limiting nutrient becomes depleted. Thus the model behaves like a 'Law of the Minimum' growth model, except during fast changes in nutrient supply rates.

The molar ratio of a cell is given by:

$$\text{C} : \text{N} : \text{P} = 106(1 + R_C^*) : 16(1 + R_N^*) : 1 + R_P^* \tag{32}$$

4.3.2 Nutrient uptake

The diffusion-limited nutrient uptake to a single phytoplankton cell, J, is given by:

$$J = \psi D \left(C_b - C_w\right) \tag{33}$$

where ψ is the diffusion shape factor ($= 4\pi r$ for a sphere), D is the molecular diffusivity of the nutrient, C_b is the average extracellular nutrient concentration, and C_w is the concentration at the wall of the cell. The diffusion shape factor is determined by equating the divergence of the gradient of the concentration field to zero ($\nabla^2 C = 0$).

A semi-empirical correction to Eq. 33, to account for fluid motion around the cell, and the calculation of non-spherical diffusion shape factors, has been applied in earlier work (Baird and Emsley, 1999). For the purposes of biogeochemical modelling these uncertain corrections for small scale turbulence and non-spherical shape are not quantitatively important, and have not been pursued here.

Numerous studies have considered diffusion-limited transport to the cell surface at low nutrient concentrations saturating to a physiologically-limited nutrient uptake from the cell wall (Hill and Whittingham, 1955; Pasciak and Gavis, 1975; Mann and Lazier, 2006) at higher concentrations. The physiological limitation is typically considered using a Michaelis-Menton type equation. Here we simply consider the diffusion-limited uptake to be saturated by the filling-up of reserves, $(1 - R^*)$. Thus, nutrient uptake is given by:

$$J = \psi D C_b \left(1 - R^*\right) \tag{34}$$

where R^* is the reserve of the nutrient being considered. As shown later when considering preferential ammonia uptake, under extreme limitation relative to other nutrients, R^* approaches 0, and uptake approaches the diffusion limitation.

4.3.3 Light capture and chlorophyll synthesis

Light absorption by microalgae cells has already been considered above Eq. 6. The same absorption cross-section, α, is used to calculate the capture of photons:

$$\frac{\partial R_C^*}{\partial t} = \left(1 - R_C^*\right) \frac{\left(10^9 hc\right)^{-1}}{A_V} \int \alpha_\lambda E_{o,\lambda} \lambda \, d\lambda \tag{35}$$

where $\left(1 - R_C^*\right)$ accounts for the reduced capture of photons as the reserves becomes saturated, and $\frac{\left(10^9 hc\right)^{-1}}{A_V}$ converts from energy to photons. The absorption cross-section is a function of intracellular pigment concentration, which is a dynamic variable determined below. While a drop-off of photosynthesis occurs as the carbon reserves become replete, this formulation does not consider photoinhibition due to photooxidation, although it has been considered elsewhere for zooxanthallae Sec. 5.4.2).

The dynamic C:Chl component determines the rate of synthesis of pigment based on the incremental benefit of adding pigment to the rate of photosynthesis. This calculation includes both the reduced benefit when carbon reserves are replete, $(1 - R_C^*)$, and the reduced benefit due to self-shading, χ. The factor χ is calculated for the derivative of the absorption cross-section per unit projected area, α/PA, with non-dimensional group $\rho = \gamma c_i r$. For a sphere of radius r (Baird et al., 2013):

$$\frac{1}{PA}\frac{\partial \alpha}{\partial \rho} = \frac{1 - e^{-2\rho}(2\rho^2 + 2\rho + 1)}{\rho^3} = \chi \tag{36}$$

where χ represents the area-specific incremental rate of change of absorption with ρ. The rate of chlorophyll synthesis is given by:

$$\frac{\partial c_i}{\partial t} = k_{\text{Chl}}^{\max}(1 - R_C^*)\overline{\chi} \quad \text{if C : Chl} > \theta_{min} \tag{37}$$

where $k_{\text{Chl}}^{\max}$ is the maximum rate of synthesis and θ_{min} is the minimum C:Chl ratio. Below θ_{min}, pigment synthesis is zero. Both self-shading, and the rate of photosynthesis itself, are based on photon absorption rather than energy absorption (Table 6), as experimentally shown in Nielsen and Sakshaug (1993).

For each phytoplankton type the model considers multiple pigments with distinct absorbance spectra. The model needs to represent all photo-absorbing pigments as the C:Chl model calculates the pigment concentration based on that required to maximise photosynthesis. If only Chl a was represented, the model would predict a Chl a concentration that was accounting for the absorption of Chl a and the auxiliary pigments, thus over-predicting the Chl a concentration when compared to observations. Thus the Chl-a predicted by the model is like a HPLC-determined Chl-a concentration, and not the sum of the photosynthetic pigments.

The state variables, equations and parameter values are listed in Tables 5, 6 and 7 respectively. The equations in Table 5 described nitrogen uptake from the DIN pool, where the partitioning between nitrate and ammonia due to preferential ammonia uptake is described in Sec. 7.1.

4.3.4 Carbon fixation / respiration

When photons are captured (photosynthesis) there is an increase in reserves of carbon, $k_I(1 - R_C^*)$, and an accompanying uptake of dissolved inorganic carbon, $\frac{106}{1060}12k_I(1-R_C^*)$, and release of oxygen, $\frac{106}{1060}32k_I(1 - R_C^*)$, per cell to the water column (Table 6).

Additionally, there is a basal respiration, representing a constant cost of cell maintenance. The loss of internal reserves, $\mu_B^{\max} m_C \phi R_C^*$, results in a gain of water column dissolved inorganic carbon per cell, $\frac{106}{1060}\frac{12}{14}\mu_B^{\max}\phi R_C^*$, as well as a loss in water column dissolved oxygen per cell, $\frac{106}{1060}\frac{32}{14}\mu_B^{\max}\phi R_C^*$ (Table 6). The loss in water column dissolved oxygen per cell represents an instantaneous respiration

of the fixed carbon of the reserves. Basal respiration decreases internal reserves, and therefore growth rate, but does not directly lead to cell mortality at zero carbon reserves. Implicit in this scheme is that the basal cost is higher when the cell has more carbon reserves, R_C^*.

A linear mortality term, resulting in the loss of structural material and carbon reserves, is considered later.

4.3.5 Conservation of mass of microalgae model

The conservation of mass during transport, growth and mortality is proven in Baird et al. (2004a). Briefly, for microalgal growth, total concentration of nitrogen in microalgae cells is given by $B + BR_N^*$. For conservation of mass, the time derivatives must equate to zero:

$$\frac{\partial B}{\partial t} + \frac{\partial \left(R_N B / R_N^{max}\right)}{\partial t} = 0. \tag{38}$$

using the product rule to differentiate the second term on the LHS:

$$\frac{\partial B}{\partial t} + \frac{\partial B}{\partial t}\frac{R_N}{R_N^{max}} + \frac{B}{R_N^{max}}\frac{\partial R_N}{\partial t} = 0 \tag{39}$$

Where:

$$\frac{\partial B}{\partial t} = +\mu_B^{max} R_C^* R_N^* R_P^* B \tag{40}$$

$$\frac{\partial B}{\partial t}\frac{R_N}{R_N^{max}} = +\mu_B^{max} R_C^* R_N^* R_P^* B \frac{R_N}{R_N^{max}} \tag{41}$$

$$\frac{B}{R_N^{max}}\frac{\partial R_N}{\partial t} = -B(1 + R_N^*)\mu_B^{max} R_C^* R_N^* R_P^* \frac{R_N}{R_N^{max}} \tag{42}$$

Thus demonstrating conservation of mass when $m_{B,N} = R_N^{max}$, as used here.

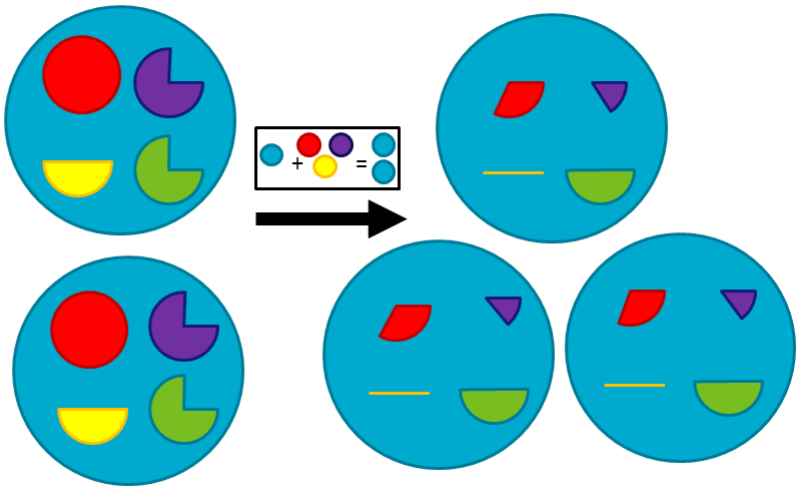

Figure 9: Schematic of the process of microalgae growth from internal reserves. Blue circle - structural material; Red pie - nitrogen reserves; Purple pie - phosphorus reserves; Yellow pie - carbon reserves; Green pie - pigment content. Here a circular pie has a value of 1, representing the normalised reserve (a value between 0 and 1). The box shows that to generate structural material for an additional cell requires the equivalent of 100 % internal reserves of carbon, nitrogen and phosphorus of one cell. This figure shows the discrete growth of 2 cells to 3, requiring both the generation of new structural material from reserves and the reserves being diluted as a result of the number of cells in which they are divided increasing from 2 to 3. Thus the internal reserves for nitrogen after the population increases from 2 to 3 is given by: two from the initial 2 cells, minus one for building structural material of the new cell, shared across the 3 offspring, to give 1/3. The same logic applies to carbon and phosphorus reserves, with phosphorus reserves being reduced to 1/6, and carbon reserves being exhausted. In contrast, pigment is not required for structural material so the only reduction is through dilution; the 3/4 content of 2 cells is shared among 3 cells to equal 1/2 in the 3 cells. This schematic shows one limitation of a population-style model whereby reserves are 'shared' across the population (as opposed to individual based modelling, Beckmann and Hense (2004)). A proof of the conservation of mass for this scheme, including under mixing of populations of suspended microalgae, is given in Baird et al. (2004a). The model equations also include terms affecting internal reserves through nutrient uptake, light absorption, respiration and mortality that are not shown in this simple schematic.

$$\frac{\partial N}{\partial t} = -\psi D_N N(1-R_N^*)\,(B/m_N) \tag{43}$$

$$\frac{\partial P}{\partial t} = -\psi D_P P(1-R_P^*)\,(B/m_N) \tag{44}$$

$$\frac{\partial DIC}{\partial t} = -\left(\frac{106}{1060}12k_I(1-R_C^*) - \frac{106}{16}\frac{12}{14}\mu_B^{\max}\phi R_C^*\right)(B/m_N) \tag{45}$$

$$\frac{\partial [\mathrm{O_2}]}{\partial t} = \left(\frac{106}{1060}32k_I(1-R_C^*) - \frac{106}{16}\frac{32}{14}\mu_B^{\max}\phi R_C^*\right)(B/m_N) \tag{46}$$

$$\frac{\partial R_N}{\partial t} = \psi D_N N(1-R_N^*) - \mu_B^{\max}\,(m_N+R_N)\,R_P^*R_N^*R_C^* \tag{47}$$

$$\frac{\partial R_P}{\partial t} = \psi D_P P(1-R_P^*) - \mu_B^{\max}\,(m_P+R_P)\,R_P^*R_N^*R_C^* \tag{48}$$

$$\frac{\partial R_C}{\partial t} = k_I(1-R_C^*) - \mu_B^{\max}\,(m_C+R_C)\,R_P^*R_N^*R_C^* - \mu_B^{\max}\phi m_C R_C^* \tag{49}$$

$$\frac{\partial B}{\partial t} = \mu_B^{\max}R_P^*R_N^*R_C^*B \tag{50}$$

$$\frac{\partial c_i}{\partial t} = k_{\mathrm{Chl}}^{\max}(1-R_C^*)\overline{\chi} - \mu_P^{\max}R_P^*R_N^*R_C^*c_i \tag{51}$$

$$\psi = 4\pi r \tag{52}$$

$$k_I = \frac{(10^9 hc)^{-1}}{A_V}\int \alpha_\lambda E_{o,\lambda}\lambda\,d\lambda \tag{53}$$

$$\alpha_\lambda = \pi r^2\left(1-\frac{2(1-(1+2\rho_\lambda)e^{-2\rho_\lambda})}{4\rho_\lambda^2}\right) \tag{54}$$

$$\overline{\chi} = \int \chi_\lambda E_{o,\lambda}\lambda\ d\lambda \ \Big/ \int E_{o,\lambda}\lambda\ d\lambda \tag{55}$$

$$\chi_\lambda = \frac{1}{\pi r^2}\frac{\partial \alpha_\lambda}{\partial \rho_\lambda} = \frac{1-e^{-2\rho_\lambda}(2\rho_\lambda^2+2\rho_\lambda+1)}{\rho_\lambda^3} \tag{56}$$

$$\rho_\lambda = \gamma c_i r \tag{57}$$

Table 6: Microalgae growth model equations. The term B/m_N is the concentration of cells. The equation for organic matter formation gives the stoichiometric constants; 12 g C mol C^{-1}; 32 g O mol $\mathrm{O_2^{-1}}$. The equations are for scalar irradiance specified as an energy flux.

	Symbol	Value
Constants		
Molecular diffusivity of NO_3	D_N	$f(T,S)$ m^2 s^{-1}
Molecular diffusivity of PO_4	D_P	$f(T,S)$ m^2 s^{-1}
Speed of light	c	2.998×10^8 m s^{-1}
Planck constant	h	6.626×10^{-34} J s^{-1}
Avogadro constant	A_V	6.02×10^{23} mol^{-1}
[a]Pigment-specific absorption coefficient	$\gamma_{\text{pig},\lambda}$	$f(\text{pig},\lambda)$ m^{-1} (mg m^{-3})$^{-1}$
[d]Minimum C:Chl ratio	θ_{min}	20.0 wt/wt
Allometric relationships		
[b]Carbon content	m_C	$12010 \times 9.14 \times 10^3 V$ mg C cell^{-1}
[c]Maximum intracellular Chl a concentration	$c_i^{\max}$	$2.09 \times 10^7 V^{-0.310}$ mg Chl m^{-3}
Nitrogen content of phytoplankton	m_N	$\frac{14}{12}\frac{16}{106} m_C$ mg N cell^{-1}

Table 7: Constants and parameter values used in the microalgae model. V is cell volume in μm^3. [a] Figs. 3 4 & 5,[b]Straile (1997),[c] Finkel (2001), Sathyendranath et al. (2009) using HPLC-determination which isolate Chl-a.

Earlier published versions of the microalgae model are described with multiple nutrient limitation (Baird et al., 2001), with variable C:N ratios (Wild-Allen et al., 2010) and variable C:Chl ratios (Baird et al., 2013). Further, demonstration of the conservation of mass during transport is given in Baird et al. (2004a). Here the microalgae model is presented with variable C:Chl ratios (with an additional auxiliary pigment), and both nitrogen and phosphorus limitation, and a preference for ammonia uptake when compared to nitrate. The strategy of dynamic supply and consumption rates of elements is a simple version of what is often called Dynamic Energy Budget (DEB) models in the ecological modelling literature (Kooijman, 2010).

4.4 Nitrogen-fixing *Trichodesmium*

The growth of *Trichodesmium* follows the microalgae growth and C:Chl model above, with the following additional processes of nitrogen fixation and physiological-dependent buoyancy adjustment, as described in Robson et al. (2013). Additional parameter values for *Trichodesmium* are given in Table 8.

4.4.1 Nitrogen fixation

Nitrogen fixation occurs when the DIN concentration falls below a critical concentration, DIN_{crit}, typically 0.3 to 1.6 μmol L^{-1} (i.e. 4 to 20 mg N m^{-3}, Robson et al. (2013)), at which point *Trichodesmium* produce nitrogenase to allow fixation of N_2. It is assumed that nitrogenase becomes available whenever ambient DIN falls below the value of DIN_{crit} and carbon and phosphorus are available to support nitrogen uptake. The rate of change of internal reserves of nitrogen, R_N, due to nitrogen fixation if $DIN < DIN_{crit}$ is given by:

$$N_{fix} = \frac{\partial R_N}{\partial t}|_{N_{fix}} = \max\left(4\pi r D_{\mathrm{NO_3}} DIN_{crit} R_P^* R_C^* (1 - R_N^*) - 4\pi r D_{\mathrm{NO_3}} \left[\mathrm{NO_3} + \mathrm{NH_4}\right](1 - R_N^*), 0\right) \tag{58}$$

where N_{fix} is the rate of nitrogen fixation per cell and r is the radius of the individual cell. Using this formulation, *Trichodesmium* is able to maintain its nitrogen uptake rate at that achieved through diffusion limited uptake at DIN_{crit} even when DIN drops below DIN_{crit}, provided phosphorus and carbon reserves, R_P^* and R_C^* respectively, are available.

The energetic cost of nitrogen fixation is represented as a fixed proportion of carbon fixation, f_{Nfix}, equivalent to a reduction in quantum efficiency, and as a proportion, $f_{nitrogenase}$, of the nitrogen fixed:

$$\frac{\partial R_C}{\partial t} = -(1 - f_{Nfix})(1 - f_{nitrogenase}) k_I \tag{59}$$

where k_I is the rate of photon absorption per cell obtain from the microalgal growth model (Table 6).

4.4.2 Buoyancy adjustment

The rate of change of *Trichodesmium* biomass, B, as a result of density difference between the cell and the water, is approximated by Stokes' Law:

$$\frac{\partial B}{\partial t} = -\frac{2}{9} \frac{g r_{col}^2}{\mu} (\rho - \rho_w) \frac{\partial B}{\partial z} \tag{60}$$

where z is the distance in the vertical (+ve up), μ is the dynamic viscosity of water, g is acceleration due to gravity, r_{col} is the equivalent spherical radius of the sinking mass representing a colony radius, ρ_w is the density of water, and ρ is the cell density is given by:

$$\rho = \rho_{min} + R_C^* (\rho_{max} - \rho_{min}) \tag{61}$$

where R_C^* is the normalised carbon reserves of the cell (see above), and ρ_{min} and ρ_{max} are the densities of the cell when there is no carbon reserves and full carbon reserves respectively. Thus, when light reserves are depleted, the cell is more buoyant, facilitating the retention of *Trichodesmium* in the surface waters.

	Symbol	Value
Maximum growth rate	μ^{max}	0.2 d^{-1}
[b]Ratio of xanthophyll to Chl *a*	f_{xan}	0.5
Linear mortality	m_L	0.10 d^{-1}
Quadratic mortality	m_Q	0.10 d^{-1} (mg N m^{-3})$^{-1}$
Cell radius	r	5 μm
Colony radius	r_{col}	5 μm
Max. cell density	ρ_{max}	1050 kg m^{-3}
Min. cell density	ρ_{min}	900 kg m^{-3}
Critical threshold for N fixation	DIN_{crit}	10 mg N m^{-3}
Fraction of energy used for nitrogenase	$f_{nitrogenase}$	0.07
Fraction of energy used for N fixation	f_{Nfix}	0.33
Nitrogen gas in equilibrium with atm.	$[N_2]$	2 $\times 10^4$ mg N m^{-3}

Table 8: Parameter values used in the *Trichodesmium* model (Robson et al., 2013). [b] The major accessory pigments in *Trichodesmium* are the red-ish phycourobilin and phycoerythrobilin (Subramaniam et al., 1999). For simplicity in this model their absorption cross-section is approximated by photosynthetic xanthophyll, which has an absorption peak approximately 10 nm less than the phycourobilin.

4.5 Water column inorganic chemistry

4.5.1 Carbon chemistry

The major pools of dissolved inorganic carbon species in the ocean are HCO_3^-, CO_3^-, and dissolved CO_2, which influence the speciation of H^+, and OH^- ions, and therefore pH. The interaction of these ions reaches an equilibrium in seawater within a few tens of seconds (Zeebe and Wolf-Gladrow, 2001). In the biogeochemical model here, where calculation timesteps are of order tens of minutes, it is reasonable to assume that the carbon chemistry system is at equilibrium.

The Ocean-Carbon Cycle Model Intercomparison Project (OCMIP) has developed numerical methods to quantify air-sea carbon fluxes and carbon dioxide system equilibria (Najjar and Orr, 1999). Here we use a modified version of the OCMIP-2 Fortran code developed for MOM4 (GFDL Modular Ocean Model version 4, (Griffies et al., 2004)). The OCMIP procedures quantify the state of the carbon dioxide (CO_2) system using two prognostic variables, the concentration of dissolved inorganic carbon, DIC, and total alkalinity, A_T. The value of these prognostic variables, along with salinity and temperature, are used to calculate the pH and partial pressure of carbon dioxide, pCO_2, in the surface waters using a set of governing chemical equations which are solved using a Newton-Raphson method (Najjar and Orr, 1999).

One alteration from the global implementation of the OCMIP scheme is to increase the search space for the iterative scheme from ±0.5 pH units (appropriate for global models) to ±2.5. With this change, the OCMIP scheme converges over a broad range of DIC and A_T values (Munhoven, 2013).

For more details see Mongin and Baird (2014); Mongin et al. (2016).

Variable	Symbol	Units
Ammonia concentration	$[NH_4]$	mg N m^{-3}
Water column Dissolved Inorganic Carbon (DIC)	DIC	mg C m^{-3}
Water column Dissolved Inorganic Phosphorus (DIP)	P	mg P m^{-3}
Water column Particulate Inorganic Phosphorus (PIP)	PIP	mg P m^{-3}
Water column Non-Algal Particulates (NAP)	NAP	kg m^{-3}
Water column dissolved oxygen concentration	$[O_2]$	mg O m^{-3}

Table 9: State and derived variables for the water column inorganic chemistry model.

$$\mathrm{NH_4^+ + 2O_2 \longrightarrow NO_3^- + H_2O + 2H^+} \tag{62}$$

$$\frac{\partial[\mathrm{NH_4}]}{\partial t} = -\tau_{nit,wc}[\mathrm{NH_4}]\frac{[\mathrm{O_2}]}{K_{nit,\mathrm{O}} + [\mathrm{O_2}]} \tag{63}$$

$$\frac{\partial[\mathrm{O_2}]}{\partial t} = -2\tau_{nit,wc}[\mathrm{NH_4}]\frac{[\mathrm{O_2}]}{K_{nit,\mathrm{O}} + [\mathrm{O_2}]} \tag{64}$$

$$\frac{\partial[\mathrm{NO_3}]}{\partial t} = \tau_{nit,wc}[\mathrm{NH_4}]\frac{[\mathrm{O_2}]}{K_{nit,\mathrm{O}} + [\mathrm{O_2}]} \tag{65}$$

$$\frac{\partial P}{\partial t} = \tau_{Pabs}\left(\frac{PIP}{k_{Pads,wc}NAP} - \frac{[\mathrm{O_2}]P}{K_{\mathrm{O_2,abs}} + [\mathrm{O_2}]}\right) \tag{66}$$

$$\frac{\partial PIP}{\partial t} = -\tau_{Pabs}\left(\frac{PIP}{k_{Pads,wc}NAP} - \frac{[\mathrm{O_2}]P}{K_{\mathrm{O_2,abs}} + [\mathrm{O_2}]}\right) \tag{67}$$

Table 10: Equations for the water column inorganic chemistry.

Description	Symbol	Units
Maximum rate of nitrification in the water column	$\tau_{nit,wc}$	0.1 d^{-1}
Oxygen half-saturation constant for nitrification	$K_{nit,\mathrm{O}}$	500 mg O m^{-3}
Rate of P adsorbed/desorbed equilibrium	τ_{Pabs}	0.004 d^{-1}
Isothermic const. P adsorption for NAP	$k_{Pads,wc}$	30 kg NAP^{-1}
Oxygen half-saturation for P adsorption	$K_{\mathrm{O_2,abs}}$	2000 mg O m^{-3}

Table 11: Constants and parameter values used in the water column inorganic chemistry.

4.5.2 Nitrification

Nitrification is the oxidation of ammonia with oxygen, to form nitrite followed by the rapid oxidation of these nitrites into nitrates. This is represented in a one step processes, with the rate of nitrification given by:

$$\frac{\partial[\mathrm{NH_4}]}{\partial t} = -\tau_{nit,wc}[\mathrm{NH_4}]\frac{[\mathrm{O_2}]}{K_{nit,\mathrm{O}} + [\mathrm{O_2}]} \tag{68}$$

where the equations and parameter values are defined in Tables 10 and 11.

4.5.3 Phosphorus absorption - desorption

The rate of phosphorus desorption from particulates is given by:

$$\frac{\partial P}{\partial t} = \tau_{Pabs}\left(\frac{PIP}{k_{Pads,wc}NAP} - \frac{[\mathrm{O_2}]P}{K_{\mathrm{O_2,abs}} + [\mathrm{O_2}]}\right) = -\frac{\partial PIP}{\partial t} \tag{69}$$

where $[\mathrm{O_2}]$ is the concentration of oxygen, P is the concentration of dissolved inorganic phosphorus, PIP is the concentration of particulate inorganic phosphorus, NAP is the sum of the non-algal inorganic particulate concentrations, and τ_{Pabs}, $k_{Pads,wc}$ and $K_{\mathrm{O_2,abs}}$ are model parameters described in Table 11.

At steady-state, the PIP concentration is given by:

$$PIP = k_{Pads,wc}P\frac{[\mathrm{O_2}]}{K_{\mathrm{O_2,abs}} + [\mathrm{O_2}]}NAP \tag{70}$$

As an example for rivers flowing into the eReefs configuration, $[\mathrm{O_2}] = 7411$ mg m^{-3} (90% saturation at T = 25, S = 0), $NAP = 0.231$ kg m^{-3}, $k_{Pads,wc} = 30$ kg NAP^{-1}, $K_{\mathrm{O_2,abs}} = 74$ mg O m^{-3}, $P = 4.2$ mg m^{-3}, thus the ratio $PIP/DIP = 6.86$ (see Fig. 10).

Limited available observations of absorption-desorption include from the Johnstone River (Pailles and Moody, 1992) and the GBR (Monbet et al., 2007).

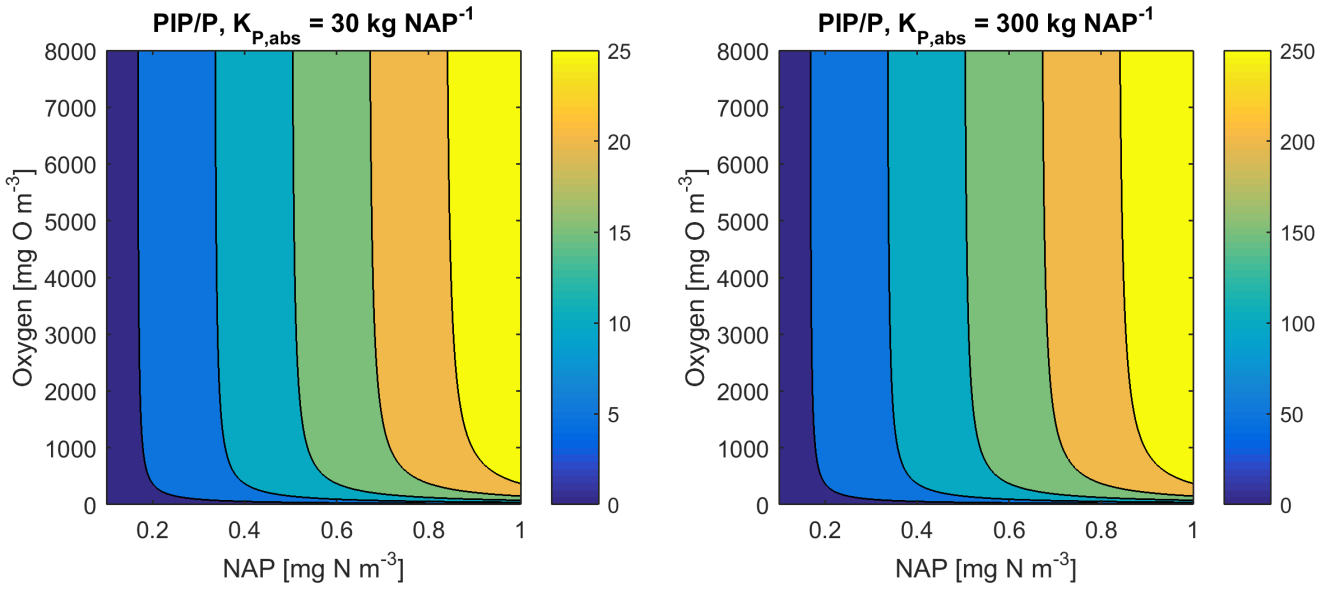

Figure 10: Phosphorus adsorption - desorption equilibria, $K_{\mathrm{O_2,abs}} = 74$ mg O m^{-3}.

4.6 Zooplankton herbivory

The simple food web of the model involves small zooplankton consuming small phytoplankton, and large zooplankton consuming large phytoplankton, microphytobenthos and *Trichodesmium*. For simplicity the state variables and equations are only given for small plankton grazing (Tables 12, 14), but the parameters are given for all grazing terms (Table 13).

The rate of zooplankton grazing is determined by the encounter rate of the predator and all its prey up until the point at which it saturates the growth of the zooplankton, and then it is constant. This is effectively a Hollings Type I grazing response (Gentleman, 2002). Under the condition of multiple prey types, there is no preferential grazing other than that determined by the chance of encounter. The encounter rate is the result of the relative motion brought about by diffusive, shear, and swimming-determined relative velocities (Jackson, 1995; Baird, 2003).

This formulation of grazing, originally proposed by Jackson (1995) but rarely used in biogeochemical modelling, is developed from considering the encounter of individuals, not populations. One particular advantage of formulating the encounter on individuals is that should the number of populations considered in the model change (i.e. an additional phytoplankton class is added), there is no need to re-parameterise. In contrast, almost all biogeochemical models, as typified by Fasham et al. (1990), consider the grazing of populations of plankton, parameterised using a saturating curve constrained by a half saturation constant. Awkwardly, the half saturation constant only has meaning for one particular diet of phytoplankton. This is best illustrated by dividing a single population into two identical populations of half the number, in which case, for the same specification of half-saturation constant, the grazing rate increases. That is:

$$\frac{\mu P}{k+P} \neq \frac{\mu P/2}{k+P/2} + \frac{\mu P/2}{k+P/2} \tag{71}$$

As the zooplankton are grazing on the phytoplankton that contain internal reserves of nutrients an addition flux of dissolved inorganic nutrients (gR^*_N for nitrogen) is returned to the water column (for more details see Sec. 4.6.1).

4.6.1 Conservation of mass in zooplankton grazing

It is important to note that the microalgae model presented above represents internal reserves of nutrients, carbon and chlorophyll as a per cell quantity. Using this representation there are no losses of internal quantities with either grazing or mortality. However the implication of their presence is represented in the (gR^*_N) terms (Table 14) that return the reserves to the water column. These terms represent the fast return of a fraction of phytoplankton nitrogen due to processes like "sloppy eating".

Variable	Symbol	Units
Ammonia concentration	$[NH_4]$	mg N m^{-3}
Water column dissolved Inorganic Carbon (DIC)	DIC	mg C m^{-3}
Water column dissolved Inorganic Phosphorus (DIP)	P	mg P m^{-3}
Water column dissolved oxygen concentration	$[O_2]$	mg O m^{-3}
Reserves of phytoplankton nitrogen	R_N	mg N $cell^{-1}$
Reserves of phytoplankton phosphorus	R_P	mg P $cell^{-1}$
Reserves of phytoplankton carbon	R_C	mmol photon $cell^{-1}$
Maximum reserves of nitrogen	$R_N^{\max}$	mg N $cell^{-1}$
Maximum reserves of phosphorus	$R_P^{\max}$	mg P $cell^{-1}$
Maximum reserves of carbon	$R_C^{\max}$	mmol photon $cell^{-1}$
Normalised reserves of nitrogen	$R_N^* \equiv R_N/R_N^{\max}$	-
Normalised reserves of phosphorus	$R_P^* \equiv R_P/R_P^{\max}$	-
Normalised reserves of carbon	$R_C^* \equiv R_C/R_C^{\max}$	-
Phytoplankton structural biomass	B	mg N m^{-3}
Zooplankton biomass	Z	mg N m^{-3}
Detritus at the Redfield ratio	D_{Red}	mg N m^{-3}
Zooplankton grazing rate	g	mg N m^{-3} s^{-1}
Encounter rate coefficient due to molecular diffusion	ϕ_{diff}	m^3 s^{-1} cell Z^{-1}
Encounter rate coefficient due to relative motion	ϕ_{rel}	m^3 s^{-1} cell Z^{-1}
Encounter rate coefficient due to turbulent shear	ϕ_{shear}	m^3 s^{-1} cell Z^{-1}
Phytoplankton cell mass	m_B	mg N $cell^{-1}$
Zooplankton cell mass	m_Z	mg N $cell^{-1}$

Table 12: State and derived variables for the zooplankton grazing. Zooplankton cell mass, $m_Z = 16000 \times 14.01 \times 10.5 V_Z$ mg N $cell^{-1}$, where V_Z is the volume of zooplankton (Hansen et al., 1997).

An alternative and equivalent formulation would be to consider total concentration of microalgal reserves in the water column, then the change in water column concentration of reserves due to mortality (either grazing or natural mortality) must be considered. This alternate representation will not be undertaken here as the above considered equations are fully consistent, but it is worth noting that the numerical solution of the model within the EMS package represents total water column concentrations of internal reserves, and therefore must include the appropriate loss terms due to mortality.

Description	Symbol	Small	Large
Maximum growth rate of zooplankton at T_{ref} (d^{-1})	μ_Z	4.0	1.33
Nominal cell radius of zooplankton (μm)	r_Z	5	320
Growth efficiency of zooplankton	E_Z	0.462	0.426
Fraction of growth inefficiency lost to detritus	γ_Z	0.5	0.5
Swimming velocity ($\mu m\ s^{-1}$)	U_Z	200	3000
Constants			
Boltzmann's constant	κ	1.38066×10^{-23}	$J\ K^{-1}$
Viscosity	ν	10^{-6}	$m^2\ s^{-1}$
Dissipation rate of TKE	ϵ	10^{-6}	$m^3\ s^{-1}$
Oxygen half-saturation for aerobic respiration	K_{OA}	256	mg O m^{-3}

Table 13: Constants and parameter values used for zooplankton grazing. Dissipation rate of turbulent kinetic energy (TKE) is considered constant.

4.7 Zooplankton carnivory

Large zooplankton consume small zooplankton. This process uses similar encounter rate and consumption rate limitations calculated for zooplankton herbivory (Table 14). As zooplankton contain no internal reserves, the equations are simplified from the herbivory case to those listed in Table 15). Assuming that the efficiency of herbivory, γ, is equal to that of carnivory, and therefore assigned the same parameter, the additional process of carnivory adds no new parameters to the biogeochemical model.

4.8 Zooplankton respiration

In the model there is no change in water column oxygen concentration if organic material is exchanged between pools with the same elemental ratio. Thus, when zooplankton plankton consume phytoplankton no oxygen is consumed due to the consumption of phytoplankton structural material (B_P). However, the excess carbon reserves represent a pool of fixed carbon, which when released from the phytoplankton must consume oxygen. Further, zooplankton mortality and growth inefficiency results in detritial production, which when remineralised consumes oxygen. Additionally, carbon released to the dissolved inorganic pool during inefficiency grazing on phytoplankton structural material also consumes oxygen. Thus zooplankton respiration is implicitly captured in these associated processes.

4.9 Non-grazing plankton mortality

The rate of change of phytoplankton biomass, B, as a result of natural mortality is given by:

$$\frac{\partial B}{\partial t} = -m_L B - m_Q B^2 \tag{93}$$

where m_L is the linear mortality coefficient and m_Q is the quadratic mortality coefficient.

A combination of linear and quadratic mortality rates are used in the model. When the mortality term is the sole loss term, such as zooplankton in the water column or benthic microalgae in the sediments, a quadratic term is employed to represent increasing predation / viral disease losses in dense populations.

Linear terms have been used to represent a basal respiration rate.

As described in Sec 4.3.5, the mortality terms need to account for the internal properties of lost microalgae.

For definitions of the state variables see Tables 16 & 17.

$$
\begin{aligned}
\frac{\partial[\mathrm{NH_4}]}{\partial t} &= g(1-E)\,(1-\gamma) + gR_N^* && (72)\\
\frac{\partial P}{\partial t} &= g\frac{1}{16}\frac{31}{14}(1-E)\,(1-\gamma) + \frac{1}{16}\frac{31}{14}gR_P^* && (73)\\
\frac{\partial DIC}{\partial t} &= g\frac{106}{16}\frac{12}{14}(1-E)\,(1-\gamma) + \frac{106}{16}\frac{12}{14}gR_C^* && (74)\\
\frac{\partial B}{\partial t} &= -g && (75)\\
\frac{\partial Z}{\partial t} &= Eg && (76)\\
\frac{\partial D_{Red}}{\partial t} &= g(1-E)\gamma && (77)\\
\frac{\partial[\mathrm{O_2}]}{\partial t} &= -\frac{\partial DIC}{\partial t}\frac{32}{12}\frac{[\mathrm{O_2}]}{K_{OA}+[\mathrm{O_2}]} && (78)\\
g &= \min\left[\mu_Z^{max} Z/E, \frac{Z}{m_{Z_L}}\left(\phi_{diff}+\phi_{rel}+\phi_{shear}\right)B\right] && (79)\\
\phi &= \phi_{diff}+\phi_{rel}+\phi_{shear} && (80)\\
\phi_{diff} &= (2\kappa T/(3\rho\nu))(1/r_Z+1/r_B)(r_B+r_Z) && (81)\\
\phi_{rel} &= \pi(r_Z+r_B)^2 U_{eff} && (82)\\
\phi_{shear} &= 1.3\sqrt{\epsilon/\nu}(r_Z+r_B)^3 && (83)\\
U_{eff} &= (U_B^2+3U_Z^2)/3U_Z && (84)
\end{aligned}
$$

Table 14: Equations for zooplankton grazing. The terms represent a predator Z consuming a phytoplankton B. Notes (1) If the zooplankton diet contains multiple phytoplankton classes, and grazing is prey saturated, then phytoplankton loss must be reduced to account for the saturation by other types of microalgae; (2) $\frac{Z}{m_Z}$ is the number of individual zooplankton; (3) Phytoplankton pigment is lost to water column without being conserved. Chl *a* has chemical formulae $C_{55}H_{72}O_5N_4Mg$, and a molecular weight of 893.49 g mol^{-1}. The uptake (and subsequent remineralisation) of molecules for chlorophyll synthesis could make up a maximum (at C:Chl = 20) of (660/893)/20 and (56/893)/20 $\times$ (16/106) $\times$ (14/12)), or $\sim$4 and $\sim$2 per cent of the exchange of C and N between the cell and water column, and will cancel out over the lifetime of a cell. Thus the error in ignoring chlorophyll loss to the water column is small.

$$
\begin{aligned}
\frac{\partial[\mathrm{NH_4}]}{\partial t} &= g(1-E)\,(1-\gamma) && (85)\\
\frac{\partial P}{\partial t} &= g\frac{1}{16}\frac{31}{14}(1-E)\,(1-\gamma) && (86)\\
\frac{\partial DIC}{\partial t} &= g\frac{106}{16}\frac{12}{14}(1-E)\,(1-\gamma) && (87)\\
\frac{\partial Z_S}{\partial t} &= -g && (88)\\
\frac{\partial Z_L}{\partial t} &= Eg && (89)\\
\frac{\partial D_{Red}}{\partial t} &= g(1-E)\gamma && (90)\\
\frac{\partial[\mathrm{O_2}]}{\partial t} &= -\frac{\partial DIC}{\partial t}\frac{32}{12}\frac{[\mathrm{O_2}]}{K_{OA}+[\mathrm{O_2}]} && (91)\\
g &= \min\left[\mu_{Z_L}^{max} Z_L/E, \frac{Z_L}{m_Z}\left(\phi_{diff}+\phi_{rel}\phi_{shear}\right) Z_S\right] && (92)
\end{aligned}
$$

Table 15: Equations for zooplankton carnivory, represent large zooplankton Z_L consuming small zooplankton Z_S. The parameters values and symbols are given in Table 13 and Table 12

.

Description	water column		sediment	
	linear d^{-1}	quadratic d^{-1} $(\mathrm{mg\ N\ m^{-3}})^{-1}$	linear d^{-1}	quadratic d^{-1} $(\mathrm{mg\ N\ m^{-3}})^{-1}$
Small phytoplankton	0.1	-	1	-
Large phytoplankton	0.1	-	10	-
Microphytobenthos	-	-	-	0.0001
Trichodesmium	0.1	0.1	-	-

Table 16: Constants and parameter values used for plankton mortality.

$$\frac{\partial[\mathrm{NH_4}]}{\partial t} = m_{L,B} B R^*_N \quad (94)$$

$$\frac{\partial DIP}{\partial t} = \frac{1}{16}\frac{31}{14} m_{L,B} B R^*_P \quad (95)$$

$$\frac{\partial DIC}{\partial t} = \frac{106}{16}\frac{12}{14} m_{L,B} B R^*_C \quad (96)$$

$$\frac{\partial[\mathrm{O_2}]}{\partial t} = -\frac{\partial DIC}{\partial t}\frac{32}{12}\frac{[\mathrm{O_2}]}{K_{OA} + [\mathrm{O_2}]} \quad (97)$$

$$\frac{\partial B}{\partial t} = -m_{L,B} B \quad (98)$$

$$\frac{\partial D_{Red}}{\partial t} = m_{L,B} B \quad (99)$$

Table 17: Equations for linear phytoplankton mortality.

$$\frac{\partial Z_S}{\partial t} = -m_{Q,ZS} Z_S^2 \quad (100)$$

$$\frac{\partial Z_L}{\partial t} = -m_{Q,ZL} Z_L^2 \quad (101)$$

$$\frac{\partial D_{Red}}{\partial t} = f_{Z2det}\left(m_{Q,ZS} Z_S^2 + m_{Q,ZL} Z_L^2\right) \quad (102)$$

$$\frac{\partial[\mathrm{NH_4}]}{\partial t} = (1 - f_{Z2det})\left(m_{Q,ZS} Z_S^2 + m_{Q,ZL} Z_L^2\right) \quad (103)$$

Table 18: Equations for the zooplankton mortality. f_{Z2det} is the fraction of zooplankton mortality that is remineralised, and is equal to 0.5 for both small and large zooplankton.

4.10 Gas exchange

Gas exchange is calculated using wind speed (we choose a cubic relationship, Wanninkhof and McGillis (1999)), saturation state of the gas (described below) and the Schmidt number of the gas (Wanninkhof, 1992). The transfer coefficient, k, is given by:

$$k = \frac{0.0283}{360000} u_{10}^3 \left(\mathrm{Sc}/660\right)^{-1/2} \tag{104}$$

where 0.0283 cm hr^{-1} is an empirically-determined constant (Wanninkhof and McGillis, 1999), u_{10}^3 is the short-term steady wind at 10 m above the sea surface [m s^{-1}], the Schmidt number, Sc, is the ratio of the diffusivity of momentum and that of the exchanging gas, and is given by a cubic temperature relationship (Wanninkhof, 1992). Finally, a conversion factor of 360000 m s^{-1} (cm hr^{-1})$^{-1}$ is used.

In practice the hydrodynamic model can contain thin surface layers as the surface elevation moves between z-levels. Further, physical processes of advection and diffusion and gas fluxes are done sequentially, allowing concentrations to build up through a single timestep. To avoid unrealistic changes in the concentration of gases in thin surface layers, the shallowest layer thicker than 20 cm receives all the surface fluxes.

4.10.1 Oxygen

The saturation state of oxygen $[\mathrm{O_2}]_{sat}$ is determined as a function of temperature and salinity following Weiss (1970). The change in concentration of oxygen in the surface layer due to a sea-air oxygen flux (+ve from sea to air) is given by:

$$\frac{\partial[\mathrm{O_2}]}{\partial t} = k_{\mathrm{O_2}} \left([\mathrm{O_2}]_{sat} - [\mathrm{O_2}]\right)/h \tag{105}$$

where $k_{\mathrm{O_2}}$ is the transfer coefficient for oxygen (Eq. 104), $[\mathrm{O_2}]$ is the dissolved oxygen concentration in the surface waters, and h is the thickness of the surface layer of the model into which sea-air flux flows.

4.10.2 Carbon dioxide

The change in surface dissolved inorganic carbon concentration, DIC, resulting from the sea-air flux (+ve from sea to air) of carbon dioxide is given by:

$$\frac{\partial DIC}{\partial t} = k_{\mathrm{CO_2}} \left([\mathrm{CO_2}]_{atm} - [\mathrm{CO_2}]\right)/h \tag{106}$$

where k_{CO_2} the transfer coefficient for carbon dioxide (Eq. 104), $[CO_2]$ is the dissolved carbon dioxide concentration in the surface waters determined from DIC and A_T using the carbon chemistry equilibria calculations described in Sec 4.5.1, $[CO_2]_{atm}$ is the partial pressure of carbon dioxide in the atmosphere, and h is the thickness of the surface layer of the model into which sea-air flux flows.

Note the carbon dioxide flux is not determined by the gradient in DIC, but the gradient in $[CO_2]$. At pH values around 8, $[CO_2]$ makes up only approximately 1/200th of DIC in seawater, significantly reducing the air-sea exchange. Counteracting this reduced gradient, note that changing DIC results in an approximately 10 fold change in $[CO_2]$ (quantified by the Revelle factor (Zeebe and Wolf-Gladrow, 2001)). Thus, the gas exchange of CO_2 is approximately $1/200 \times 10 = 1/20$ of the oxygen flux for the same proportional perturbation in DIC and oxygen. At a Sc number of 524 (25°C seawater) and a wind speed of 12 m s^{-1}, 1 m of water equilibrates with CO_2 in the atmosphere with an e-folding timescale of approximately 1 day.

5 Epibenthic processes

In the model, benthic communities are quantified as a biomass per unit area, or areal biomass. At low biomass, the community is composed of a few specimens spread over a small fraction of the bottom, with no interaction between the nutrient and energy acquisition of individuals. Thus, at low biomass the areal fluxes are a linear function of the biomass.

As biomass increases, the individuals begin to cover a significant fraction of the bottom. For nutrient and light fluxes that are constant per unit area, such as downwelling irradiance and sediment releases, the flux per unit biomass decreases with increasing biomass. Some processes, such as photosynthesis in a thick seagrass meadow or nutrient uptake by a coral reef, become independent of biomass (Atkinson, 1992) as the bottom becomes completely covered. To capture the non-linear effect of biomass on benthic processes, we use an effective projected area fraction, A_{eff}.

To restate, at low biomass, the area on the bottom covered by the benthic community is a linear function of biomass. As the total leaf area approaches and exceeds the projected area, the projected area for the calculation of water-community exchange approaches 1, and becomes independent of biomass. This is represented using:

$$A_{eff} = 1 - \exp(-\Omega_B \ B) \tag{107}$$

where A_{eff} is the effective projected area fraction of the benthic community (m^2 m^{-2}), B is the biomass of the benthic community (g N m^{-2}), and Ω_B is the nitrogen-specific leaf area coefficient (m^2 g N^{-1}). For further explanation of Ω_B see Baird et al. (2016a).

The parameter Ω_B is critical: it provides a means of converting between biomass and fractions of the bottom covered, and is used in calculating the absorption cross-section of the leaf and the nutrient uptake of corals and macroalgae. That Ω_B has a simple physical explanation, and can be determined from commonly undertaken morphological measurement (see below), gives us confidence in its use throughout the model.

5.1 Epibenthic optical model

The spectrally-resolved light field at the base of the water column is attenuated, in vertical order, by macroalgae, seagrass (*Zostera* then shallow and then deep forms of *Halophila*), followed by the zooxanthellae in corals. The downwelling irradiance at wavelength λ after passing through each macroalgae and seagrass species is given by, $E_{below,\lambda}$:

$$E_{below,\lambda} = E_{d,above,\lambda} e^{-A_\lambda \Omega_X X} \tag{108}$$

where $E_{above,\lambda}$ for macroalgae is $E_{d,bot,\lambda}$, the downwelling irradiance of the bottom water column layer, A_λ is the absorbance of the leaf, Ω is the nitrogen specific leaf area, and X is the leaf nitrogen biomass.

The light absorbed by corals is assumed to be entirely due to zooxanthellae, and is given by:

$$E_{below,\lambda} = E_{above,\lambda} e^{-n\alpha_\lambda} \tag{109}$$

where $n = CS/m_{N,CS}$ is the areal density of zooxanthellae cells and α_λ is the absorption cross-section of a cell a result of the absorption of multiple pigment types.

The optical model for microphytobenthic algae, and the bottom reflectance due to sediment and bottom types, is described in Sec. 6.1.

5.2 Macroalgae

The macroalgae model considers the diffusion-limited supply of dissolved inorganic nutrients (N and P) and the absorption of light, delivering N, P and fixed C respectively. Unlike the microalgae model, no internal reserves are considered, implying that the macroalgae has a fixed stoichiometry that can be specified as:

$$550CO_2 + 30NO_3^- + PO_4^{3-} + 792H_2O \xrightarrow{5500 \text{ photons}} (CH_2O)_{550}(NH_3)_{30}H_3PO_4 + 716O_2 \tag{110}$$

where the stoichiometry is based on Atkinson and Smith (1983) (see also Baird and Middleton (2004); Hadley et al. (2015a,b)). Note that when ammonia is taken up instead of nitrate there is a slightly different O_2 balance (Sec. 7.1). In the next section will consider the maximum nutrient uptake and light absorption, and then bring them together to determine the realised growth rate.

5.2.1 Nutrient uptake

Nutrient uptake by macroalgae is a function of nutrient concentration, water motion (Hurd, 2000) and internal physiology. The maximum flux of nutrients is specified as a mass transfer limit per projected area of macroalgae and is given by (Falter et al., 2004; Zhang et al., 2011):

$$S_\mathrm{x} = 2850 \left(\frac{2\tau}{\rho}\right)^{0.38} \mathrm{Sc_x}^{-0.6}, \mathrm{Sc_x} = \frac{\nu}{D_\mathrm{x}} \tag{111}$$

where S_x is the mass transfer rate coefficient of element x = N, P, τ is the shear stress on the bottom, ρ is the density of water and $\mathrm{Sc_x}$ is the Schmidt number. The Schmidt number is the ratio of the diffusivity of momentum, ν, and mass, D_x, and varies with temperature, salinity and nutrient species. The rate constant S can be thought of as the height of water cleared of mass per unit of time by the water-macroalgae exchange.

Variable	Symbol	Units
Downwelling irradiance	E_d	W m^{-2}
Macroalgae biomass	MA	g N m^{-2}
Water column detritus, C:N:P = 550:30:1	D_{Atk}	g N m^{-3}
Effective projected area of macroalgae	A_{eff}	m^2 m^{-2}
Leaf absorbance	$A_{L,\lambda}$	-
Bottom stress	τ	N m^{-2}
Wavelength	λ	nm
Bottom water layer thickness	h_{wc}	m

Table 19: State and derived variables for the macroalgae model. For simplicity in the equations all dissolved constituents are given in grams, although elsewhere they are shown in milligrams.

5.2.2 Light capture

The calculation of light capture by macroalgae involves estimating the fraction of light that is incident upon the leaves, and the fraction that is absorbed. The rate of photon capture is given by:

$$k_I = \frac{(10^9 hc)^{-1}}{A_V} \int E_{d,\lambda} \left(1 - \exp\left(-A_{L,\lambda} \Omega_{MA} MA\right)\right) \lambda d\lambda \tag{112}$$

where h, c and A_V are fundamental constants, 10^9 nm m^{-1} accounts for the typical representation of wavelength, λ in nm, and $A_{L,\lambda}$ is the spectrally-resolved absorbance of the leaf. As shown in Eq. 107, the term $1 - \exp\left(-\Omega_{MA} MA\right)$ gives the effective projected area fraction of the community. In the case of light absorption of macroalgae, the exponent is multiplied by the leaf absorbance, $A_{L,\lambda}$, to account for the transparency of the leaves. At low macroalgae biomass, absorption at wavelength λ is equal to $E_{d,\lambda} A_{L,\lambda} \Omega_{MA} MA$, increasing linearly with biomass as all leaves at low biomass are exposed to full light (i.e. there is no self-shading). At high biomass, the absorption by the community asymptotes to $E_{d,\lambda}$, at which point increasing biomass does not increase the absorption as all light is already absorbed.

For more details on the calculation of Ω_{MA} see the Sec. 5.3.2.

5.2.3 Growth

The growth rate combines nutrient, light and maximum organic matter synthesis rates following:

$$\mu_{MA} = \min\left[\mu_{MA}^{max}, \frac{30}{5500} 14 \frac{k_I}{MA}, \frac{S_N A_{eff} N}{MA}, \frac{30}{1}\frac{14}{31}\frac{S_P A_{eff} P}{MA}\right] \tag{113}$$

and the production of macroalgae is given by $\mu_{MA}MA$. Note, as per seagrass, that the maximum growth rates sits within the minimum operator. This allows the growth of macroalgae to the independent of temperature at low light, but still have an exponential dependence at maximum growth rates (Baird et al., 2003).

$$\frac{\partial N}{\partial t} = -\mu_{MA}MA/h_{wc} \tag{114}$$

$$\frac{\partial P}{\partial t} = -\frac{1}{30}\frac{31}{14}\mu_{MA}MA/h_{wc} \tag{115}$$

$$\frac{\partial DIC}{\partial t} = -\frac{550}{30}\frac{12}{14}\mu_{MA}MA/h_{wc} \tag{116}$$

$$\frac{\partial [\mathrm{O_2}]}{\partial t} = \frac{716}{30}\frac{32}{14}\left(\mu_{MA}MA\right)/h_{wc} \tag{117}$$

$$\frac{\partial MA}{\partial t} = \mu_{MA}MA - \zeta_{MA}MA \tag{118}$$

$$\frac{\partial D_{Atk}}{\partial t} = \zeta_{MA}MA/h_{wc} \tag{119}$$

$$\mu_{MA} = \min\left[\mu_{MA}^{max}, \frac{30}{5500}14\frac{k_I}{MA}, \frac{S_N A_{eff} N}{MA}, \frac{30}{1}\frac{14}{31}\frac{S_P A_{eff} P}{MA}\right] \tag{120}$$

$$S_{\mathrm{x}} = 2850\left(\frac{2\tau}{\rho}\right)^{0.38}\mathrm{Sc}^{-0.6}, Sc = \frac{\nu}{D_{\mathrm{x}}} \tag{121}$$

$$k_I = \frac{(10^9 hc)^{-1}}{A_V}\int E_{d,\lambda}\left(1 - \exp\left(-A_{L,\lambda}\Omega_{MA}MA\right)\right)\lambda d\lambda \tag{122}$$

$$A_{eff} = 1 - \exp(-\Omega_{MA}\ MA) \tag{123}$$

$$550\mathrm{CO_2} + 30\mathrm{NO_3^-} + \mathrm{PO_4^{3-}} + 792\mathrm{H_2O} \xrightarrow{5500\ \text{photons}} (\mathrm{CH_2O})_{550}(\mathrm{NH_3})_{30}\mathrm{H_3PO_4} + 716\mathrm{O_2} + 391\mathrm{H^+} \tag{124}$$

Table 20: Equations for the macroalgae model. Other constants and parameters are defined in Table 21. 14 g N mol N^{-1}; 12 g C mol C^{-1}; 31 g P mol P^{-1}; 32 g O mol $\mathrm{O_2^{-1}}$. Uptake shown here is for nitrate, see Sec. 7.1 for ammonia uptake.

	Symbol	Value	Units
Parameters			
Maximum growth rate of macroalgae	μ_{MA}^{max}	1.0	d^{-1}
Nitrogen-specific area of macroalgae	Ω_{MA}	1.0	$(g\ N\ m^{-2})^{-1}$
[a]Leaf absorbance	$A_{L,\lambda}$	~ 0.7	-
Mortality rate	ζ_{MA_A}	0.01	d^{-1}

Table 21: Constants and parameter values used to model macroalgae. [a]Spectrally-resolved values

5.2.4 Mortality

Mortality is defined as a simple linear function of biomass:

$$\frac{\partial MA}{\partial t} = -\zeta_{MA} MA \tag{125}$$

A quadratic formulation is not necessary as both the nutrient and light capture rates become independent of biomass as $MA \gg 1/\Omega_{MA}$. Thus the steady-state biomass of macroalgae under nutrient limitation is given by:

$$(MA)_{SS} = \frac{S_N A_{eff} N}{\zeta} \tag{126}$$

and for light-limited growth by:

$$(MA)_{SS} = \frac{k_I}{\zeta} \tag{127}$$

The full macroalgae equations, parameters and symbols are listed in Tables 19, 20 and 21.

5.3 Seagrass

Seagrasses are quantified per m^2 with a constant stoichiometry (C:N:P = 550:30:1) for both above-ground, SG_A, and below-ground, SG_B, biomass, and can translocate organic matter at this constant stoichiometry between the two stores of biomass. Growth occurs only in the above-ground biomass, but losses (grazing, decay etc.) occur in both. Multiple seagrass varieties are represented. The varieties are modelled using the same equations for growth, respiration and mortality, but with different parameter values.

Variable	Symbol	Units
Downwelling irradiance	E_d	W m^{-2}
Porewater DIN concentration	N_s	g N m^{-3}
Porewater DIP concentration	P_s	g P m^{-3}
Water column DIC concentration	DIC	g C m^{-3}
Water column oxygen concentration	$[O_2]$	g O m^{-3}
Above-ground seagrass biomass	SG_A	g N m^{-2}
Below-ground seagrass biomass	SG_B	g N m^{-2}
Detritus at 550:30:1 in sediment	$D_{Atk,sed}$	g N m^{-3}
Effective projected area of seagrass	A_{eff}	m^2 m^{-2}
Bottom stress	τ	N m^{-2}
Thickness of sediment layer l	$h_{s,l}$	m
Bottom water layer thickness	h_{wc}	m
Wavelength	λ	nm
Translocation rate	Υ	g N m^{-2} s^{-1}
Porosity	ϕ	-

Table 22: State and derived variables for the seagrass model. For simplicity in the equations all dissolved constituents are given in grams, although elsewhere they are shown in milligrams. The bottom water column thickness varies is spatially-variable, depending on bathymetry.

$$\frac{\partial N_w}{\partial t} = -\left(\mu_{SG} - \frac{\mu_{SG}^{max}\overline{N_s}}{K_{SG,N} + \overline{N_s}}\right)/h_{wc} \quad (128)$$

$$\frac{\partial P_w}{\partial t} = -\left(\frac{1}{30}\frac{31}{14}\mu_{SG} - \frac{\mu_{SG}^{max}\overline{P_s}}{K_{SG,P} + \overline{P_s}}\right)/h_{wc} \quad (129)$$

$$\frac{\partial N_{s,l}}{\partial t} = -f_{N,l}/\left(h_{s,l}\phi_l\right) \quad (130)$$

$$\frac{\partial P_{s,l}}{\partial t} = -\frac{1}{30}\frac{31}{14}f_{P,l}/\left(h_{s,l}\phi_l\right) \quad (131)$$

$$\frac{\partial DIC}{\partial t} = -\frac{550}{30}\frac{12}{14}\left(\mu_{SG_A}SG_A\right)/h_{wc} \quad (132)$$

$$\frac{\partial [O_2]}{\partial t} = \frac{716}{30}\frac{32}{14}\left(\mu_{SG_A}SG_A\right)/h_{wc} \quad (133)$$

$$\frac{\partial SG_A}{\partial t} = \mu_{SG_A}SG_A - \left(\zeta_{SG_A} + \zeta_{SG,\tau}\right)\left(SG_A - \frac{f_{seed}}{\Omega_{SG}}\left(1 - f_{below}\right)\right) - \Upsilon \quad (134)$$

$$\frac{\partial SG_B}{\partial t} = -\left(\zeta_{SG_B} + \zeta_{SG,\tau}\right)\left(SG_B - \frac{f_{seed}}{\Omega_{SG}}f_{below}\right) + \Upsilon \quad (135)$$

$$\frac{\partial D_{Atk,sed}}{\partial t} = \left(\left(\zeta_{SG_A} + \zeta_{SG,\tau}\right)\left(SG_A - \frac{f_{seed}}{\Omega_{SG}}\left(1 - f_{below}\right)\right)\right)/\left(h_{sed}\phi\right) + \left(\left(\zeta_{SG_B} + \zeta_{SG,\tau}\right)\left(SG_B - \frac{f_{seed}}{\Omega_{SG}}f_{below}\right)\right)/\left(h_{sed}\phi\right) \quad (136)$$

$$\mu_{SG_A} = \min\left[\frac{\mu_{SG}^{max}\overline{N_s}}{K_{SG,N} + \overline{N_s}} + S_N A_{eff} N, \frac{\mu_{SG}^{max}\overline{P_s}}{K_{SG,P} + \overline{P_s}} + S_P A_{eff} P, \frac{30}{5500}14\frac{\max(0, k_I - k_{resp})}{SG_A}\right] \quad (137)$$

$$\overline{N_s} = \frac{\sum_{l=1}^{L} N_{s,l}h_{s,l}\phi_l}{\sum_{l=1}^{L} h_{s,l}\phi_l} \quad (138)$$

$$\overline{P_s} = \frac{\sum_{l=1}^{L} P_{s,l}h_{s,l}\phi_l}{\sum_{l=1}^{L} h_{s,l}\phi_l} \quad (139)$$

$$f_{N,l} = \frac{N_{s,l}h_{s,l}\phi_l}{\sum_{l=1}^{L} N_{s,l}h_{s,l}\phi_l}\mu_{SG}SG_A \quad (140)$$

$$f_{P,l} = \frac{P_{s,l}h_{s,l}\phi_l}{\sum_{l=1}^{L} P_{s,l}h_{s,l}\phi_l}\mu_{SG}SG_A \quad (141)$$

$$k_I = \frac{\left(10^9 hc\right)^{-1}}{A_V}\int E_{d,\lambda}\left(1 - \exp\left(-A_{L,\lambda}\Omega_{SG}SG_A\sin\beta_{blade}\right)\right)\lambda d\lambda \quad (142)$$

$$k_{resp} = 2\left(E_{comp}A_L\Omega_{SG}\sin\beta_{blade} - \frac{5500}{30}\frac{1}{14}\zeta_{SG_A}\right)SG_A \quad (143)$$

$$\Upsilon = \left(f_{below} - \frac{SG_B}{SG_B + SG_A}\right)\left(SG_A + SG_B\right)\tau_{tran} \quad (144)$$

$$550CO_2 + 30NO_3^- + PO_4^{3-} + 792H_2O \xrightarrow{5500\ \text{photons}} (CH_2O)_{550}(NH_3)_{30}H_3PO_4 + 716O_2 + 391H \quad (145)$$

Table 23: Equations for the seagrass model. Other constants and parameters are defined in Table 24.

	Symbol	*Zostera capricorni*	*Halophila ovalis*	*Halophila decipens*	Units
Parameters					
[a]Maximum growth rate of seagrass	μ_{SG}^{max}	0.4	0.4	0.4	d^{-1}
[b]Nitrogen-specific area of seagrass	Ω_{SG}	1.5	1.9	1.9	$(g\ N\ m^{-2})^{-1}$
[c]Leaf absorbance	$A_{L,\lambda}$	~ 0.7	~ 0.7	~ 0.7	-
[d]Fraction biomass below ground	f_{below}	0.75	0.25	0.5	-
[e]Translocation rate	τ_{tran}	0.033	0.033	0.033	d^{-1}
[f]Half-saturation P uptake	$K_{SG,P}$	96	96	96	$mg\ P\ m^{-3}$
[g]Half-saturation N uptake	$K_{SG,N}$	420	420	420	$mg\ N\ m^{-3}$
[h]Compensation scalar PAR irradiance	E_{comp}	4.5	2.0	1.5	$mol\ photon\ m^{-2}\ d^{-1}$
[h]Leaf loss rate	ζ_{SG_A}	0.04	0.08	0.06	d^{-1}
[h]Root loss rate	ζ_{SG_B}	0.004	0.004	0.004	d^{-1}
Seed biomass as a fraction of 63 % cover	f_{seed}	0.01	0.01	0.01	-
[i]Seagrass root depth	z_{root}	0.15	0.08	0.05	m
Sine of nadir canopy bending angle	$\sin\beta_{blade}$	0.5	1.0	1.0	-
Mortality critical shear stress	$\tau_{SG,shear}$	1.0	1.0	1.0	$N\ m^{-2}$
Mortality shear stress time-scale	$\tau_{SG,time}$	0.5	0.5	0.5	d
Max. shear stress loss rate	$\zeta_{SG,\tau}^{\max}$	2	2	2	d^{-1}

Table 24: Constants and parameter values used to model seagrass. [a] $\times 2$ for nighttime $\times 2$ for roots; [b] Zostera - calculated from leaf characteristics in (Kemp et al., 1987; Hansen et al., 2000), *Halophia ovalis* - calculated from leaf dimensions in Vermaat et al. (1995) - Ω_{SG} can also be determined from specific leaf area such as determined in Cambridge and Lambers (1998) for 9 Australian seagrass species; [c] Spectrally-resolved values in Fig. 11; [d] Duarte and Chiscano (1999); [e] loosely based on Kaldy et al. (2013); [f] *Thalassia testudinum* Gras et al. (2003); [g] *Thalassia testudinum* (Lee and Dunton, 1999); [h] Chartrand et al. (2012); Longstaff (2003); Chartrand et al. (2017); [i] Roberts (1993).

5.3.1 Nutrient uptake

Nutrient uptake can occur through the roots, or the leaves. The model considers nutrient uptake from the roots first. If the rate of uptake of each constituent (N and P) from the roots does not saturate growth, then uptake from the leaves can supplement the growth up to the maximum growth rate. Considering uptake by the roots first.

Depth-resolved sediment nutrient uptake. Dissolved inorganic nutrients are taken up by the root system following a Michaelis-Menton form:

$$k_N = \frac{\mu_{SG}^{\max} N_s}{K_{SG,N} + N_s} \tag{146}$$

where $\mu_{SG}^{\max}$ is the maximum growth rate of the above-ground seagrass biomass, N_s is the concentration of dissolved inorganic nitrogen in the sediment pore waters of porosity ϕ, and $K_{SG,N}$ is the concentration at which nutrient uptake is half the maximum.

Nutrients are taken from the sediment porewaters to a depth of z_{root}. The nutrient concentration used in Eq. 146 is weighted by the volume of porewater in each of L layers:

$$\overline{N_s} = \frac{\sum_{l=1}^{L} N_{s,l} h_{s,l} \phi_l}{\sum_{l=1}^{L} h_{s,l} \phi_l} \tag{147}$$

where $h_{s,l}$ and ϕ_l are the thickness and porosity of sediment layer l.

As a further caveat, ammonia is preferentially absorbed relative to nitrate (see Sec. 7.1).

The nutrient taken up from each layer, as a fraction of the total growth rate, $\mu_{SG} SG_A$, also matches this weighting. Thus the nutrient uptake from layer l is given by:

$$f_{N,l} = \frac{N_{s,l} h_{s,l} \phi_l}{\sum_{l=1}^{L} N_{s,l} h_{s,l} \phi_l} \mu_{SG} SG_A \tag{148}$$

Leaf nutrient uptake. Like macroalgae leaf nutrient uptake, seagrass leaf uptake is a function of nutrient concentration, water motion (Hurd, 2000) and internal physiology. The maximum flux of nutrients is:

$$S_{\mathrm{x}} = 2850 \left(\frac{2\tau}{\rho}\right)^{0.38} \mathrm{Sc_x}^{-0.6}, \mathrm{Sc_x} = \frac{\nu}{D_{\mathrm{x}}} \tag{149}$$

where S_{x} is the mass transfer rate coefficient of element x = N, P, τ is the shear stress on the bottom, ρ is the density of water and $\mathrm{Sc_x}$ is the Schmidt number. The Schmidt number is the ratio of the diffusivity of momentum, ν, and mass, D_{x}, and varies with temperature, salinity and nutrient species. As a further caveat, ammonia is preferentially absorbed relative to nitrate (see Sec. 7.1), although nitrate in the sediments is preferred over ammonia in the water column.

5.3.2 Light capture

The spectrally-resolved leaf absorbance, $A_{L,\lambda}$, of two common Australian seagrass species, *Zostera capriconia* and *Halophila ovalis*, are given in Fig. 11. It is assumed that when co-existing *Zostera* shades *Halophila*.

Following Eq. 108, the light below successive seagrass canopies is given by:

$$E_{below,\lambda} = E_{d,above,\lambda} e^{-A_\lambda \Omega_{SG} SG_A \sin \beta_{blade}} \tag{150}$$

where $E_{d,above,\lambda}$ is the downwelling light above the canopy, $E_{d,below,\lambda}$, is the downwelling irradiance below the canopy, A_λ is the absorbance of the leaf, Ω_{SG} is the nitrogen-specific leaf area, SG is the leaf nitrogen biomass, and $\sin \beta_{blade}$ is the sine of the nadir bending angle of the leaf. This formulation captures the phenomena that seagrass biomass cannot be infinitely spread on the bottom, but must be in leaves that shade a fraction of the bottom, while the remaining light passes through the canopy without attenuation. For more information see the epibenthic light model (Sec. 6.2.2).

The rate of photon capture by seagrass is given by:

$$k_I = \frac{(10^9 hc)^{-1}}{A_V} \int E_{d,\lambda} \left(1 - \exp\left(-A_{L,\lambda} \Omega_{SG} SG_A \sin \beta_{blade}\right)\right) \lambda d\lambda \tag{151}$$

where h, c and A_V are fundamental constants, 10^9 nm m^{-1} accounts for the typical representation of wavelength, λ, in nm, and $A_{L,\lambda}$ is the spectrally-resolved absorbance of the seagrass leaf. As shown in Eq. 107, the term $1 - \exp(-\Omega_{SG} SG_A)$ gives the effective projected area fraction of the community. In the case of light absorption of seagrass, the exponent includes leaf absorbance, $A_{L,\lambda}$, to account for the transparency of the leaves, and $\sin \beta_{blade}$ to account for the orientation of the leaf. At low seagrass biomass, absorption at wavelength λ is equal to the $E_{d,\lambda} A_{L,\lambda} \Omega_{SG} SG_A \sin \beta_{blade}$, increasing linearly with biomass at low biomass as all leaves are exposed to full light (i.e. there is no self-shading). As biomass increases, the absorption by the community asymptotes to $E_{d,\lambda}$, at which point increasing biomass does not increase the absorption as all light is already absorbed. These end points arise for the same reasons as given in Eq. 107 for A_{eff}.

For *H. ovalis*, the leaf weighs 0.0035 g and has dimensions 15.4 mm × 8.5 mm, thus $\Omega_{SG,Halophila} = 1.9$ (g N m^{-2})$^{-1}$. Observations from Cairns Harbour suggest seagrass meadows of *Z. capriconia* can reach a leaf area of approximately 6 times their surface area (McKenzie, 1994). This corresponds to a biomass of 6 / Ω = 4 g N m^{-2}, or 200 g DW m^{-2}.

5.3.3 Respiration

The seagrass model does not consider internal reserves of carbon and nutrients, and therefore cannot respire using carbon from reserves like in the model representation of microalgae. Furthermore,

growth is represented as net production, not gross production. Given growth timescales of many days, this is a reasonable approximation for the purposes of estimating seagrass biomass, and the daily fluxes of metabolites.

Nonetheless, the cost due to respiration needs to be taken into account. Observations from Port Curtis (Petrou et al., 2013) suggest that *Zostera* is unable to survive at less than 4.5 mol photon m^{-2} d^{-1} (Petrou et al., 2013). Presuming this is for a leaf without self-shading (i.e. absorption given by $A_L \Omega_{SG} SG_A$), the loss rate of photons through respiration as a turnover time becomes:

$$k_{resp} = 2 \left(E_{comp} A_L \Omega_{SG} \sin \beta_{blade} - \frac{5500}{30} \frac{1}{14} \zeta_{SG_A} \right) SG_A \tag{152}$$

where E_{comp} is the PAR-weighted by photons compensation scalar irradiance at which respiration equals gross production. Since the observed compensation irradiance will include other loss terms, the respiration turnover rate is calculated from the compensation irradiance minus the mortality rate. The factor of two accounts for mortality occurring throughout a 24 period, but photosynthesis only during the light.

The respiration rate, k_{resp}, is subtracted from the rate of absorption, k_I, to give the growth rate at a particular light intensity. If k_{resp} exceeds k_I, then no growth occurs (Table 23).

5.3.4 Seagrass net production

Gross production, the combination of C, N and P elements at 550:30:1 to form seagrass biomass, only occurs in the leaves, using 5500 photons. Net growth is the gross growth minus respiratory losses. As mentioned above, the realised net growth rate of the above-ground biomass, μ_{SG_A}, is represented using a law of the minimum formulation limited by either by nitrogen, phosphorus, light availability or the maximum growth rate:

$$\mu_{SG_A} = \min \left[\mu_{SG}^{max}, \frac{\mu_{SG}^{max} \overline{N_s}}{K_{SG,N} + \overline{N_s}} + S_N A_{eff} N, \frac{\mu_{SG}^{max} \overline{P_s}}{K_{SG,P} + \overline{P_s}} + S_P A_{eff} P, \frac{30}{5500} 14 \frac{\max(0, k_I - k_{resp})}{SG_A} \right] \tag{153}$$

where μ_{SG}^{max} is the maximum growth rate of seagrass leaves. In the model, seagrass production occurs only in the day. Thus, μ_{SG}^{max} is equal to approximately twice that obtained from measurements of leaf growth over a 24-hour cycle, to account for zero growth at night in the model. Further, if the measurements of realised growth are obtained considering the change in biomass of both leaves and roots, then μ_{SG}^{max} must be multiplied by a further quantity, approximately 2 for a plant with a below-ground biomass to total biomass ratio, f_{below}, of 0.5, such that the net growth within the leaves can account for the biomass change in both the leaves and roots. Thus $\mu_{SG}^{max} = 0.4$ d^{-1}, as used for both *Zostera* and *Halophila* represents the maximum turnover of the whole plant over 24 hours of 0.1 d^{-1} (Table 24).

5.3.5 Translocation between above- and below-ground biomass

Translocation is modelled as a rate, Υ, with a time constant, τ_{tran}, at which the above and below ground biomasses approach a steady state, specified by a fraction of below ground biomass, f_{below}.

$$\Upsilon = \left(f_{below} - \frac{SG_B}{SG_B + SG_A} \right) (SG_A + SG_B)\, \tau_{tran} \tag{154}$$

5.3.6 Mortality

Seagrass are exposed to a linear, quadratic and shear-stress dependent mortality rate. The shear-stress dependent mortality rate is equal for both leaves and roots and is given by:

$$\zeta_{SG,\tau} = \min \left[\zeta^{\max}_{SG,\tau}, \max \left[\frac{\tau - \tau_{SG,shear}}{\tau_{SG,shear}} \frac{1}{\tau_{SG,time}}, 0 \right] \right] \tag{155}$$

where $\tau_{SG,shear}$ is the critical shear stress above which mortality occurs ($\sim$ 1 N m^{-2}), $\tau_{SG,time}$ is the time-scale over which shear stress occurs ($\sim$ 0.5 d), and $\zeta^{\max}_{SG,\tau}$ is the maximum shear stress dependent loss rate (2 d^{-1}).

A linear mortality rate is defined for above ground biomass, ζ_{SG_A}, transforming above ground seagrass biomass into labile detritus at the Atkinson ratio. Additionally, seeds are represented as a component of the seagrass biomass which is unaffected by mortality. The fraction of the seagrass biomass at $1/\Omega_{SG}$ which is seeds is given byf_{seed}. Thus, the above (and similiarly below ground) mortality is:

$$\frac{\partial SG_A}{\partial t} = -\left(\zeta_{SG_A} + \zeta_{SG,\tau}\right) \left(SG_A - f_{seed}/\Omega_{SG}\,(1 - f_{below})\right) \tag{156}$$

The below ground mortality is:

$$\frac{\partial SG_B}{\partial t} = -\left(\zeta_{SG_B} + \zeta_{SG,\tau}\right) \left(SG_B - (f_{seed}/\Omega_{SG})\, f_{below}\right) \tag{157}$$

The inclusion of the term f_{below} in the above equations allows the mortality of both above and below ground biomass to asymptote to zero at a seed fraction, at which translocation is also zero.

The quadratic mortality term, which only applies to the above-ground biomass, is given by:

$$\frac{\partial SG_A}{\partial t} = -mQ_{SG_A}(SG_A)^2 \tag{158}$$

where mQ_{SG_A} is the quadratic mortality rate coefficient. Eq. 158 does not need to include the consideration of seed fractions because $mQ_{SG_A}(SG_A)^2$ asymptotes to zero at low seagrass biomass.

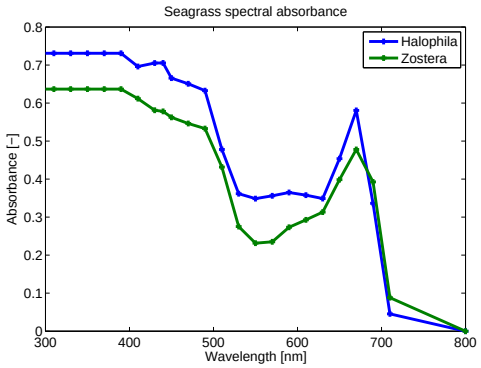

Figure 11: The spectrally-resolved leaf absorbance, $A_{L,\lambda}$, of two common Australian seagrass species (Petrou et al., 2013).

The quadratic loss rate was found to be necessary in slow-growing deep seagrass where light just exceeds respiration losses, other limitations such as nutrients or shear stress loss were unimportant, so over time biomass could accumulate to unrealistic levels. Thus for shallow seagrass, $mQ_{SG_A} = 0$.

5.4 Coral polyps

The coral polyp parameterisation consists of a microalgae growth model to represent zooxanthellae growth based on Baird et al. (2013), and the parameterisation of coral - zooxanthellae interaction based on the host - symbiont model of Gustafsson et al. (2013), a new photoadaptation, photoinhibition and reaction centre dynamics models. The extra detail on the zooxanthellae photosystem is required due to its important role in thermal-stress driven coral bleaching (Yonge, 1930; Suggett et al., 2008).

5.4.1 Coral host, symbiont and the environment

The state variables for the coral polyp model (Table 25) include the biomass of coral tissue, CH (g N m^{-2}), and the structure material of the zooxanthellae cells, CS (mg N m^{-2}). The structure material of the zooxanthellae, CS, in addition to nitrogen, contains carbon and phosphorus at the Redfield ratio. The zooxanthellae cells also contain reserves of nitrogen, R_N (mg N m^{-2}), phosphorus, R_P (mg P m^{-2}), and carbon, R_C (mg C m^{-2}).

The zooxanthellae light absorption capability is resolved by considering the time-varying concentrations of pigments chlorophyll a, Chl, diadinoxanthin, X_p, and diatoxanthin X_h, for which the state variable represents the areal concentration. A further three pigments, chlorophyll c_2, peridinin, and β-carotene are considered in the absorption calculations, but their concentrations are in fixed ratios to chlorophyll a. Exchanges between the coral community and the overlying water can alter the water column concentrations of dissolved inorganic carbon, DIC, nitrogen, N, and phosphorus, P, as well as particulate phytoplankton, B, zooplankton, Z, and detritus, D, where multiple nitrogen, plankton and detritus types are resolved (Table 25).

The coral host is able to assimilate particulate organic nitrogen either through translocation from the zooxanthellae cells or through the capture of water column organic detritus and/or plankton (Fig. 12). The zooxanthellae varies its intracellular pigment content depending on potential light limitation of growth, and the incremental benefit of adding pigment, allowing for the package effect (Baird et al., 2013). The coral tissue is assumed to have a Redfield C:N:P stoichiometry (Redfield et al., 1963), as shown by Muller-Parker et al. (1994). The zooxanthellae are modelled with variable C:N:P ratios (Muller-Parker et al., 1994), based on a structure material at the Redfield ratio, but with variable internal reserves. The fluxes of C, N and P with the overlying water column (nutrient uptake and detritial / mucus release) can therefore vary from the Redfield ratio.

An explanation of the individual processes follows, with tables in the Appendix listing all the model state variables (Table 25), derived variables (Table 26), equations (Tables 27, 28, 29 and 30), and parameters values (Tables 31 and 32).

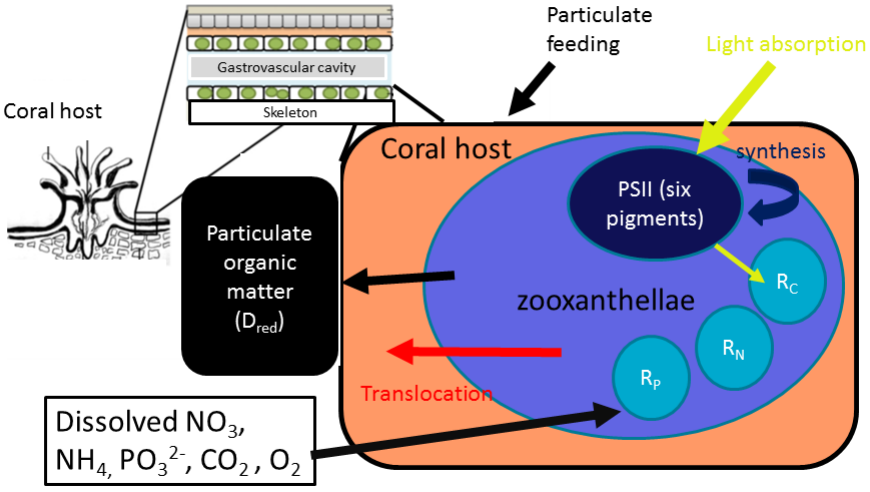

Figure 12: Schematic showing the coral-symbiont relationship and its interaction with the overlying water column.

Effective projected area fraction of corals. A key component of the coral-symbiont model is to relate the biomass of the polyp to coral cover (the fraction of the bottom covered when viewed from above), which follows the relationship for other benthic communities (Eq. 107) such that $A_{eff} = 1 - \exp(-\Omega_{CH} CH)$ where A_{eff} is the effective projected area fraction of the coral community ($\mathrm{m}^2\ \mathrm{m}^{-2}$), CH is the biomass of the coral host, and Ω_{CH} is the nitrogen-specific polyp area coefficient ($\mathrm{m}^2\ \mathrm{g\ N}^{-1}$).

In the coarser configurations, coral communities are restricted to a size that is often much less than the model grid size, due to their existence on the rims of reefs (Baird et al., 2004b). To consider this sub-grid scale patchiness, Eq. 107 is slightly modified resulting in the effective projected area for corals calculated by:

$$A_{eff} = A_{CH}\,(1 - \exp(-\Omega_{CH}\ CH/A_{CH})) \tag{159}$$

The area coefficient, A_{CH}, represents the fraction of a grid cell that the corals can occupy. In the case of 200 m grids, this will be up to 1, representing dense corals on the whole cell. For coarser grids, A_{CH} is reduced to represent that the cell contains both dense coral communities on the forereef / reef crest and also sparse coral communities on the reef flat / lagoon areas. In the 1 km grid, A_{CH} represents the fraction of the area of dense corals to total reef area, and is of order 0.36. The geometrically-derived equation for A_{CH} is given by (Fig. 13):

$$A_{CH} = 1 - \frac{(R-x)^2}{R^2}, \quad R = \sqrt{h_1 h_2/\pi}, \quad R > x \tag{160}$$

where x is the width of dense coral communities on the reef, and R is the equivalent circular radius

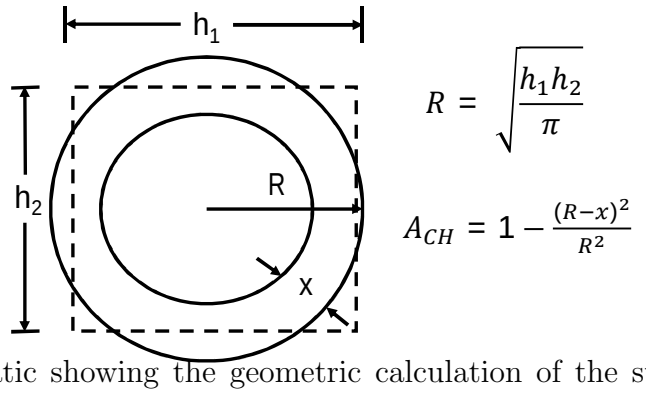

Figure 13: Schematic showing the geometric calculation of the sub-grid parameterisation of the effective projected area fraction of corals, A_{CH}. Nominal width of dense coral communities, $x = 200$ m, grid cell dimensions h_1 and h_2 are 1000 m for the 1 km grid, and R is the equivalent circular radius of the grid cell.

of the grid cell.

The impact of concentrating corals into one portion of a grid cell, as quantified by A_{CH}, only affects the calculations when the concentrated area begins self-shading. Thus, in Eq. 159, when $\Omega_{CH}\, CH/A_{CH}$ is small, $A_{eff} \sim (1 - \exp(-\Omega_{CH} CH))$. But if $\Omega_{CH}\, CH/A_{CH} \to 1$ and $A_{CH} < 1$ the coral biomass saturates due to space limitation at a lower biomass than it would for $A_{CH} = 1$.

The model contains macroalgae that grow above the corals at the seabed. For the case of macroalgae over-growing corals, the effective projected area occupied by corals is further reduced by the presence of macroalgal leaves:

$$A_{eff} = A_{CH} \exp(-\Omega_{MA}\ MA)\,(1 - \exp(-\Omega_{CH}\ CH/A_{CH})) \tag{161}$$

where MA is the biomass of macroalgae, and Ω_{MA} is the nitrogen-specific leaf area coefficient (m^2 g N^{-1}). We assume that the fraction of the bottom covered by the macroalgae, $\exp(-\Omega_{MA}\ MA)$, is evenly spread across the surface. Thus the portion covered by corals is also reduced by the same factor, resulting in the multiplication of the $\exp(-\Omega_{MA}\ MA)$ and $A_{CH}\,(1 - \exp(-\Omega_{CH}\ CH/A_{CH}))$ in Eq. 161.

Growth rate of zooxanthellae. The zooxanthellae growth from reserves is identical to microalgae growth described in Sec. 4.3.1, although the light and nutrient uptake processes are different.

Uptake of nutrients and particulate matter from the overlying water. The maximum flux of nutrients and prey to the surface of the coral is specified as a mass transfer limit per projected area of coral (Atkinson and Bilger, 1992; Baird et al., 2004b), as given by (Falter et al., 2004; Zhang et al., 2011):

$$S_{\mathrm{x}} = 2850 \left(\frac{2\tau}{\rho}\right)^{0.38} \mathrm{Sc_x}^{-0.6}, \mathrm{Sc_x} = \frac{\nu}{D_{\mathrm{x}}} \tag{162}$$

where S_x is the mass transfer rate coefficient of element x = N, P, τ is the shear stress on the bottom, ρ is the density of water and Sc_x is the Schmidt number. The Schmidt number is the ratio of the diffusivity of momentum, ν, and mass, D_x, and varies with temperature, salinity and nutrient species. The mass transfer rate constant S_x can be thought of as the height of water cleared of nutrient per unit of time by the water-coral exchange.

The capture of organic particles (phytoplankton, zooplankton, labile detritus) is also represented as an areal flux. Ribes and Atkinson (2007) considered whether mass transfer limits apply to particulate matter on reefs, and found for coral rubble communities only a weak velocity dependence, suggesting filter feeders overcame any diffusion limitations (see also Monismith et al. (2010)). Thus, instead of using a velocity-dependent mass transfer rate like was used for dissolved tracers (Eq. 162), capture of organic particles, G, is represented by a constant mass transfer rate coefficient, S_{part}, multiplied by the sum of the concentration of each of organic constituents in the water column. The calculated capture rate is limited to the maximum growth rate of the coral tissue, $\mu_{CH}^{max} CH$ (Table 28).

The maximum fluxes of both nutrients and particulates from the overlying water are multiplied by the effective projected area fraction of the coral (A_{eff}) to account for corals covering only a fraction of the bottom.

Translocation between zooxanthellae and coral host. Translocation here represents the one-way consumption of zooxanthellae organic matter produced through either zooxanthellae growth or mortality.

A fraction, f_{tran}, of zooxanthellae growth is translocated to the coral tissue. This fraction is given by the ratio of the projected area of the zooxanthellae cells to twice the surface area of the coral polyp, $2CH\Omega_{CH}$:

$$f_{tran} = \frac{\pi r_{CS}^2 CS/m_N}{2CH\Omega_{CH}} \tag{163}$$

where r_{CS} is the radius of the zooxanthellae cells. When $f_{tran} < 0.5$, zooxanthellae growth is primarily used for increasing symbiont population, and for $f_{tran} > 0.5$, it is primarily translocated. The initial number of symbiont cells is set so that $(\pi r_{CS}^2 CS/m_N) \,/\, (2CH\Omega_{CH})$ is less than 1. Under this initial condition, as $(\pi r_{CS}^2 CS/m_N) \,/\, (2CH\Omega_{CH})$ approaches 1, all symbiont growth is translocated, so f_{tran} never has a value above 1.

This translocation formulation represents a geometrically-derived space limitation on zooxanthellae, being located within two layers of gastrodermal cells (Gustafsson et al., 2013). The geometric derivation has avoided the need for uncertain and/or poorly-defined mass-specific space limitation coefficients.

Coral polyp net production. Coral host biomass, CH, grows at a maximum rate, $\mu_{CH}^{max} CH$, conditional on the availability of organic matter either taken up from the water column as particulate

organic matter by the host itself (Eq. 162), or through translocation from zooxanthellae. It is assumed that the realised hetertrophic feeding rate of zooxanthellae, G', is independent of the physiology of the coral host, and further, that the fraction of the zooxanthellae growth that is translocated depends only on the unavailability of space for the zooxanthellae population to reside in (see above).

$$G' = \min\left[\min\left[\mu_{CH}^{max} CH - f_{tran}\mu_{CS} CS - \zeta_{CS} CS, 0\right], G\right] \tag{164}$$

Should this rate of translocation, plus the flux of organic matter due to zooxanthellae mortality, exceed the maximum growth rate of coral host biomass, $\mu_{CH}^{max} CH$, then the coral host grows at its maximum rate, and the excess is released into the environment as mucus. Should the translocation rate and the particulate organic matter flux be less than $\mu_{CH}^{max} CH$, then the coral host grows at the sum of the two. Finally, should the sum of the translocation rate and the particulate organic matter flux be greater than $\mu_{CH}^{max} CH$, then the host will use all of the translocated organic matter, and a fraction of captured particulate organic matter, with the fraction being composed of fractions of each particulate components based on the relative concentration of organic matter in each category.

Non-bleaching mortality of coral polyps. There are two mortality terms: the mortality of the entire polyp (ζ_{CH}), affecting both coral and zooxanthellae biomass, and mortality of the zooxanthellae (ζ_{CS}). The polyp mortality term has a quadratic mortality coefficient, ζ_{CH}, that stabilises the biomass of coral tissue to μ_{CH}/ζ_{CH}. For a maximum growth rate of coral, $\mu_{CH}^{max} = 0.05$ d^{-1}, ζ_{CH} has been set to 0.01 (g N m^{-2})$^{-1}$ d^{-1}, so the biomass of coral tissue CH stabilises at 0.05 / 0.01 = 5 g N m^{-2}. As this biomass is per unit area, and includes a correction for corals being only viable on A_{eff} of the area, ζ_{CH} needs to be divided by A_{eff} in the equations.

The model does not consider coral host mortality due to thermal stress directly. The impact of zooxanthellae expulsion on the host is a reduced translocation of organic matter from the symbiont to the host, reducing growth if heterotrophic feeding is growth limiting.

5.4.2 Photoadaptation through pigment synthesis and the xanthophyll cycle

The model considers the photoacclimation or photoadaptation of the zooxanthellae cells through the processes of pigment synthesis and xanthophyll pigment cycling (Fig. 14, left). The model assumes a constant ratio of xanthophyll pigments to chlorophyll a, $\Theta_{chl2xan}$. This ratio is maintained constant through time by assuming xanthophyll synthesis is $\Theta_{chl2xan}$ multiplied by the chlorophyll a synthesis. For simplicity we assume all synthesised xanthophyll is of the photosynthesising form. Similarly, a constant ratio of synthesis of peridinin, chlorophyll c_2 and β-carotene accessory pigments to chlorophyll a ensures these accessory pigments also maintain a constant ratio. The de-coupling of zooxanthellae growth and pigment synthesis results in a variable carbon to chlorophyll ratio through time.

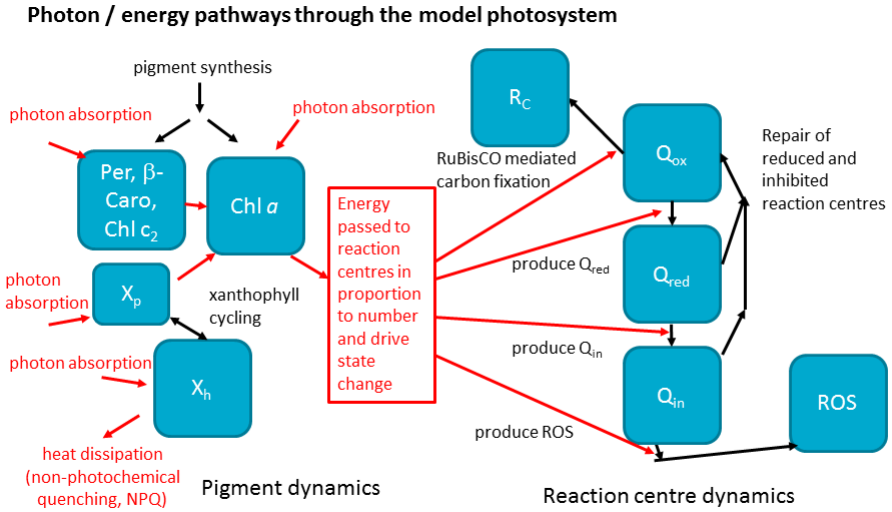

Figure 14: Schematic showing photosynthetic (Chl a, peridinin, β-carotene, Chl c_2, and the photosynthetic xanthophyll diadinoxanthin, X_p) and the photoprotective (xanthophyll diatoxanthin, X_h), xanthophyll cycling and reaction centre dynamics. Red arrows depict fluxes of photons / electrons. Black arrows show transformations of state of either reaction centres or xanthophyll cycle pigments. Note that energy (or photons) are conserved in this flow, significantly reducing the need for empirical rate constants.

The rate of synthesis of pigment is based on the incremental benefit of adding pigment to the rate of photosynthesis. This calculation includes a reduced benefit when carbon reserves are replete, $(1 - R_C^*)$, the reduced benefit due to self-shading, χ, and the fraction of inhibited reaction centres, (Q_{in}/Q_T). The factor χ is calculated for the derivative of the absorption cross-section per unit projected area, α/PA, with non-dimensional group $\rho = \gamma c_i r$. For a sphere of radius r (Baird et al., 2013):

$$\frac{1}{PA}\frac{\partial \alpha}{\partial \rho} = \frac{1 - e^{-2\rho}(2\rho^2 + 2\rho + 1)}{\rho^3} = \chi \tag{165}$$

where χ represents the area-specific incremental rate of change of absorption with ρ. For the multi-spectral calculation used in this paper, we calculate the quantum-weighted mean of χ, $\overline{\chi}$.

The rate of chlorophyll a synthesis is given by:

$$\frac{\partial c_i}{\partial t} = k_{\mathrm{Chl}}^{\max}(1 - R_C^*)\,(1 - Q_{in}/Q_T)\,\overline{\chi} \quad \text{if C : Chl } a > \theta_{min} \tag{166}$$

where $k_{\mathrm{Chl}}^{\max}$ is the maximum rate of synthesis and θ_{min} is the minimum C:Chl ratio. Below θ_{min}, pigment synthesis is zero. Both self-shading, and the rate of photosynthesis itself, are based on

photon absorption rather than energy absorption as experimentally shown in microalgae (Nielsen and Sakshaug, 1993).

Xanthophyll cycle. The symbiont cell contains six pigments, chlorophyll *a*, chlorophyll c_2, peridinin, β-carotene and diadinoxanthin that absorb light and pass the photons on through the photosystem; and diatoxanthin, that absorbs light and dissipates it as heat. Diadinoxanthin and diatoxanthin are almost identical molecules. Diatoxanthin is the de-epoxidised form of diadinoxanthin. The xanthophyll cycle (Falkowski and Raven, 2007) is the reversible switching of diadinoxanthin to diatoxanthin under potentially damaging excess light, and vice-versa under light-limiting conditions. The xanthophyll cycle in the model is represented by two state variables, the areal concentration of diadinoxanthin (X_p) and of diatoxanthin (X_h), and requires one new parameter, τ_{xan}, the time-scale of switching.

The rate at which the xanthophyll pigments switch from diadinoxanthin to diatoxanthin (or vice versa) is assumed to be relatively fast when compared to the synthesis of pigments. The reversible processes is given by:

$$\frac{\partial X_p}{\partial t} = -8\left(Q_{in}/Q_{\mathrm{T}} - 0.5\right)^3 \tau_{xan} \Phi (X_p + X_h) = -\frac{\partial X_h}{\partial t} \tag{167}$$

where the time scale, $1/\tau_{xan}$, is order of 10 minutes (Gustafsson et al., 2014). The direction of switching in Eq. 167 is set by the term $\left(Q_{in}/Q_{\mathrm{T}} - 0.5\right)^3$, such that cells with a large fraction of inhibited reaction centres ($Q_{in}/Q_{\mathrm{T}} > 0.5$) switch from diadinoxanthin (X_p) to diatoxanthin (X_h), and a small fraction of oxidised reaction centres vice versa. The term $8(Q_{in}/Q_{\mathrm{T}} - 0.5)^3$ also increases cubically from zero to 1 (for $Q_{in}/Q_{\mathrm{T}} > 0.5$) or decreases from zero to -1 (for $Q_{in}/Q_{\mathrm{T}} < 0.5$) as the cell becomes more or less inhibited respectively. Using a cubic power that takes a small value in the vicinity of 0.5 prevents fast switching between diadinoxanthin (X_p) and diatoxanthin (X_h) in the region of 0.5. The constant 8 arises from $8 \times 0.5^3 = 1$, where 3 is the cubic power. A odd power is necessary to retain the direction of switching.

The final bracketed term, $(X_p + X_h)$, recognises that the switching is quantified for the population of cells, and so is proportional to the total xanthophyll pigment concentration of the population.

Finally, the rate of conversion slows as one pigment pool is reduced to zero, as determined by a parabolic term Φ (Eq. 168). If $Q_{in}/Q_{\mathrm{T}} < 0.5$ and $X_h > X_p$ (i.e. uninhibited reaction centres with more heat dissipating than light absorbing pigment) or $Q_{in}/Q_{\mathrm{T}} > 0.5$ and $X_p > X_h$ (i.e. inhibited reaction centres with more light absorbing than heat dissipating pigment) then $\Phi = 1$, and the rate of switching is independent of the present mix of heat and light absorbing pigment. Otherwise, a parabolic form for Φ is used to reduce the rate of switching as the process completes:

$$\Phi = 1 - 4\left(\frac{X_p}{X_p + X_h} - 0.5\right)^2 \tag{168}$$

The parabola is at a maximum at $X_p = X_h$, but decreases by the square of the difference between the fraction of diadinoxanthin (X_p) and 0.5. The square ensures that the fractional term does not change the overall sign of the switching, which, as already mentioned, is set by the reaction centre status (i.e. $8\left(Q_{in}/Q_{\mathrm{T}} - 0.5\right)^3$). The value of the parabolic term is zero at $X_p = X_h$. At $X_p >> X_h$, or $X_p << X_h$, the parabolic term is equal to 0.25. The parabolic term is multiplied by 4 so that when switching is complete, $\Phi = 1 - 1 = 0$, thus preventing X_p or X_h either exceeding $X_p + X_h$, or becoming negative. In summary, the full switching term (Eq. 167) results in the relatively quick switching of the xanthophyll pigments between light absorbing and heat dissipating based on the oxidation status of the reaction centres.

The processes of light absorption by diadinoxanthin, chlorophyll *a*, chlorophyll c_2, peridinin and β-carotene is called photochemical quenching (PQ), while light absorbed and dissipated by diatoxanthin (X_h) is called non-photochemical quenching (NPQ). A common measure of PQ is (1-Fv/Fm) (Raven, 1997), where Fv is the difference between maximum fluorescence, Fm, and minimum fluorescence (i.e. variable fluorescence). Fv/Fm is a measurable ratio that represents the maximum potential quantum efficiency of Photosystem II if all capable reaction centres are open, which is equivalent in this model to Q_{ox}/Q_{T}.

Carbon fixation / respiration. Photosynthesis is represented in a similar way to suspended microalage, except a photoinhibition term is introduced. When photons are captured by oxidised reaction centres (photosynthesis) there an increase in the cellular reserves of carbon, R_C, and an accompanying uptake of dissolved inorganic carbon, $\frac{106}{1060} 12 k_I \left(Q_{ox}/Q_{\mathrm{T}}\right) a^*_{Q_{ox}} (1 - R^*_C)$, and release of oxygen per cell, $\frac{106}{1060} 32 k_I \left(Q_{ox}/Q_{\mathrm{T}}\right) a^*_{Q_{ox}} (1 - R^*_C)$, to the water column (Table 27) [$a_{Q_{ox}}$ is the activity of the enzyme facilitating carbon fixation, which is introduced in next section]. While the reserves of nutrients have been defined generically above (a quantity of N, P taken up but not yet combined at the Redfield ratio), the reserves of carbon are a generic photosynthate - they represent the point at which a photon has been absorbed and its energy used to produce fixed carbon and release oxygen. For interest, the photoinhibition term, or the fraction of reduced photosynthesis due to photosystem stress, is $1 - \left(Q_{ox}/Q_{\mathrm{T}}\right) a^*_{Q_{ox}}$.

Basal respiration represents a constant cost of cell maintenance. The loss of internal reserves, $\mu^{\max}_{CS} m_C \phi R^*_C$, results in a gain of water column dissolved inorganic carbon per cell, $\frac{106}{1060}\frac{12}{14}\mu^{\max}_{CS}\phi R^*_C$, as well as a loss in water column dissolved oxygen per cell, $\frac{106}{1060}\frac{32}{14}\mu^{\max}_{CS}\phi R^*_C$ (Table 27). The loss in water column dissolved oxygen per cell represents an instantaneous respiration of the fixed carbon of the reserves. Basal respiration decreases internal reserves, and therefore growth rate, but does not directly lead to cell mortality at zero carbon reserves. Implicit in this scheme is that the basal cost is higher when the cell has more carbon reserves, R^*_C. A linear mortality term, resulting in the loss of structural material and carbon reserves, is considered below.

5.4.3 Photosynthesis, reaction centre dynamics and reactive oxygen production

To model the processes of photoinhibition we include a submodel of reaction centre dynamics that captures the fate of photons absorbed by the cell as a changing oxidation state of the reaction centre of photosystem II (PSII). The model contains state variables for the concentration of oxidised reaction centre, Q_{ox}, reduced reaction centre concentration, Q_{red}, and inhibited reaction centre concentration, Q_{in}, as well as the concentration of reactive oxygen species, [ROS] (Fig. 14). The reaction centre dynamics is based on stoichiometric relationships between reaction centre numbers, photons absorbed and the rate of generation of reactive oxygen species.

To follow the path of a photon as it moves through the reaction centres (Fig. 14), photons are absorbed by either a photosynthetic pigment, or a heat dissipating pigment, in the ratio of the concentration of the two pigment types. If the photon is absorbed by a heat dissipating pigment it is lost. If the photon is absorbed by a photosynthetic pigment, then it will result in a change in either the internal reserves of carbon, the reaction centre state, or the concentration of reactive oxygen species. Like absorption by pigments, the photons interact with the reaction centres as a proportion of the total number of reaction centres. If the photon encounters an oxidised reaction centre, the reserves are deplete and the RuBisCO enzyme active, then the only change will be an increase in carbon reserves (i.e. carbon fixation). If the photon encounters an oxidised reaction centre, but fixation is inhibited, then an oxidised reaction centre becomes reduced. If the photon hits a reduced reaction centre, then a reduced reaction centre becomes inhibited. The final alternative, if the photon interactions with an inhibited reaction centre, then the reaction centre remains inhibited, and a reactive oxygen species is generated, adding to the reactive oxygen pool. The following sections derives rates for these pathways.

Light absorption and photoinhibition. The total rate of photon absorption due to photosynthetic pigments (chlorophyll *a*, chlorophyll c_2, peridinin, β-carotene and diadinoxanthin) across all wavelengths, λ, is given by:

$$k_I = \frac{(10^9 hc)^{-1}}{A_V} \int \alpha_\lambda E_{d,\lambda} \lambda \, d\lambda \tag{169}$$

where h, c and A_V are fundamental constants (Table 31). The absorption-cross section (α) of a spherical cell of radius (r), with a wavelength-dependent pigment-specific absorption coefficient of chlorophyll and accessory pigments (γ_{chl+}) and diadinoxanthin (γ_{dia}), and homogeneous intracellular pigment concentration (c_i and x_p respectively), can be calculated using geometric optics (i.e. ray tracing) without considering internal scattering, and is given by (Duysens, 1956; Kirk, 1975):

$$\alpha = \pi r^2 \left(1 - \frac{2(1 - (1 + 2\left(\gamma_{chl+} c_i + \gamma_{dia} x_p\right) r) e^{-2(\gamma_{chl+} c_i + \gamma_{dia} x_p) r}\right)}{\left(2\left(\gamma_{chl+} c_i + \gamma_{dia} x_p\right) r\right)^2}\right) \tag{170}$$

where πr^2 is the projected area of the spherical zooxanthellae, and the bracketed term is 0 for no absorption ($(\gamma_{chl} c_i + \gamma_{dia} x_p)\, r = 0$) and approaches 1 as the cell becomes fully opaque ($(\gamma_{chl} c_i + \gamma_{dia} x_p)\, r \rightarrow$

∞). The pigment-specific absorption coefficient of chlorophyll and accessory pigments (γ_{chl+}, Fig. 15 black line) is given by:

$$\gamma_{chl+} = \gamma_{chl_a} + \Theta_{chla2chlc}\gamma_{chl_c} + \Theta_{chla2per}\gamma_{per} + \Theta_{chla2caro}\gamma_{car} \tag{171}$$

The component of light absorbed by oxidised reaction centres, and therefore available for carbon fixation, is:

$$k_{I,fix} = k_I \left(\frac{Q_{\text{ox}}}{Q_{\text{T}}}\right) a^*_{Q_{ox}} \left(1 - R^*_C\right) \tag{172}$$

where the oxidised fraction of reaction centres is $(Q_{\text{ox}}/Q_{\text{T}})$ and the fixation rate can be limited by the carbon reserves $(1 - R^*_C)$. If the carbon reserves are full (R^*_C approaches 1) then fixation does not consume photons.

Carbon fixation is also reduced by the temperature inhibition of the active component of the reaction centres. This is the key term in coral bleaching. The mechanism through which this occurs is understood to be the inactivation of the Ribulose-1,5-bisphosphate carboxylase/oxygenase (RuBisCO, Lilley et al. (2010)). Field observations show bleaching occurs relative to the climatological value for each reef site (Liu et al., 2014), suggesting a mechanism for corals to adapt to local conditions. For practical purposes, we propose the following equation for the temperature-dependent inhibition of carbon fixation:

$$a^*_{Q_{ox}} = \left(1 - \exp(-\left(2 - \Delta T\right))\right) / \left(1 - \exp(-2)\right) \tag{173}$$

where ΔT is the temperature anomaly and is calculated as the difference between the model bottom temperature and the spatially and temporally-varying climatological temperature at that depth (Ridgway and Dunn, 2003). The form of Eq. 173 was based on a general line of reasoning that bleaching stress begins at a temperature anomaly of 1°C (the NOAA bleaching index uses 1°C above climatology that would reduce $a^*_{Q_{ox}}$ in Eq. 173 to 0.73), and that for a sustained period (2 summer months) 2°C (equivalent to 16 degree heating weeks) causes maximal stress ($a^*_{Q_{ox}} = 0$). If the climatological temperature is below 26°C, then ΔT is given by the model bottom temperature minus 26°C. The constant 2°C represents the temperature anomaly above which activity of oxidised reaction centres is zero. For $\Delta T < 0$°C, $a^*_{Q_{ox}} = 1$, and all oxidised reaction centres are active, and $\Delta T > 2$°C, $a^*_{Q_{ox}} = 0$, and all oxidised reaction centres are inactive.

The component of total absorption that is absorbed by oxidised reaction centres but not used in fixation and therefore responsible for moving reaction centres from an oxidised to reduced state is the remaining light absorbed at the oxidised centres:

$$k_{I,unfix} = k_I \left(\frac{Q_{\text{ox}}}{Q_{\text{T}}}\right) - k_{I,fix} \tag{174}$$

Photons are absorbed by the reaction centres in each of the three oxidation states in proportion to the fraction in each state, independent of the carbon reserves. Absorption of a photon by an

oxidised state is discussed above. Absorption by a reduced state moves it to an inhibited state. Absorption by an inhibited state does not change the state but produces ROS (see below):

$$\frac{\partial Q_{\text{ox}}}{\partial t} = -k_I n\, m_{\text{RCII}} \frac{Q_{\text{ox}}}{Q_{\text{T}}} \left(1 - a^*_{Q_{ox}} \left(1 - R^*_C\right)\right) \tag{175}$$

$$\frac{\partial Q_{\text{red}}}{\partial t} = k_I n\, m_{\text{RCII}} \frac{Q_{\text{ox}}}{Q_{\text{T}}} \left(1 - a^*_{Q_{ox}} \left(1 - R^*_C\right)\right) - k_I n\, m_{\text{RCII}} \frac{Q_{\text{red}}}{Q_{\text{T}}} \tag{176}$$

$$\frac{\partial Q_{\text{in}}}{\partial t} = k_I n\, m_{\text{RCII}} \frac{Q_{\text{red}}}{Q_{\text{T}}} \tag{177}$$

where k_I is the rate of photon absorption (Eq. 169), n is the number of zooxanthellae cells and m_{RCII} is a stoichiometric coefficient, and is one over the number of photons needed to reduce a whole reaction centre (Table 32).

The reaction centre turn-over time is shorter than the chlorophyll synthesis or carbon fixation terms. To illustrate this point, Suggett et al. (2008) gives the cross-sectional area of an individual reaction centre as 385×10^{-20} m^2. Thus for a photon flux of 250 mol photon m^{-2} d^{-1}, a relatively low light level for midday, the time-interval between individual photon interceptions is $385 \times 10^{-20} / (250/A_V) \times (1/86400) \approx 0.1$ s. As this turnover is much quicker than other processes represented in the photosystem model, it has the potential to slow the model integration. A solution is to divide the terms in Eqs. 176 - 178 by 10^6. This results in reaction centre dynamics varying on an hourly, rather than second, time-scale. The slower response of the reaction centres has only small feedbacks to other terms in the photosystem model, and maintains conservation of reaction centre numbers in the calculation.

Production of reactive oxygen. Photons absorbed by inhibited reaction centres generate reactive oxygen species, [ROS]:

$$\frac{\partial [\text{ROS}]}{\partial t} = 32 \frac{1}{10} k_I n\, m_{\text{RCII}} \left(\frac{Q_{\text{in}}}{Q_{\text{T}}}\right) \tag{178}$$

where the stoichiometric conversions are 32 g O mol O_2^{-1}, $\frac{106}{106}$ mol O mol C^{-1}, $\frac{1}{10}$ mol C mol photon^{-1}. Reactive oxygen species are not considered part of the oxygen mass balance, as it is assumed to be sourced and returned to the mass of water (H_2O).

Repair rate of inhibited reaction centres. The repair rate of inhibited reactions centres is difficult to quantify, and may be a function of temperature (Hill et al., 2011). We took the assumption that the reaction centres would need to be able to repair damaged caused by 10 mol photon m^{-2} d^{-1}. This relatively low daily averaged light intensity represents a threshold below which surface-adapted coral species show an impact due to low light, and might therefore be a reasonable minimum repair rate. As discussed later, this is one of the most uncertain components of the model.

To repair damaged caused by 10 mol photon m^{-2} d^{-1},

$$\frac{\partial Q_{\text{in}}}{\partial t} = -268 \; m_{\text{RCII}} Q_{\text{in}} = -\frac{\partial Q_{\text{ox}}}{\partial t} \tag{179}$$

where m_{RCII} is a stoichiometric coefficient [mol photon (mol reaction centre)$^{-1}$], and the constant 268 arises from the 10 mol photon m^{-2} d^{-1} limit.

Rate of detoxification of reactive oxygen species. Reactive oxygen species are reduced through a temperature-dependent processes (Hill et al., 2011):

$$\frac{\partial [\text{ROS}]}{\partial t} = -f(T) R_N^* R_P^* R_C^* [\text{ROS}] \tag{180}$$

where $f(T)$ is a function of temperature, and here is set at the maximum growth rate of the zooxanthellae cells. This particularly uncertain assumption results in the cells detoxifying at the same rate as they grow. The logic for this term is as simple as a healthier symbiont is one that grows faster, and coincidently, would have more resources for detoxification.

5.4.4 Zooxanthellae expulsion

The rate of expulsion of zooxanthellae cells is function of the reactive oxygen concentration, [ROS]:

$$\frac{\partial CS}{\partial t} = -\min\left[\gamma, \max\left[0, \frac{[\text{ROS}] - [\text{ROS}_{threshold}]}{m_O}\right]\right] CS \tag{181}$$

where γ is the maximum expulsion rate, $m_O = (106/16)(32/14)m_N$ is the stoichiometric coefficient for the oxygen content of the structural component of a cell, and $[\text{ROS}_{threshold}]$ is the limit below which no bleaching occurs. A similar rate of loss is applied to Q_{ox}, Q_{red}, Q_{in}, Chl, X_p, X_h, R_C, R_N, R_P and [ROS]. Expulsion leads to an increase in detritus at the Redfield ratio, D_{Red}, in the bottom water column layer from the zooxanthellae structural material, and an increased in dissolved nutrients (carbon, DIC, nitrogen in the form of ammonia $[NH_4]$, and phosphorus, P) due to the loss of reserves (Table 30).

5.4.5 Coral calcification

The rate of coral calcification is a function of the water column aragonite saturation, Ω_a, and the normalised reserves of fixed carbon in the symbiont, R_C^*. The rates of change of DIC and total alkalinity, A_T, in the bottom water column layer of thickness h_{wc} due to calcification becomes:

$$\frac{\partial DIC}{\partial t} = -12 g A_{eff} / h_{wc} \tag{226}$$

$$\frac{\partial A_T}{\partial t} = -2gA_{eff}/h_{wc} \tag{227}$$

$$g = k_{day}(\Omega_a - 1)(R_C^*)^2 + k_{night}(\Omega_a - 1) \tag{228}$$

where g is the rate of net calcification, k_{day} and k_{night} are defined in Table 31 with habitat-specific values (Anthony et al., 2011; Mongin and Baird, 2014). The fluxes are scaled by the effective projected area of the community, A_{eff}. The power of 2 for R_C^* ensures that generally light replete symbionts provide the host with sufficient energy for calcification.

5.4.6 Dissolution of shelf carbonate sands

In addition to the dissolution of carbonate sands on a growing coral reef, which is captured in the net dissolution quantified above, the marine carbonates on the continental shelf dissolve (Eyre et al., 2018). Like above, the dissolution of marine carbonates is approximated as a source of DIC and alkalinity but does not affect the properties (mass, porosity etc.) of the underlying sediments.

We assume carbonate dissolution from the sediment bed is proportional to the fraction of the total surface sediment is composed of either sand or mud carbonates. Other components, whose fraction do not release DIC and alkalinity, including carbonate gravel and non-carbonate mineralogies. Thus the change in DIC and A_T in the bottom water column layer is given by:

$$\frac{\partial DIC}{\partial t} = -12d_{\mathrm{CaCO_3}}\left(\frac{Mud_{\mathrm{CaCO_3}} + Sand_{\mathrm{CaCO_3}}}{M}\right)/h_{wc} \tag{229}$$

$$\frac{\partial A_T}{\partial t} = -2d_{\mathrm{CaCO_3}}\left(\frac{Mud_{\mathrm{CaCO_3}} + Sand_{\mathrm{CaCO_3}}}{M}\right)/h_{wc} \tag{230}$$

where M is the total mass of surface layer inorganic sediments, $d_{\mathrm{CaCO_3}}$ is the dissolution rate of $CaCO_3$, and is the reverse reaction to calcification and h_{wc} is the thickness of the water column layer. The dissolution rate, $d_{\mathrm{CaCO_3}}$ [mmol m^{-2} d^{-1}] is assumed to be a function of Ω_a (Eyre et al., 2018):

$$d_{\mathrm{CaCO_3}} = -11.51\Omega_a + 33.683 \tag{231}$$

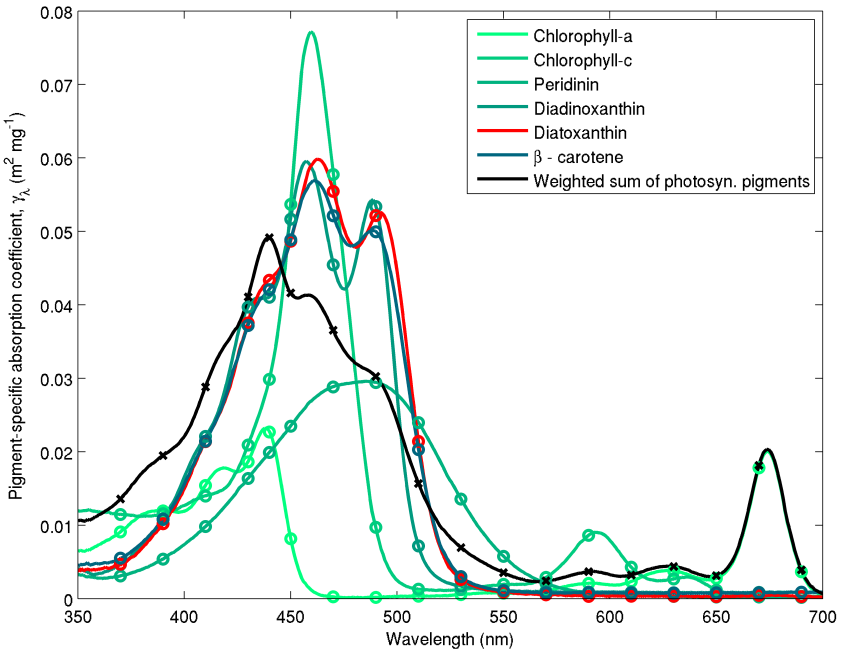

Figure 15: Pigment-specific absorption coefficients for the dominant pigments found in *Symbiodinium* determined using laboratory standards in solvent in a 1 cm vial undertaken. Green lines are photosynthetic pigments, red lines are photoprotective pigments constructed from 563 measured wavelengths. Circles represent the wavelengths at which the optical properties are calculated in the simulations. The black line represents the weighted sum of the photosynthetic pigments (Eq. 171), with the weighting calculated from the ratio of each pigment concentration to chlorophyll *a*. Black crosses represent the chl *a*-specific absorption coefficient of all pigments at the wavelengths used in the simulations. The spectra are wavelength-shifted from their raw measurement by the ratio of the refractive index of the solvent to the refractive index of water (1.352 for acetone used with chlorophyll *a*, chlorophyll c_2 and β-carotene; 1.361 for ethanol used with peridinin, diadinoxanthin and diatoxanthin; 1.330 for water). The integral from 340 to 700 nm of the chl *a*-specific absorption coefficient using the 23 model wavelengths is only 0.72 % greater than using the 563 measured wavelengths. Thus for white light incident on cells with a zero package effect, 23 wavelengths is sufficient to compute the spectrally-resolved absorption. For highly packaged cells, the absorption cross-section is flattened (Kirk, 1994), so the error will be even less than 0.72 %.

Variable	Symbol	Units
Dissolved inorganic nitrogen (DIN)	N	mg N m^{-3}
Dissolved inorganic phosphorus (DIP)	P	mg P m^{-3}
Zooxanthellae biomass	CS	mg N m^{-2}
Reserves of nitrogen	R_N	mg N $cell^{-1}$
Reserves of phosphorus	R_P	mg P $cell^{-1}$
Reserves of carbon	R_C	mg C $cell^{-1}$
Coral biomass	CH	g N m^{-2}
Suspended phytoplankton biomass	B	mg N m^{-3}
Suspended zoooplankton biomass	Z	mg N m^{-3}
Suspended detritus at 106:16:1	D_{Red}	mg N m^{-3}
Macroalgae biomass	MA	mg N m^{-3}
Temperature	T	°C
Absolute salinity	S_A	kg m^{-3}
zooxanthellae chlorophyll *a* concentration	Chl	mg m^{-2}
zooxanthellae diadinoxanthin concentration	X_p	mg m^{-2}
zooxanthellae diatoxanthin concentration	X_h	mg m^{-2}
Oxidised reaction centre concentration	Q_{ox}	mg m^{-2}
Reduced reaction centre concentration	Q_{red}	mg m^{-2}
Inhibited reaction centre concentration	Q_{in}	mg m^{-2}
Reactive oxygen species concentration	[ROS]	mg m^{-2}
Chemical oxygen demand	COD	mg O_2 m^{-3}

Table 25: Model state variables for the coral polyp model. Note that water column variables are 3 dimensional, benthic variables are 2 dimensional, and unnormalised reserves are per cell.

Variable	Symbol	Units
Downwelling irradiance	E_d	W m^{-2}
Maximum reserves of nitrogen	$R_N^{\max}$	mg N cell^{-1}
Maximum reserves of phosphorus	$R_P^{\max}$	mg P cell^{-1}
Maximum reserves of carbon	$R_C^{\max}$	mg C cell^{-1}
Normalised reserves of nitrogen	$R_N^* \equiv R_N/R_N^{\max}$	-
Normalised reserves of phosphorus	$R_P^* \equiv R_P/R_P^{\max}$	-
Normalised reserves of carbon	$R_C^* \equiv R_C/R_C^{\max}$	-
Intracellular chlorophyll a concentration	c_i	mg m^{-3}
Intracellular diadinoxanthin concentration	x_p	mg m^{-3}
Intracellular diatoxanthin concentration	x_h	mg m^{-3}
Total reaction centre concentration	Q_{T}	mg m^{-2}
Total active reaction centre concentration	Q_{a}	mg m^{-2}
Concentration of zooxanthellae cells	n	cell m^{-2}
Thickness of the bottom water column layer	h_{wc}	m
Effective projected area fraction	A_{eff}	m^2 m^{-2}
Area density of zooxanthellae cells	n_{CS}	cell m^{-2}
Absorption cross-section	α	m^2 cell^{-1}
Rate of photon absorption	k_I	mol photon cell^{-1} s^{-1}
Photon-weighted average opaqueness	$\overline{\chi}$	-
Maximum Chl. synthesis rate	$k_{\mathrm{Chl}}^{\max}$	mg Chl m^{-3} d^{-1}
Density of water	ρ	kg m^{-3}
Bottom stress	τ	N m^{-2}
Schmidt number	Sc	-
Mass transfer rate coefficient for particles	S_{part}	m d^{-1}
Heterotrophic feeding rate	G	g N m^{-2} d^{-1}
Wavelength	λ	nm
Translocation fraction	f_{tran}	-
Active fraction of oxidised reaction centres	$a_{Q_{ox}}^*$	-

Table 26: Derived variables for the coral polyp model.

$$\frac{\partial N}{\partial t} = -S_N N(1-R_N^*)A_{eff} \quad (182)$$

$$\frac{\partial P}{\partial t} = -S_P P(1-R_P^*)A_{eff} \quad (183)$$

$$\frac{\partial DIC}{\partial t} = -\left(\frac{106}{1060}12k_I\frac{Q_{\rm ox}}{Q_{\rm T}}a_{Q_{ox}}^*(1-R_C^*) - \frac{106}{16}\frac{12}{14}\mu_{CS}^{\max}\phi R_C^*\right)(CS/m_N) \quad (184)$$

$$\frac{\partial [{\rm O}_2]}{\partial t} = \left(\frac{106}{1060}32k_I\frac{Q_{\rm ox}}{Q_{\rm T}}a_{Q_{ox}}^*(1-R_C^*) - \frac{106}{16}\frac{32}{14}\mu_{CS}^{\max}\phi R_C^*\right)(CS/m_N) \quad (185)$$

$$\frac{\partial R_N}{\partial t} = S_N N(1-R_N^*)/(CS/m_N) - \mu_{CS}^{\max}R_P^*R_N^*R_C^*(m_N+R_N) \quad (186)$$

$$\frac{\partial R_P}{\partial t} = S_P P(1-R_P^*)/(CS/m_N) - \mu_{CS}^{\max}R_P^*R_N^*R_C^*(m_P+R_P) \quad (187)$$

$$\frac{\partial R_C}{\partial t} = k_I\left(\frac{Q_{\rm ox}}{Q_{\rm T}}\right)a_{Q_{ox}}^*(1-R_C^*) - \mu_{CS}^{\max}R_P^*R_N^*R_C^*(m_C+R_C) - \mu_{CS}^{\max}\phi m_C R_C^* \quad (188)$$

$$\frac{\partial CS}{\partial t} = \mu_{CS}^{\max}R_P^*R_N^*R_C^*CS - \zeta_{CS}CS \quad (189)$$

$$\frac{\partial c_i}{\partial t} = (k_{\rm Chl}^{\max}(1-R_C^*)(1-Q_{in}/Q_T)\overline{\chi} - \mu_P^{\max}R_P^*R_N^*R_C^*c_i)(CS/m_N) \quad (190)$$

$$\frac{\partial X_p}{\partial t} = \Theta_{xan2chl}(k_{\rm Chl}^{\max}(1-R_C^*)(1-Q_{in}/Q_T)\overline{\chi}) \quad (191)$$

$$-8(Q_{in}/Q_t - 0.5)^3\tau_{xan}\Phi(X_p+X_h) \quad (192)$$

$$\frac{\partial X_h}{\partial t} = 8(Q_{in}/Q_{\rm T} - 0.5)^3\tau_{xan}\Phi(X_p+X_h) \quad (193)$$

$$\frac{\partial CS}{\partial t} = (1-f_{tran})\mu_{CS}CS - \zeta_{CS}CS + f_{remin}\frac{\zeta_{CH}}{A_{eff}}CH^2 \quad (194)$$

$$k_I = \frac{(10^9 hc)^{-1}}{A_V}\int \alpha_\lambda E_{d,\lambda}\lambda\, d\lambda \quad (195)$$

$${\rm S_x} = 2850\left(\frac{2\tau}{\rho}\right)^{0.38}{\rm Sc_x}^{-0.6}, {\rm Sc_x} = \frac{\nu}{D_{\rm x}} \quad (196)$$

$$\Phi = 1 - 4\left(\frac{X_p}{X_p+X_h} - 0.5\right)^2 \text{ or } \Phi = 1 \quad (197)$$

Table 27: Equations for the interactions of coral host, symbiont and environment excluding bleaching loss terms that appear in Table 30. The term CS/m_N is the concentration of zoothanxellae cells. The equation for organic matter formation gives the stoichiometric constants; 12 g C mol C^{-1}; 32 g O mol O_2^{-1}.

$$
\begin{aligned}
\frac{\partial CH}{\partial t} &= G' - \frac{\zeta_{CH}}{A_{eff}} CH^2 && (198)\\
\frac{\partial B}{\partial t} &= -S_{part} A_{eff} B \frac{G'}{G} / h_{wc} && (199)\\
\frac{\partial Z}{\partial t} &= -S_{part} A_{eff} Z \frac{G'}{G} / h_{wc} && (200)\\
\frac{\partial D_{Red}}{\partial t} &= \left(-S_{part} A_{eff} D_{Red} \frac{G'}{G} + (1 - f_{remin}) \frac{\zeta_{CH}}{A_{eff}} CH^2 \right) / h_{wc} && (201)\\
f_{tran} &= \frac{\pi r_{CS}^2 n_{CS}}{2 CH \Omega_{CH}} && (202)\\
G &= S_{part} A_{eff} \left(B + Z + D_{Red} \right) && (203)\\
G' &= \min \left[\min \left[\mu_{CH}^{max} CH - f_{tran} \mu_{CS} CS - \zeta_{CS} CS, 0 \right], G \right] && (204)\\
A_{eff} &= 1 - \exp(-\Omega_{CH} CH) && (205)
\end{aligned}
$$

Table 28: Equations for the coral polyp model. The term CS/m_N is the concentration of zoothanxellae cells. The equation for organic matter formation gives the stoichiometric constants; 12 g C mol C^{-1}; 32 g O mol O_2^{-1}. Other constants and parameters are defined in Table 32.

$$
\begin{aligned}
\frac{\partial Q_{\text{ox}}}{\partial t} &= -k_I n \, m_{\text{RCII}} \left(\frac{Q_{\text{ox}}}{Q_{\text{T}}} \right) \left(1 - a_{Q_{ox}}^* \left(1 - R_C^* \right) \right) + f_2(T) R_N^* R_P^* R_C^* Q_{\text{in}} && (206)\\
\frac{\partial Q_{\text{red}}}{\partial t} &= k_I n \, m_{\text{RCII}} \left(\frac{Q_{\text{ox}}}{Q_{\text{T}}} \right) \left(1 - a_{Q_{ox}}^* \left(1 - R_C^* \right) \right) - k_I n m_{RCII} \frac{Q_{\text{red}}}{Q_T} && (207)\\
\frac{\partial Q_{\text{in}}}{\partial t} &= -268 \; m_{RCII} Q_{\text{in}} + k_I n m_{RCII} \frac{Q_{\text{red}}}{Q_T} && (208)\\
\frac{\partial [\text{ROS}]}{\partial t} &= -f(T) R_N^* R_P^* R_C^* [\text{ROS}] + 32 \frac{1}{10} k_I n \, m_{\text{RCII}} \left(\frac{Q_{\text{in}}}{Q_{\text{T}}} \right) && (209)
\end{aligned}
$$

Table 29: Equations for symbiont reaction centre dynamics. Bleaching loss terms appear in Table 30.

$$\frac{\partial[\mathrm{NH_4}]}{\partial t} = \min\left[\gamma, \max\left[0, \frac{[\mathrm{ROS}]-[\mathrm{ROS}_{threshold}]}{m_O}\right]\right] CSR^*_N/h_{wc} \quad (210)$$

$$\frac{\partial P}{\partial t} = \frac{1}{16}\frac{31}{14}\min\left[\gamma, \max\left[0, \frac{[\mathrm{ROS}]-[\mathrm{ROS}_{threshold}]}{m_O}\right]\right] CSR^*_P/h_{wc} \quad (211)$$

$$\frac{\partial DIC}{\partial t} = \frac{106}{16}\frac{12}{14}\min\left[\gamma, \max\left[0, \frac{[\mathrm{ROS}]-[\mathrm{ROS}_{threshold}]}{m_O}\right]\right] CSR^*_C/h_{wc} \quad (212)$$

$$\frac{\partial[\mathrm{O_2}]}{\partial t} = -\frac{\partial DIC}{\partial t}\frac{32}{12}\frac{[\mathrm{O_2}]^2}{K^2_{OA}+[\mathrm{O_2}]^2} \quad (213)$$

$$\frac{\partial[\mathrm{COD}]}{\partial t} = \frac{\partial DIC}{\partial t}\frac{32}{12}\left(1-\frac{[\mathrm{O_2}]^2}{K^2_{OA}+[\mathrm{O_2}]^2}\right) \quad (214)$$

$$\frac{\partial CS}{\partial t} = -\min\left[\gamma, \max\left[0, \frac{[\mathrm{ROS}]-[\mathrm{ROS}_{threshold}]}{m_O}\right]\right] CS \quad (215)$$

$$\frac{\partial R_N}{\partial t} = -\min\left[\gamma, \max\left[0, \frac{[\mathrm{ROS}]-[\mathrm{ROS}_{threshold}]}{m_O}\right]\right] R_N \quad (216)$$

$$\frac{\partial R_P}{\partial t} = -\min\left[\gamma, \max\left[0, \frac{[\mathrm{ROS}]-[\mathrm{ROS}_{threshold}]}{m_O}\right]\right] R_P \quad (217)$$

$$\frac{\partial R_C}{\partial t} = -\min\left[\gamma, \max\left[0, \frac{[\mathrm{ROS}]-[\mathrm{ROS}_{threshold}]}{m_O}\right]\right] R_C \quad (218)$$

$$\frac{\partial Chl}{\partial t} = -\min\left[\gamma, \max\left[0, \frac{[\mathrm{ROS}]-[\mathrm{ROS}_{threshold}]}{m_O}\right]\right] Chl \quad (219)$$

$$\frac{\partial X_p}{\partial t} = -\min\left[\gamma, \max\left[0, \frac{[\mathrm{ROS}]-[\mathrm{ROS}_{threshold}]}{m_O}\right]\right] X_p \quad (220)$$

$$\frac{\partial X_h}{\partial t} = -\min\left[\gamma, \max\left[0, \frac{[\mathrm{ROS}]-[\mathrm{ROS}_{threshold}]}{m_O}\right]\right] X_h \quad (221)$$

$$\frac{\partial Q_{\mathrm{ox}}}{\partial t} = -\min\left[\gamma, \max\left[0, \frac{[\mathrm{ROS}]-[\mathrm{ROS}_{threshold}]}{m_O}\right]\right] Q_{\mathrm{ox}} \quad (222)$$

$$\frac{\partial Q_{\mathrm{red}}}{\partial t} = -\min\left[\gamma, \max\left[0, \frac{[\mathrm{ROS}]-[\mathrm{ROS}_{threshold}]}{m_O}\right]\right] Q_{\mathrm{red}} \quad (223)$$

$$\frac{\partial Q_{\mathrm{in}}}{\partial t} = -\min\left[\gamma, \max\left[0, \frac{[\mathrm{ROS}]-[\mathrm{ROS}_{threshold}]}{m_O}\right]\right] Q_{\mathrm{in}} \quad (224)$$

$$\frac{\partial D_{Red}}{\partial t} = \min\left[\gamma, \max\left[0, \frac{[\mathrm{ROS}]-[\mathrm{ROS}_{threshold}]}{m_O}\right]\right] CS/h_{wc} \quad (225)$$

Table 30: Equations describing the expulsion of zooxanthellae, and the resulting release of inorganic and organic molecules into the bottom water column layer.

	Symbol	Value
Constants		
Molecular diffusivity of NO_3	D	$f(T, S_A) \sim 17.5 \times 10^{-10}$ m^2 s^{-1}
Speed of light	c	2.998×10^8 m s^{-1}
Planck constant	h	6.626×10^{-34} J s^{-1}
Avogadro constant	A_V	6.02×10^{23} mol^{-1}
[a]Pigment-specific absorption coefficients	γ_λ	$f(\text{pig}, \lambda)$ m^{-1} (mg m^{-3})$^{-1}$
Kinematic viscosity of water	ν	$f(T, S_A) \sim 1.05 \times 10^{-6}$ m^2 s^{-1}
Parameters		
[b]Nitrogen content of zooxanthellae cells	m_N	5.77×10^{-12} mol N cell^{-1}
[c]Carbon content of zooxanthellae cells	m_C	$(106/16)\ m_N$ mol C cell^{-1}
[d]Maximum intracellular Chl concentration	$c_i^{\max}$	3.15×10^6 mg Chl m^{-3}
Radius of zooxanthellae cells	r_{CS}	5 μm
Maximum growth rate of coral	μ_{CH}^{max}	0.05 d^{-1}
[e]Rate coefficient of particle capture	S_{part}	3.0 m d^{-1}
Maximum growth rate of zooxanthellae	μ_{CS}^{max}	0.4 d^{-1}
Quadratic mortality coefficient of polyps	ζ_{CH}	0.01 d^{-1} (g N m^{-2})$^{-1}$
Linear mortality of zooxanthellae	ζ_{CS}	0.04 d^{-1}
[g]Remineralised fraction of coral mortality	f_{remin}	0.5
Nitrogen-specific host area coefficient of polyps	Ω_{CH}	2.0 m^2 g N^{-1}
Fractional (of μ_{CS}^{max}) respiration rate	ϕ	0.1

Table 31: Constants and parameter values used to model coral polyps. V is zooxanthellae cell volume in μm^3. [a]Fig. 15,[c]Redfield et al. (1963) and Kirk (1994),[d]Finkel (2001),[e]Ribes and Atkinson (2007); Wyatt et al. (2010),[f,g]Gustafsson et al. (2013, 2014).

	Symbol	Value
Constants		
Parameters		
Maximum growth rate of zooxanthellae	μ_{CS}^{max}	1 d^{-1}
Rate coefficient of xanthophyll switching	τ_{xan}	1/600 s^{-1}
[a]Atomic ratio of Chl a to RCII in *Symbiodinium*	A_{RCII}	500 mol Chl mol $RCII^{-1}$
[a]Stoichiometric ratio of RCII units to photons	m_{RCII}	0.1 mol RCII mol $photon^{-1}$
Maximum rate of zooxanthellae expulsion	γ	1 d^{-1}
Oxygen half-saturation for aerobic respiration	K_{OA}	500 mg O m^{-3}
Molar mass of Chl a	M_{Chla}	893.49 g mol^{-1}
[b]Ratio of Chl a to xanthophyll	$\Theta_{chla2xan}$	0.2448 mg Chl mg X^{-1}
[b]Ratio of Chl a to Chl c	$\Theta_{chla2chlc}$	0.1273 mg Chl-a mg Chl-c^{-1}
[b]Ratio of Chl a to peridinin	$\Theta_{chla2per}$	0.4733 mg Chl mg^{-1}
[b]Ratio of Chl a to β-carotene	$\Theta_{chla2caro}$	0.0446 mg Chl mg^{-1}
[c]Lower limit of ROS bleaching	$[\mathrm{ROS}_{threshold}]$	5×10^{-4} mg O $cell^{-1}$

Table 32: Constants and parameter values used in the coral bleaching model. [a]In Suggett et al. (2009). [b] ratio of constant terms in multivariate analysis in Hochberg et al. (2006). [c]Fitted parameter based on the existence of non-bleaching threshold (Suggett et al., 2009), and a comparison of observed bleaching and model output in the ∼1 km model.

Calcification

$$\frac{\partial A_T}{\partial t} = -2gA_{eff}/h_{wc} \quad (232)$$

$$\frac{\partial DIC}{\partial t} = -12gA_{eff}/h_{wc} \quad (233)$$

$$k_{day}(\Omega_a - 1)(R_C^*)^2 + k_{night}(\Omega_a - 1) \quad (234)$$

$$\Omega_a = \frac{[\mathrm{CO_3^{2-}}][\mathrm{Ca^{2+}}]}{K_{sp}} \quad (235)$$

$$\mathrm{Ca^{2+}} + 2\mathrm{HCO_3^-} \longrightarrow \mathrm{CaCO_3} + \mathrm{CO_2} + \mathrm{H_2O} \quad (236)$$

Dissolution

$$\frac{\partial A_T}{\partial t} = 2d_{\mathrm{CaCO_3}} \left(\frac{Mud_{\mathrm{CaCO_3}} + Sand_{\mathrm{CaCO_3}}}{M} \right) / h_{wc} \quad (237)$$

$$\frac{\partial DIC}{\partial t} = 12d_{\mathrm{CaCO_3}} \left(\frac{Mud_{\mathrm{CaCO_3}} + Sand_{\mathrm{CaCO_3}}}{M} \right) / h_{wc} \quad (238)$$

$$d_{\mathrm{CaCO_3}} = -11.51\Omega_a + 33.683 \quad (239)$$

$$\mathrm{CaCO_3} + \mathrm{CO_2} + \mathrm{H_2O} \longrightarrow \mathrm{Ca^{2+}} + 2\mathrm{HCO_3^-} \quad (240)$$

Table 33: Equations for coral polyp calcification and dissolution. The concentration of carbonate ions, $[\mathrm{CO_3^{2-}}]$, is determined from equilibrium carbon chemistry as a function of A_T, DIC, temperature and salinity, and the concentration of calcium ions, $[\mathrm{Ca^{2+}}]$, is a mean oceanic value. 12 g C mol $\mathrm{C^{-1}}$. Other constants and parameters are defined in Table 31.

6 Processes in the sediments

6.1 Brief summary of processes in the sediments

The EMS model contains a multi-layered sediment compartment with time and space-varying vertical layers, and the same horizontal grid as the water column and epibenthic models. All state variables that exist in the water column layers have an equivalent in the sediment layers (and are specified by `<variable name>_sed`). The dissolved tracers are given as a concentration in the porewater, while the particulate tracers are given as a concentration per unit volume (see Sec. 8.5.2).

The sediment model contains inorganic particles of different size (Dust, Mud, Sand and Gravel) and different mineralogies (carbonate and non-carbonate). The critical shear stress for resuspension, and the sinking rates, are generally larger for large particles, while and mineralogy only affects the optical properties. The size-class Dust comes only in a non-carbonate mineralogy, and the Mud-carbonate class contains a category of FineSed-mineral that has the same physical and optical properties as Mud-mineral, except that it is initialised with a zero value and only enters the domain from rivers.

The organic matter classes are discussed in the Sec. 7.3. The inorganic and organic particulate classes are summarised in Table 34.

Name	Nom. size μm	Sinking vel. m d^{-1}	Organic	Origin	Phosphorus adsorption	Colour
Gravel $CaCO_3$	10^4	60,480	N	I	N	W
Gravel non-$CaCO_3$	10^4	60,480	N	I	N	B
Sand $CaCO_3$	10^2	172.8	N	I	N	W
Sand non-$CaCO_3$	10^2	172.8	N	I	N	B
Mud $CaCO_3$	30	17.2	N	I	Y	W
Mud non-$CaCO_3$	30	17.2	N	I	Y	B
FineSed	30	17.2	N	C	Y	B
Dust	1	1	N	C	Y	B
D_{Atk}	-	10	Y	OM	N	B
D_{Red}	-	10	Y	OM	N	B
D_C,D_N,D_P	-	100	Y	OM	N	B

Table 34: Characteristics of the particulate classes. Y - Yes, N - No, I - initial condition, C - catchment, OM - remineralistion from organic matter, B - brown, W - white (Condie et al., 2009; Margvelashvili, 2009).

6.2 Sediment optical model

6.2.1 Light absorption by benthic microalgae

The calculation of light absorption by benthic microalgae assumes they are the only attenuating component in a layer (biofilm) that lies on top layer of sediment, with a perfectly absorbing layer below and no scattering by any other components in the layer. Thus no light penetrates through to the second sediment layer where benthic microalgae also reside. Thus the downwelling irradiance at wavelength λ at the bottom of a layer, $E_{d,\lambda,bot}$, is given by:

$$E_{d,bot,\lambda} = E_{d,top,\lambda} e^{-n\alpha_\lambda h} \tag{241}$$

where $E_{d,top,\lambda}$ is the downwelling irradiance at wavelength λ at the top of the layer and α_λ is the absorption cross-section of the cell at wavelength λ, and n is the concentration of cells in the layer. The layer thickness used here, h, is the thickness of the top sediment layer, so as to convert the concentration of cells in that layer, n, into the areal concentration of cells in the biofilm, nh.

Given no scattering in the cell, and that the vertical attenuation coefficient is independent of azimuth angle, the scalar irradiance that the benthic microalgae are exposed to in the surface biofilm is given by:

$$E_{o,\lambda} = \left(E_{d,top,\lambda} - E_{d,bot,\lambda}\right) / \left(n\alpha_\lambda h\right) \tag{242}$$

The photons captured by each cell, and the microalgae process, follow the same equations as for the water column (Sec. 4.3.3).

6.2.2 Bottom reflectance of macrophytes, benthic microalgae and sediment types

In the water column optical (Sec 4.2.3), the calculation of remote-sensing reflectance required the contribution to water-leaving irradiance from bottom reflection. In order to calculate the importance of bottom reflectance, the integrated weighting of the water column must be calculated (Sec. 4.2.3), with the remaining being ascribed to the bottom. Thus, the weighting of the bottom reflectance as a component of surface reflectance is given by:

$$w_{\lambda,bot} = 1 - \frac{1}{z_{bot}} \int_0^{z_{bot}} \exp\left(-2K_{\lambda,z'}\right) dz' \tag{243}$$

where K_λ is the attenuation coefficient at wavelength λ described above, the factor of 2 accounts for the pathlength of both downwelling and upwelling light.

The bottom reflectance between 400 and 800 nm of $\sim$ 100 substrates (including turtles and giant clams!) have been measured on Heron Island using an Ocean Optics 2000 (Roelfsema and Phinn,

2012; Leiper et al., 2012). The data for selected substrates are shown in Fig. 17. When the bottom is composed of mixed communities, the surface reflectance is weighted by the fraction of the end members visible from above, with the assumption that the substrates are layered from top to bottom by macroalgae, seagrass (*Zostera* then *Halophila*), corals (zooxanthellae then skeleton), benthic microalgae, and then sediments. Since the sediment is sorted in the simulation by the sediment process, the sediments are assumed to be well mixed in surface sediment layer. Implicit in this formulation is that the scattering of one substrate type (i.e. benthic microalgae) does not contribute to the relectance of another (i.e. sand). In terms of an individual photon, it implies that if it first intercepts substrate A, then it is only scattered and/or absorbed by A.

Calculation of bottom fraction.

The fraction of the bottom taken up by a benthic plant of biomass B is $A_{eff} = 1-\exp(-\Omega_B B)$, with $\exp(-\Omega_B B)$ uncovered. Thus the fraction of the bottom covered by macroalgae, seagrass (Zostera then shallow and deep Halophila) and corals polyps is given by:

$$f_{MA} = 1 - \exp(-\Omega_{MA} MA) \tag{244}$$

$$f_{SG} = (1 - f_{MA})\,(1 - \exp(-\Omega_{SG} SG)) \tag{245}$$

$$f_{SGH} = (1 - f_{MA} - f_{SG})\,(1 - \exp(-\Omega_{SGH} SGH)) \tag{246}$$

$$f_{SGD} = (1 - f_{MA} - f_{SG} - f_{SGH})\,(1 - \exp(-\Omega_{SGD} SGD)) \tag{247}$$

$$f_{polyps} = (1 - f_{MA} - f_{SG} - f_{SGH} - f_{SGD})\,(1 - \exp(-\Omega_{CH} CH)) \tag{248}$$

Of the fraction of the bottom taken up by the polyps, f_{polyps}, zooxanthellae are first exposed. Assuming the zooxanthellae are horizontally homogeneous, the fraction taken up by the zooxanthellae is given by:

$$f_{zoo} = \min[f_{polyps}, \frac{\pi}{2\sqrt{3}} n\pi r_{zoo}^2] \tag{249}$$

where πr^2 is the projected area of the cell, n is the number of cells, and $\pi/(2\sqrt{3}) \sim 0.9069$ accounts for the maximum packaging of spheres. Thus the zooxanthellae can take up all the polyp area. The fraction, if any, of the exposed polyp area remaining is assumed to be coral skeleton:

$$f_{skel} = f_{polyps} - \min[f_{polyps}, \frac{\pi}{2\sqrt{3}} n\pi r_{zoo}^2] \tag{250}$$

The benthic microalgae overlay the sediments. Following the zooxanthellae calculation above, the fraction taken up by benthic microalgae is given by:

$$f_{MPB} = \min[(1 - f_{MA} - f_{SG} - f_{SGH} - f_{SGD} - f_{polyps}), \frac{\pi}{2\sqrt{3}} n\pi r_{MPB}^2] \tag{251}$$

Finally, the sediment fractions are assigned relative to their density in the surface layer, assuming the finer fractions overlay gravel:

$$M = Mud_{\mathrm{CaCO_3}} + Sand_{\mathrm{CaCO_3}} + Mud_{\mathrm{non-CaCO_3}} + Sand_{\mathrm{non-CaCO_3}} + FineSed + Dust \tag{252}$$

$$f_{CaCO_3} = (1 - f_{MA} - f_{SG} - f_{SGH} - f_{SGD} - f_{polyps} - f_{MPB}) \left(\frac{Mud_{\mathrm{CaCO_3}} + Sand_{\mathrm{CaCO_3}}}{M} \right) \tag{253}$$

$$f_{non-CaCO_3} = (1 - f_{MA} - f_{SG} - f_{SGH} - f_{SGD} - f_{polyps} - f_{MPB}) \left(\frac{Mud_{\mathrm{non-CaCO_3}} + Sand_{\mathrm{non-CaCO_3}}}{M} \right) \tag{254}$$

$$f_{FineSed} = (1 - f_{MA} - f_{SG} - f_{SGH} - f_{SGD} - f_{polyps} - f_{MPB}) \left(\frac{FineSed + Dust}{M} \right) \tag{255}$$

with the porewaters not being considered optically-active. Now that the fraction of each bottom type has been calculated, the fraction of backscattering to absorption plus backscattering for the benthic surface as seen just below the surface, $u_{bot,\lambda}$, is given by:

$$\begin{aligned} u_{bot,\lambda} \quad = \quad & w_{\lambda,bot}(f_{MA}\rho_{MA,\lambda} \\ & + f_{SG}\rho_{SG,\lambda} \\ & + f_{SGH}\rho_{SGH,\lambda} \\ & + f_{SGD}\rho_{SGD,\lambda} \\ & + f_{zoo}\frac{b_{zoo,\lambda}}{a_{zoo,\lambda} + b_{zoo,\lambda}} \\ & + f_{skel}\rho_{skel,\lambda} \\ & + f_{MPB}\frac{b_{MPB,\lambda}}{a_{MPB,\lambda} + b_{MPB,\lambda}} \\ & + f_{\mathrm{CaCO_3}}\rho_{\mathrm{CaCO_3},\lambda} + f_{non-\mathrm{CaCO_3}}\rho_{non-\mathrm{CaCO_3},\lambda} + f_{FineSed}\rho_{non-\mathrm{CaCO_3},\lambda}) \end{aligned} \tag{256}$$

where the absorption and backscattering are calculated as given in Sec. 4.2.1, and ρ is the measured bottom refectance of each end member (Dekker et al., 2011; Hamilton, 2001; Reichstetter et al., 2015).

For the values of surface reflectance for sand and mud from Heron Island (Roelfsema and Phinn, 2012; Leiper et al., 2012), and microalgal optical properties calculated as per Sec. 4.2, a ternary plot can be used to visualise the changes in true colour with sediment composition (Fig. 16).

It is important to note that while the backscattering of light from the bottom is considered in the model for the purposes of calculating reflectance (and therefore comparing with observations), it is not included in the calculation of water column scalar irradiance, which would require a radiative transfer model (Mishchenko et al., 2002).

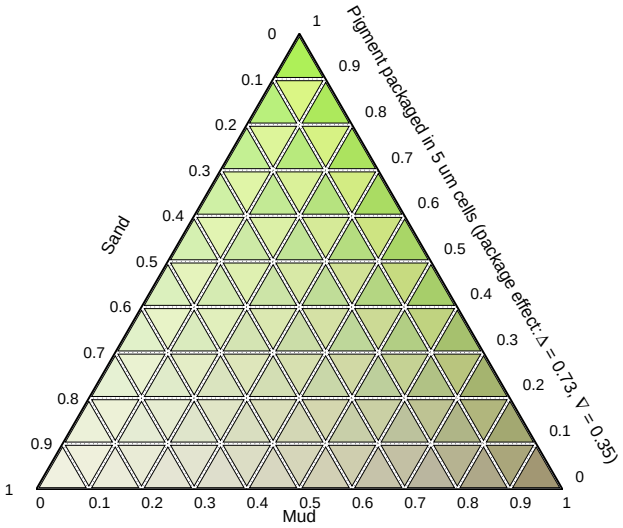

Figure 16: Modelled true colour surface reflectance for mixed sand, mud and microalgae sediment composition. The number of cells, n, required to fill the fraction without sand and mud, f_{MPB}, is calculated as $n = f_{MPB} / \left(\pi^2 r^2 / \left(2\sqrt{3}\right)\right)$ (from Eq. 251). The ternary plot shows cells of 5 μm radius with two internal concentrations of pigment (and therefore absorption). The generic parameter for the effect of cell pigment concentration on the reflectance is the packaging effect, $\alpha_\lambda/(\pi r^2)$, which varies between 0 and 1. A value of zero is a transparent cell with no self-shading, and a value of 1 is fully opaque at the specified wavelength. The upward pointing triangles, Δ, show the effect of cells with a package effect at 470 nm of 0.73, while the downward pointing triangles, ∇, show the effects of cells with a package effect at 470 nm of 0.35. Sand reflectance is based on observations from Heron Island (Roelfsema and Phinn, 2012), and mud from Janet Anstee (CSIRO). To read the counterclockwise ternary plot: At each point in the triangle the sum of sand, mud and microalgal fractions equals 1. Follow the grid in a SE direction from the sand axis, a NE from the mud axis, and W from the microalgae axis. Thus, the bottom left corner is 100 % light yellow sand, the bottom right corner is 100 % brown mud, and the top corner is 100 % green algal cells. The reflectance is enhanced using the MODIS true colour algorithm (Sec. B.2).

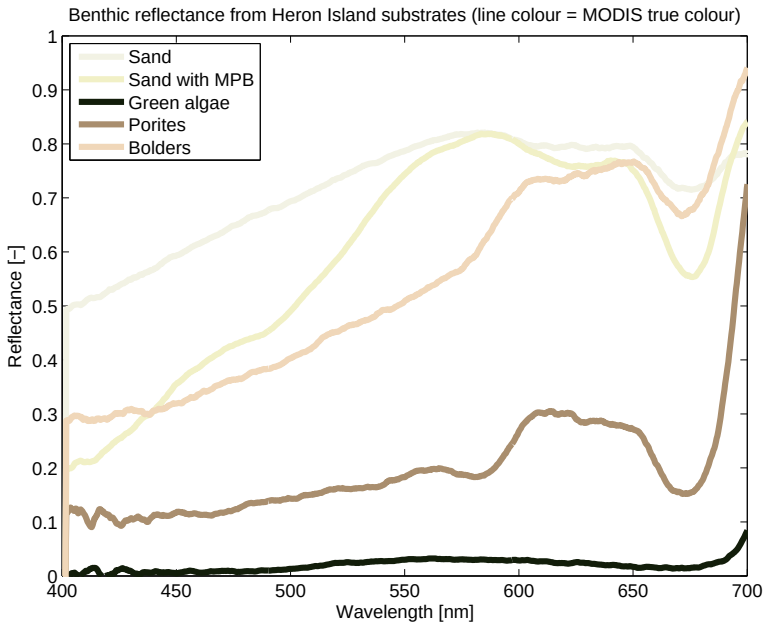

Figure 17: Observed substrate reflectance from 400 to 800 nm from Heron Island. Photos of the substrates, and the data, are available in Roelfsema and Phinn (2012). The line colour is calculated from the MODIS true colour algorithm (Gumley et al., 2010), giving the colour of the substrate lit by a spectrally-flat light source. Green algae appears almost black as there is low reflectance across all wavelengths, while sand is the whitest.

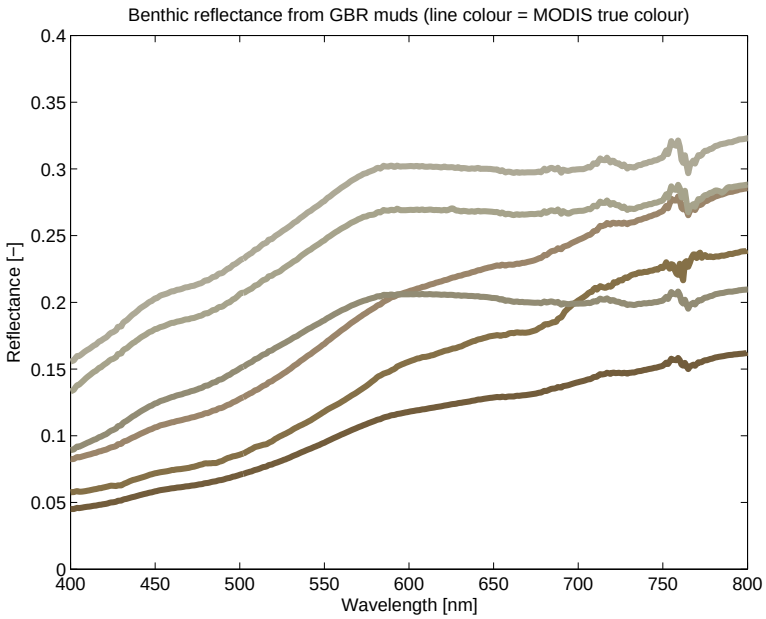

Figure 18: Observed substrate reflectance from 400 to 800 nm from terrestrial muds in the Whitsunday Islands region. The line colour is calculated from the MODIS true colour algorithm (Gumley et al., 2010), giving the colour of the substrate lit by a spectrally-flat light source. Reflectance measured as π [sr sr^{-1}] Lu [W m^{-2} nm^{-1} sr^{-1}] divided by Ed [W m^{-2} nm^{-1}], or percent reflectance.

6.3 Sediment chemistry

6.3.1 Sediment nitrification - denitrification

Nitrification in the sediment is similar to the water-column, but with a sigmoid rather than hyperbolic relationship at low oxygen, for numerical reasons. Denitrification occurs only in the sediment.

Variable	Symbol	Units
Ammonia concentration	$[NH_4]$	mg N m^{-3}
Sediment Dissolved Inorganic Carbon (DIC)	DIC	mg C m^{-3}
Sediment Dissolved Inorganic Phosphorus (DIP)	P	mg P m^{-3}
Sediment Particulate Inorganic Phosphorus (PIP)	PIP	mg P m^{-3}
Sediment Immobolised Particulate Inorganic Phosphorus (PIPI)	$PIPI$	mg P m^{-3}
Sediment Non-Algal Particulates (NAP)	NAP	kg m^{-3}
Sediment dissolved oxygen concentration	$[O_2]$	mg O m^{-3}

Table 35: State and derived variables for the sediment inorganic chemistry model.

Description	Symbol	Units
Maximum rate of nitrification in the water column	$\tau_{nit,wc}$	0.1 d^{-1}
Maximum rate of nitrification in the sediment	$\tau_{nit,sed}$	20 d^{-1}
Oxygen half-saturation constant for nitrification	$K_{O_2,nit}$	500 mg O m^{-3}
Maximum rate of denitrification	τ_{denit}	0.8 d^{-1}
Oxygen half-saturation constant for de-nitrification	$K_{O_2,denit}$	10000 mg O m^{-3}
Rate of P adsorbed/desorbed equilibrium	τ_{Pabs}	0.04 d^{-1}
Isothermic const. P adsorption for NAP	$k_{Pads,wc}$	300 kg NAP^{-1}
Oxygen half-saturation for P adsorption	$K_{O_2,\mathrm{abs}}$	2000 mg O m^{-3}
Rate of P immobilisation	τ_{Pimm}	0.0012 d^{-1}

Table 36: Constants and parameter values used in the sediment inorganic chemistry.

6.3.2 Sediment phosphorus absorption - desorption

Sediment phosphorus absorption - desorption is similar to water column.

There is an additional pool of immobilised particulate inorganic phosphorus, $PIPI$, which accumulates in the model over time as PIP becomes immobilised, and represents permanent sequestration.

$$\text{Nitrification} : \mathrm{NH_4^+ + 2O_2} \longrightarrow \mathrm{NO_3^- + H_2O + 2H^+} \quad (257)$$

$$\text{De} - \text{nitrification} : \mathrm{NO_3^- + \frac{1}{2}O_2} \longrightarrow \mathrm{\frac{1}{2}N_{2(g)} + 2O_2} \quad (258)$$

$$(259)$$

$$\frac{\partial[\mathrm{NH_4}]}{\partial t} = -\tau_{nit,wc}[\mathrm{NH_4}]\frac{[\mathrm{O_2}]^2}{K^2_{\mathrm{O_2},nit} + [\mathrm{O_2}]^2} \quad (260)$$

$$\frac{\partial[\mathrm{O_2}]}{\partial t} = -2\frac{32}{14}\tau_{nit,wc}[\mathrm{NH_4}]\frac{[\mathrm{O_2}]^2}{K^2_{\mathrm{O_2},nit} + [\mathrm{O_2}]^2} + 2\frac{32}{14}\tau_{denit}[\mathrm{NO_3}]\frac{K_{\mathrm{O_2},denit}}{K_{\mathrm{O_2},denit} + [\mathrm{O_2}]} \quad (261)$$

$$\frac{\partial[\mathrm{NO_3}]}{\partial t} = \tau_{nit,wc}[\mathrm{NH_4}]\frac{[\mathrm{O_2}]^2}{K^2_{\mathrm{O_2},nit} + [\mathrm{O_2}]^2} - \tau_{denit}[\mathrm{NO_3}]\frac{K_{\mathrm{O_2},denit}}{K_{\mathrm{O_2},denit} + [\mathrm{O_2}]} \quad (262)$$

$$\frac{\partial P}{\partial t} = \left(\tau_{Pabs}\left(\frac{PIP}{k_{Pads,sed}NAP} - \frac{[\mathrm{O_2}]P}{K_{\mathrm{O_2,abs}} + [\mathrm{O_2}]}\right)\right)/\phi \quad (263)$$

$$\frac{\partial PIP}{\partial t} = -\tau_{Pabs}\left(\frac{PIP}{k_{Pads,wc}NAP} - \frac{[\mathrm{O_2}]P}{K_{\mathrm{O_2,abs}} + [\mathrm{O_2}]}\right) - \tau_{Pimm}PIP \quad (264)$$

$$\frac{\partial PIPI}{\partial t} = \tau_{Pimm}PIP \quad (265)$$

Table 37: Equations for the sediment inorganic chemistry.

7 Common water / epibenthic / sediment processes

7.1 Preferential uptake of ammonia

The model contains two forms of dissolved inorganic nitrogen (DIN), dissolved ammonia (NH_4) and dissolved nitrate (NO_3):

$$N = [\mathrm{NH_4}] + [\mathrm{NO_3}] \quad (266)$$

where N is the concentration of DIN, $[NH_4]$ is the concentration of dissolved ammonia and $[NO_3]$ is the concentration of nitrate. In the model, the ammonia component of the DIN pool is assumed to be taken up first by all primary producers, followed by the nitrate, with the caveat that the uptake of ammonia cannot exceed the diffusion limit for ammonia. The underlying principle of this assumption is that photosynthetic organisms preference is at the upper limit of that which is

physically possibly.

As the nitrogen uptake formulation varies for the different autotrophs, the formulation of the preference of ammonia also varies. As the diffusion coefficient of ammonia and nitrate are only 3 % different, the nitrate diffusion coefficient has been used for both.

Thus, for microalgae with internal reserves of nitrogen, the partitioning of nitrogen uptake is given by:

$$\frac{\partial N}{\partial t} = -\psi D_N N(1 - R_N^*)\,(B/m_N) \tag{267}$$

$$\frac{\partial [\mathrm{NH_4}]}{\partial t} = -\min\left[\psi D_N N(1 - R_N^*), \psi D_N [\mathrm{NH_4}]\right](B/m_N) \tag{268}$$

$$\frac{\partial [\mathrm{NO_3}]}{\partial t} = -\left(\psi D_N N(1 - R_N^*) - \min\left[\psi D_N N(1 - R_N^*), \psi D_N [\mathrm{NH_4}]\right]\right)(B/m_N) \tag{269}$$

For macroalgae (and similarly for zooxanthellae), which also have diffusion limits to uptake, but are not represented with internal reserves of nitrogen, the terms are:

$$\frac{\partial N}{\partial t} = -\mu_{MA} MA \tag{270}$$

$$\frac{\partial [\mathrm{NH_4}]}{\partial t} = -\min\left[SA_{eff}[\mathrm{NH_4}], \mu_{MA} MA\right] \tag{271}$$

$$\frac{\partial [\mathrm{NO_3}]}{\partial t} = -\left(\mu_{MA} MA - \min\left[SA_{eff}[\mathrm{NH_4}], \mu_{MA} MA\right]\right) \tag{272}$$

In the case of nutrient uptake by seagrass, which has a saturating nitrogen uptake functional form, the terms are:

$$\frac{\partial N_s}{\partial t} = -\mu_{SG} SG \tag{273}$$

$$\frac{\partial [\mathrm{NH_4}]_s}{\partial t} = -\min\left[\mu_{SG} SG, \frac{\mu_{SG}^{max} [\mathrm{NH_4}]_s SG}{K_N + [\mathrm{NH_4}]_s}\right] \tag{274}$$

$$\frac{\partial [\mathrm{NO_3}]_s}{\partial t} = -\left(\mu_{SG} SG - \min\left[\mu_{SG} SG, \frac{\mu_{SG}^{max} [\mathrm{NH_4}]_s SG}{K_N + [\mathrm{NH_4}]_s}\right]\right) \tag{275}$$

where K_N is a function of the ratio of above ground to below ground biomass described above.

Oxygen release during nitrate uptake. For all autotrophs, the uptake of a nitrate ion results in the retention of the one N molecule in their reserves or structural material, and the release of the three oxygen molecules into the water column or porewaters.

$$\frac{\partial [\mathrm{O}]}{\partial t} = -\frac{48}{14}\frac{\partial [\mathrm{NO_3}]}{\partial t} \tag{276}$$

The oxygen that is part of the structural material is assumed to have been taken up through photosynthesis.

One feature worth noting is that the above formulation for preferential ammonia uptake requires no additional parameters, which is different to other classically applied formulations (Fasham et al., 1990) that require a new parameter, potentially for each autotroph. Given that there are at least 6 autotrophs, this simple formulation has an important role in reducing model complexity.

7.2 Temperature dependence of ecological rates

Physiological rate parameters (maximum growth rates, mortality rates, remineralisation rates) have a temperature dependence that is determined from:

$$r_T = r_{Tref} Q_{10}^{(T-T_{ref})/10} \tag{277}$$

where r_T is the physiological rate parameter (e.g. μ, ζ etc.) at temperature T, T_{ref} is the reference temperature (nominally 20°C for GBR), r_T the physiological rate parameter at temperature T_{ref}, Q_{10} is the Q10 temperature coefficient and represents the rate of change of a biological rate as a result of increasing temperature by 10°C.

Note that while physiological rates may be temperature-dependent, the ecological processes they are included in may not. For example, for extremely light-limited growth, all autotrophs capture light at a rate independent of temperature. With the reserves of nutrients replete, the steady-state realised growth rate, μ, becomes the rate of photon capture, k. This can be shown algebracially: $\mu = \mu^{max} R_C^* = k(1 - R^*)$, where R^* is the reserves of carbon. Rearranging, $R^* = k/(\mu^{max} + k)$. At $k << \mu^{max}$, $R^* = k/\mu^{max}$, thus $\mu = \mu^{max} k/\mu^{max} = k$. This corresponds with observations of no temperature dependence of photosynthesis at low light levels (Kirk, 1994).

Similar arguments show that extremely nutrient limited autorophs will have the same temperature dependence to that of the diffusion coefficient. Thus, the autotroph growth model has a temperature-dependence that adjust appropriately to the physiological condition of the autotroph, and is a combination of constant, exponential, and polynomial expressions.

Physiological rates in the model that are not temperature dependent are: mass transfer rate constant for particulate grazing by corals, S_{Part}; net coral calcification g; maximum chlorophyll synthesis, k_{Chl}^{max};and rate of translocation between leaves and roots in seagrass, τ_{tran}.

Variable	Symbol	Units
Ammonia concentration	$[NH_4]$	mg N m^{-3}
Dissolved Inorganic Carbon (DIC)	DIC	mg C m^{-3}
Dissolved Inorganic Phosphorus (DIP)	P	mg P m^{-3}
Dissolved oxygen concentration	$[O_2]$	mg O m^{-3}
Labile detritus at Redfield ratio	D_{Red}	mg N m^{-3}
Labile detritus at Atkinson ratio	D_{Atk}	mg N m^{-3}
Refractory Detritus C	D_C	mg C m^{-3}
Refractory Detritus N	D_N	mg N m^{-3}
Refractory Detritus P	D_P	mg P m^{-3}
Dissolved Organic C	O_C	mg C m^{-3}
Dissolved Organic N	O_N	mg N m^{-3}
Dissolved Organic P	O_P	mg P m^{-3}
Chemical Oxygen Demand (COD)	COD	mg O m^{-3}

Table 38: State and derived variables for the detritus remineralisation model in both the sediment and water column.

7.3 Detritus remineralisation

The non-living components of C, N, and P cycles include the particulate labile and refractory pools, and a dissolved pool (Fig. 2). The labile detritus has a pool at the Redfield ratio, D_{Red}, and at the Atkinson ratio, D_{Atk}, resulting from dead organic matter at these ratios. The labile detritus from both pools then breaks down into refractory detritus and dissolved organic matter. The refractory detritus and dissolved organic matter pools are quantified by individual elements (C, N, P), in order to account for the mixed source of labile detritus. Finally, a component of the breakdown of each of these pools is returned to dissolved inorganic components. The variables, parameters and equations can be found in Tables 38, 40 & 39 respectively.

As the refractory and dissolved components are separated into C, N and P components, this introduces the possibility to have P components break down quicker than C and N. This is specified as the breakdown rate of P relative to N, Φ_{RD_P} and Φ_{DOM_P} respectively for refractory and dissolved detritus respectively.

7.3.1 Steady-state detritus and organic matter concentrations

The steady-state concentration of labile and refractory detritus and organic matter can be derived from equating derivatives in Tab. 39 to zero and adding net primary production as a source of

labile detritus. Considering only carbon and labile detritus at the Redfield ratio, the equations at steady-state become:

$$
\begin{aligned}
-r_{Red} D_{Red} + PP &= 0 && (291)\\
\frac{106}{16}\frac{12}{14}\zeta_{Red} r_{Red} D_{Red} - r_R D_C &= 0 && (292)\\
\frac{106}{16}\frac{12}{14}\vartheta_{Red} r_{Red} D_{Red} + \vartheta_{Ref} r_R D_C - r_O O_C &= 0 && (293)
\end{aligned}
$$

where PP is net primary production in units of mg N m^{-3} d^{-1}. Solving for D_{Red}, D_C and O_C:

$$
\begin{aligned}
D_{Red} &= PP/r_{Red} && (294)\\
D_C &= \frac{106}{16}\frac{12}{14}\zeta_{Red} r_{Red} D_{Red}/r_R = \frac{106}{16}\frac{12}{14}\zeta_{Red} PP/r_R && (295)\\
O_C &= \left(\frac{106}{16}\frac{12}{14}\vartheta_{Red} r_{Red} D_{Red} + \vartheta_{Ref} r_R D_C\right)/r_O && (296)\\
&= \left(\frac{106}{16}\frac{12}{14}\vartheta_{Red} PP + \vartheta_{Ref}\zeta_{Red} PP\right)/r_O && (297)\\
&= \frac{106}{16}\frac{12}{14}\frac{PP}{r_O}\left(\vartheta_{Red} + \vartheta_{Ref}\zeta_{Red}\right) && (298)
\end{aligned}
$$

Thus, the steady state of O_C is proportional to the primary production divided by the breakdown rate of dissolved organic carbon, multiplied by the fractions of D_C, ϑ_{Ref} and D_{Red}, $\vartheta_{Ref}\zeta_{Red}$, that remain organics thought the breakdown process. Using values in Tab. 40, the pelagic-driven component of dissolved organic carbon, O_C, at the reference temperature for a primary production rate of 2 mg N m^{-3} d^{-1} is 767 mg C m^{-3}, which is within the range of 760-960 observed globally for tropical and sub-tropical systems (Hansell et al., 2009).

In order to have an absorption coefficient of DOC matter at 443 nm of 0.1 m^{-1}, requires a DOC-specific absorption coefficient, $k_{DOC,443}$ of 0.1/767 = 0.0013 m^{-2} mg C. Using these steady-state results, and assuming equal breakdown rates of all elements, the initial conditions detrital and dissolved organic C, N and P pools can be calculated (Tab. 41).

$$\frac{\partial D_{Red}}{\partial t} = -r_{Red} D_{Red} \tag{278}$$

$$\frac{\partial D_{Atk}}{\partial t} = -r_{Atk} D_{Atk} \tag{279}$$

$$\frac{\partial D_C}{\partial t} = \frac{106}{16}\frac{12}{14}\zeta_{Red} r_{Red} D_{Red} + \frac{550}{30}\frac{12}{14}\zeta_{Atk} r_{Atk} D_{Atk} - r_R D_C \tag{280}$$

$$\frac{\partial D_N}{\partial t} = \zeta_{Red} r_{Red} D_{Red} + \zeta_{Atk} r_{Atk} D_{Atk} - r_R D_N \tag{281}$$

$$\frac{\partial D_P}{\partial t} = \frac{1}{16}\frac{31}{14}\zeta_{Red} r_{Red} D_{Red} + \frac{1}{30}\frac{31}{14}\zeta_{Atk} r_{Atk} D_{Atk} - \Phi_{RD_P} r_R D_P \tag{282}$$

$$\frac{\partial O_C}{\partial t} = \frac{106}{16}\frac{12}{14}\vartheta_{Red} r_{Red} D_{Red} + \frac{550}{30}\frac{12}{14}\vartheta_{Atk} r_{Atk} D_{Atk} + \vartheta_{Ref} r_R D_C - r_O O_C \tag{283}$$

$$\frac{\partial O_N}{\partial t} = \vartheta_{Red} r_{Red} D_{Red} + \vartheta_{Atk} r_{Atk} D_{Atk} + \vartheta_{Ref} r_R D_N - r_O O_N \tag{284}$$

$$\frac{\partial O_P}{\partial t} = \frac{1}{16}\frac{31}{14}\vartheta_{Red} r_{Red} D_{Red} + \frac{1}{30}\frac{31}{14}\vartheta_{Atk} r_{Atk} D_{Atk} + \vartheta_{Ref}\Phi_{RD_P} r_R D_P - \Phi_{DOM_P} r_O O_P \tag{285}$$

$$\frac{\partial [\mathrm{NH_4}]}{\partial t} = r_{Red} D_{Red}(1 - \zeta_{Red} - \vartheta_{Red}) + r_{Atk} D_{Atk}(1 - \zeta_{Atk} - \vartheta_{Atk}) + r_R D_N (1 - \vartheta_{Ref}) + r_O O_N \tag{286}$$

$$\frac{\partial DIC}{\partial t} = \frac{106}{16}\frac{12}{14} r_{Red} D_{Red}(1 - \zeta_{Red} - \vartheta_{Red}) + \frac{550}{30}\frac{12}{14} r_{Atk} D_{Atk}(1 - \zeta_{Atk} - \vartheta_{Atk}) + r_R D_C (1 - \vartheta_{Ref}) + r_O O_C \tag{287}$$

$$\frac{\partial P}{\partial t} = \frac{1}{16}\frac{31}{14} r_{Red} D_{Red}(1 - \zeta_{Red} - \vartheta_{Red}) + \frac{1}{30}\frac{31}{14} r_{Atk} D_{Atk}(1 - \zeta_{Atk} - \vartheta_{Atk}) + \Phi_{RD_P} r_R D_P (1 - \vartheta_{Ref}) + \Phi_{DOM_P} r_O O_P \tag{288}$$

$$\frac{\partial [\mathrm{O_2}]}{\partial t} = -\frac{32}{12}\frac{\partial DIC}{\partial t}\frac{[\mathrm{O_2}]^2}{K_{OA}^2 + [\mathrm{O_2}]^2} \tag{289}$$

$$\frac{\partial [COD]}{\partial t} = \frac{32}{12}\frac{\partial DIC}{\partial t}\left(1 - \frac{[\mathrm{O_2}]^2}{K_{OA}^2 + [\mathrm{O_2}]^2}\right) \tag{290}$$

Table 39: Equations for detritus remineralisation in the water column and sediment.

Description	Symbol	Red	Atk	Refractory	Dissolved
Detritus breakdown rate (d^{-1})	$r_{Red,Atk,R,O}$	0.04	0.01	0.001	0.0001
Fraction of detritus to refractory	$\zeta_{Red,Atk}$	0.19	0.19	-	-
Fraction of detritus to DOM	$\vartheta_{Red,Atk,R}$	0.1	0.1	0.05	
Breakdown rate of P relative to N	$\Phi_{R,O}$	N/A	N/A	2	2

Table 40: Constants and parameter values used in the water column detritus remineralisation model. Red = Redfield ratio (C:N:P = 106:16:1); Atk = Atkinson ratio (C:N:P = 550:30:1); Ref = Refractory. See Lønborg et al. (2017).

	Labile Det., D_{Red}	Refractory Det., D	Dissolved Organic, O
Redfield	25	-	-
Carbon	-	27	767
Nitrogen	-	4.75	135
Phosphorus	-	0.66	18.7

Table 41: Steady-state detrital and dissolved organic C, N and P concentrations for primary production equal to 2 mg N m^{-1}

7.3.2 Anaerobic and anoxic respiration

The processes of remineralisation, phytoplankton mortality and zooplankton grazing return carbon dioxide to the water column. In oxic conditions, these processes consume oxygen in a ratio of $DIC : \frac{32}{12}[O_2]$. At low oxygen concentrations, the oxygen consumed is reduced:

$$\frac{\partial [O_2]}{\partial t} = -\frac{\partial DIC}{\partial t}\frac{32}{12}\frac{[O_2]^2}{K_{OA}^2 + [O_2]^2} \tag{299}$$

where $K_{OA} = 256$ mg O m^{-3} is the half-saturation constant for anoxic respiration (Boudreau, 1996). A sigmoid saturation term is used because it is more numerically stable as the oxygen concentration approaches 0. The anoxic component of remineralisation results in an increased chemical oxygen demand (COD):

$$\frac{\partial COD}{\partial t} = \frac{\partial DIC}{\partial t}\frac{32}{12}\left(1 - \frac{[O_2]^2}{K_{OA}^2 + [O_2]^2}\right) \tag{300}$$

COD is a dissolved tracer, with the same units as oxygen.

When oxygen and COD co-exist they react to reduce both, following:

$$\frac{\partial [O_2]}{\partial t} = -\tau_{COD}\min[COD, 8000]\frac{[O_2]}{8000} \tag{301}$$

$$\frac{\partial COD}{\partial t} = -\tau_{COD} \min[COD, 8000] \frac{[O_2]}{8000} \quad (302)$$

where 8000 mg O m^{-3} is approximately the saturation concentration of oxygen in seawater, and τ_{COD} is the timescale of this reduction. The term $\min[COD, 8000]$ is required because COD represents the end stage of anoxic reduction and can become large for long simulations. Even with this limitation, if $\tau_{COD} = 1$ hr^{-1}, the processes in Eqs. 301 and 302 proceed faster than most of the other porewater processes.

8 Numerical integration

8.1 Splitting of physical and ecological integrations

The numerical solution of the time-dependent advection-diffusion-reaction equations for each of the ecological tracers is implemented through sequential solving of the partial differential equations (PDEs) for advection and diffusion, and the ordinary differential equations for reactions. This technique, called operator splitting, is common in geophysical science (Hundsdorfer and Verwer, 2003).

The time-step of the splitting is typically 15 min - 1 hour (Table 42). Under the sequential operator splitting technique used, first the advection-diffusion processes are solved for the period of the time-step. The value of the tracers at the end of this PDE integration, and the initial time, are then used as initial conditions for the ODE integration. After the ODE integration has run for same time period, the value of the tracers is update, and time is considered to have moved forward just one time-step. The integration continues to operate sequentially for the whole model simulation.

The PDE solutions are described in the physical model description available at:

`www.emg.cmar.csiro.au/www/en/emg/software/EMS/hydrodynamics.html`.

8.2 Diffusive exchange of dissolved tracers across sediment-water interface

Due to the thin surface sediment layer, and the potentially large epibenthic drawndown of porewater dissolved tracers, the exchange of dissolved tracers between the bottom water column layer and the top sediment layer is solved in the same numerical operation as the ecological tracers (other transport

processes occurring between ecological timesteps). The flux, J, is given by:

$$J = k(C_s - C) \tag{303}$$

where C and C_s are the concentration in water column and sediment respectively, $k = 4.6 \times 10^{-7}$ m s^{-1} is the transfer coefficient. In the model parameterisation, $k = D/h$ where $D = 3 \times 10^{-9}$ m^2 s^{-1} is the diffusion coefficient and $h = 0.0065$ mm is the thickness of the diffusive layer.

While in reality k would vary with water column and sediment hydrodynamics as influenced by community type etc, these complexities has not been considered. In addition to the diffusive flux between the sediment and water column, particulate deposition entrains water column water into the sediments, and particulate resuspension releases porewaters into the water column. Sediment model details can be found at: `https://research.csiro.au/cem/software/ems/ems-documentation/`.

8.3 Optical integration

The inherent and apparent optical properties are calculated between the physical and ecological integrations. The spectral resolution of 25 wavebands has been chosen to resolve the absorption peaks associated with Chl *a*, and to span the optical wavelengths. As IOPs can be calculated at any wavelength given the model state, IOPs and AOPs at observed wavelengths are recalculated after the integration.

Additionally, the wavelengths integrated have been chosen such that the lower end of one waveband and the top end of another fall on 400 and 700 nm respectively, allowing precise calculation of photosynthetically available radiation (PAR).

8.4 Adaptive solution of ecological processes

A 5th-order Dormand-Prince ordinary differential equation integrator (Dormand. and Prince, 1980) with adaptive step control is used to integrate the local rates of changes due to ecological processes. This requires 7 function evaluations for the first step and 6 for each step after. A tolerance of 1×10^{-5} mg N m^{-3} is required for the integration step to be accepted.

For an n_{wc}-layer water column and n_{sed}-layer sediment, the integrator sequentially solves the top $n_{wc} - 1$ water column layers; the nth water column layer, epibenthic and top sediment layer together; and then the $n_{sed} - 1$ to bottom sediment layers.

8.5 Additional integration details

8.5.1 Approximation of stoichiometric coefficients

In this model description we have chosen to explicitly include atomic mass as two significant figure values, so that the conversion are more readable in the equations than if they had all been rendered as mathematical symbols. Nonetheless these values are more precisely given in the numerical code (Table 43).

It is worth remembering that the atomic masses are approximations assuming the ratio of isotopes found in the Periodic Table (Atkins, 1994), based on the natural isotopic abundance of the Earth. So, for example, ^{14}N and ^{15}N have atomic masses of 14.00307 and 15.00011 respectively, with ^{14}N making up 99.64 % of the abundance on Earth. Thus the value 14.01 comes from $14.00307 \times 99.64 + 15.00011 \times 0.36 = 14.0067$. The isotopic discrimination in the food web of 3 ppt per trophic level would increase the mean atomic mass by $(15.00011 - 14.00307) \times 0.003 = 0.003$ per trophic level. Perhaps more importantly, if the model had state variables for ^{14}N and ^{15}N, then the equations would change to contain coefficients of 14 for the ^{14}N isotope equations, and 15 for the ^{15}N isotope equations, that would be applied in the numerical code using 14.00 and 15.00 respectively.

8.5.2 Mass conservation in water column and sediment porewaters

The model checks the conservation of Total C, TC, Total N, TN, Total P, TP, and oxygen, $[O_2]$, within each grid cell at each time step using the following conservation laws. To establish mass conservation, the sum of the change in mass (of N, P, C and O) with time and the mass of sinks / sources (such as sea-air fluxes, denitrification) must equate to zero.

The total mass and conservation equations are same for the water column and porewaters, with the caveats that (1) air-sea fluxes only affect surface layers of the water, (2) denitrification only occurs in the sediment, and (3) the porosity, ϕ, of the water column is 1. In the sediment, the concentration of particulates is given in per unit volume of space, while the concentration of dissolved tracers is given in per unit volume of porewater. The concentration of dissolved tracer, X, per unit space is given by ϕX.

Thus the total carbon in a unit volume of space, and its conservation, are given by:

$$TC = \phi\left(DIC + O_C\right) + \left(\frac{550}{30}\frac{12}{14}D_{Atk} + D_C + \frac{106}{16}\frac{12}{14}\left(D_{red} + \sum B(1 + R_C^*) + \sum Z\right)\right) \tag{304}$$

$$\frac{\partial TC}{\partial t} + \underbrace{k_{CO_2}\left([CO_2] - [CO_2]_{atm}\right)/h}_{\text{sea-air flux}} = 0 \tag{305}$$

The total nitrogen in a unit volume of space, and its conservation, are given by:

$$TN = \phi\left([\mathrm{NO_3}] + [\mathrm{NH_4}] + O_N\right) + \left(D_{Atk} + D_{red} + D_N + \sum B(1 + R_N^*) + \sum Z\right) \tag{306}$$

$$\frac{\partial TN}{\partial t} + \left(\text{denitrification} - \text{nitrogen fixation}\right)/\phi - \text{dust input}/h = 0 \tag{307}$$

The total phosphorus in a unit volume of space, and its conservation, are given by:

$$TP = \phi\left(DIP + O_P\right) + PIP + PIPI + \frac{1}{30}\frac{31}{14}D_{Atk} + D_P + \frac{1}{16}\frac{31}{14}\left(D_{red} + \sum B(1 + R_P^*) + \sum Z\right) \tag{308}$$

$$\frac{\partial TP}{\partial t} - \text{dust input}/h = 0 \tag{309}$$

The concept of oxygen conservation in the model is more subtle than that of C, N and P due to the mass of oxygen in the water molecules themselves not being considered. When photosynthesis occurs, C is transferred from the dissolved phase to reserves within the cell. With both dissolved and particulate pools considered, mass conservation of C is straightforward. In contrast to C, during photosynthesis oxygen is drawn from the water molecules (i.e. H_2O), whose mass is not being considered, and released into the water column. Conversely, when organic matter is broken down oxygen is consumed from the water column and released as H_2O.

In order to obtain a mass conservation for oxygen, the concept of Biological Oxygen Demand (BOD) is used. Often BOD represents the biological demand for oxygen in say a 5 day incubation, BOD_5. Here, for the purposes of mass conservation checks, we use BOD_∞, the oxygen demand over an infinite time for breakdown. This represents the total oxygen removed from the water molecules for organic matter creation.

Anaerobic respiration reduces BOD_∞ without reducing O_2, but instead creating reduced-oxygen species. This is accounted for in the oxygen balance by the prognostic tracer Chemical Oxygen Demand (COD). In other biogeochemical modelling studies this is represented by a negative oxygen concentration.

Thus at any time point the biogeochemical model will conserve the oxygen concentration minus BOD_∞ minus COD, plus or minus any sources and sinks such as sea-air fluxes. The total oxygen minus BOD_∞ minus COD in a unit volume of water, and its conservation, is given by:

$$[\mathrm{O_2}] + \frac{48}{14}[\mathrm{NO_3}] - BOD_\infty - COD =$$
$$\phi\left([\mathrm{O_2}] + \frac{48}{14}[\mathrm{NO_3}] - COD + \frac{32}{12}O_C\right) - \left(\frac{550}{30}\frac{32}{14}D_{Atk} + \frac{32}{12}D_C + \frac{106}{16}\frac{32}{14}\left(D_{red} + \sum B_N(1 + R_C^*)\right)\right) \tag{310}$$

$$\frac{\partial([\mathrm{O_2}]+\frac{48}{14}[\mathrm{NO_3}]-BOD_\infty-COD)}{\partial t}+\mathcal{R}-\overbrace{\frac{k_{\mathrm{O_2}}\left([\mathrm{O_2}]_{sat}-[\mathrm{O_2}]\right)}{h}}^{sea-air\ flux}\underbrace{-2\frac{106}{16}\frac{32}{14}\tau_{nit,wc}[\mathrm{NH_4}]\frac{[\mathrm{O_2}]}{K_{nit,\mathrm{O}}+[\mathrm{O_2}]}}_{nitrification}=0 \tag{311}$$

where $\mathcal{R}$ is respiration of organic matter.

In addition to dissolved oxygen, BOD and COD, nitrate (NO_3) appears in the oxygen mass balance. This is necessary because the N associated with nitrate uptake is not taken into the autotrophs, but rather released into the water column or porewater. Other entities that contain oxygen in the ocean include the water molecule (H_2O) and the phosphorus ion (PO_4). In the case of water, this oxygen reservoir is considered very large, with the small flux associated with its change balanced by BOD. In the case of PO_4, this is a small reservoir. As oxygen remains bound to P through the entire processes of uptake into reserves and incorporated into structural material and then release, it is not necessary to include it in the oxygen balance for the purposes of ensuring consistency. Nonetheless, strictly the water column and porewater oxygen reservoirs could include a term $+\frac{64}{31}[\mathrm{PO_4}]$, and the BOD would have similar quantities for reserves and structural material.

8.5.3 Mass conservation in the epibenthic

Mass conservation in the epibenthos requires consideration of fluxes between the water column, porewaters and the epibenthic organisms (macroalgae, seagrass and coral hosts and symbionts).

The total carbon in the epibenthos, and its conservation, is given by:

$$TC=\frac{550}{30}\frac{12}{14}\left(MA+SG_A+SG_B\right)+\frac{106}{16}\frac{12}{14}\left(CS\left(1+R_C^*\right)+CH\right) \tag{312}$$

$$\left.\frac{\partial TC}{\partial t}\right|_{epi}+h_{wc}\left.\frac{\partial TC}{\partial t}\right|_{wc}+h_{sed}\left.\frac{\partial TC}{\partial t}\right|_{sed}+\underbrace{12\left(gA_{eff}-d_{\mathrm{CaCO_3}}\right)}_{coral\ calcification\ -\ dissolution}=0 \tag{313}$$

where h_{wc} and h_{sed} are the thickness of the bottom water column and top sediment layers, R_C^* is the normalised internal reserves of carbon in zooxanthallae, $12g$ is the rate coral calcification per unit area of coral, A_{eff} is the area of the bottom covered by coral per m^{-2}, and the diffusion terms between porewaters and the water column cancel, so do not appear in the equations. Note the units of mass of CS needs to be in g N, and some configurations may have multiple seagrass and macroalgae species.

Similarly for nitrogen, phosphorus and oxygen in the epibenthos:

$$TN=MA+SG_A+SG_B+CS\left(1+R_N^*\right)+CH \tag{314}$$

$$\left.\frac{\partial TN}{\partial t}\right|_{epi} + h_{wc}\left.\frac{\partial TN}{\partial t}\right|_{wc} + h_{sed}\left.\frac{\partial TN}{\partial t}\right|_{sed} = 0 \tag{315}$$

$$TP = \frac{1}{30}\frac{31}{14}\left(MA + SG_A + SG_B\right) + \frac{1}{16}\frac{31}{14}\left(CS\left(1 + R_P^*\right) + CH\right) \tag{316}$$

$$\left.\frac{\partial TP}{\partial t}\right|_{epi} + h_{wc}\left.\frac{\partial TP}{\partial t}\right|_{wc} + h_{sed}\left.\frac{\partial TP}{\partial t}\right|_{sed} = 0 \tag{317}$$

$$BOD_\infty = \frac{550}{30}\frac{32}{14}\left(MA + SG_A + SG_B\right) + \frac{106}{16}\frac{32}{14}\left(CS\left(1 + R_C^*\right) + CH\right) \tag{318}$$

$$-\left.\frac{\partial BOD_\infty}{\partial t}\right|_{epi} + h_{wc}\left.\frac{\partial([\mathrm{O}_2] - BOD_\infty)}{\partial t}\right|_{wc} + h_{sed}\left.\frac{\partial([\mathrm{O}_2] - BOD_\infty)}{\partial t}\right|_{sed} = 0 \tag{319}$$

where there is no dissolved oxygen in the epibenthos.

8.5.4 Wetting and drying

When a water column becomes dry (the sea level drops below the seabed depth) ecological processes are turned off.

8.5.5 Unconditional stability

In addition to the above standard numerical techniques, a number of innovations are used to ensure model solutions are reached. Should an integration step fail in a grid cell, no increment of the state variables occurs, and the model is allowed moves the next vertical column, with a warning flag registered (as `Ecology Error`). Generally the problem does not reoccur due to the transport of tracers alleviating the stiff point in phase space of the model.

Description	Values
Timestep of hydrodynamic model	90 s (GBR4), 20 s (GBR1)
[a]Timestep of ODE ecological model	3600 s (GBR4), 1800 s (GBR1)
Timestep of optical and carbon chemistry models	3600 s
Optical model resolution in PAR	$\sim$ 20 nm
ODE integrator	5th order Dormand-Prince
ODE tolerance	10^{-5} mg N m^{-3}
Maximum number of ODE steps in ecology	2000
Maximum number of iterations in carbon chemistry	100
Accuracy of carbon chemistry calculations	$[H^+] = 10^{-12}$ mol

Table 42: Integration details. Optical wavelengths (nm): 290 310 330 350 370 390 410 430 440 450 470 490 510 530 550 570 590 610 630 650 670 690 710 800.[a]Since the integrator is 5th order, the ecological derivatives are evaluated at least every approximately 3600/5 = 900 s, and more regularly for stiff equations.

Element	Value in symbolic equations	Value in code
Nitrogen, N	14	14.01
Carbon, C	12	12.01
Oxygen, O_2	32	32.00
Phosphorus, P	31	30.97

Table 43: Atomic mass of the C, N, P and O_2, both in the model description where two significant figures are used for brevity, and in the numerical code, where precision is more important.

9 Peer-review publications

The following list includes peer-reviewed papers using the biogeochemical and / or optical models of the EMS package.

Baird, M. E., Walker, S. J., Wallace, B. B., Webster, I. T., Parslow, J. S., 2003. The use of mechanistic descriptions of algal growth and zooplankton grazing in an estuarine eutrophication model. Est., Coastal and Shelf Sci. 56, 685–695.

Baird, M. E., Ralph, P. J., Rizwi, F., Wild-Allen, K. A., Steven, A. D. L., 2013. A dynamic model of the cellular carbon to chlorophyll ratio applied to a batch culture and a continental shelf ecosystem. Limnol. Oceanogr. 58, 1215–1226.

Baird, M. E., M. P. Adams, R. C. Babcock, K. Oubelkheir, M. Mongin, K. A. Wild-Allen, J. Skerratt, B. J. Robson, K. Petrou, P. J. Ralph, K. R. O'Brien, A. B. Carter, J. C. Jarvis, M. A. Rasheed (2016) A biophysical representation of seagrass growth for application in a complex shallow-water biogeochemical model. Ecol. Mod. 325, 13–27.

Baird, M. E., Cherukuru, N., Jones, E., Margvelashvili, N., Mongin, M., Oubelkheir, K., Ralph, P. J., Rizwi, F., Robson, B. J., Schroeder, T., Skerratt, J., Steven A. D. L., Wild-Allen, K. A. (2016). Remote-sensing reflectance and true colour produced by a coupled hydrodynamic, optical, sediment, biogeochemical model of the Great Barrier Reef, Australia: comparison with satellite data. Env. Model. Software. 78, 79–96.

Baird, M. E., J. Andrewartha, M. Herzfeld, E. Jones, N. Margvelashvili, M. Mongin, F. Rizwi, J. Skerratt, M. Soja-Wozniak, K. Wild-Allen, T. Schroeder, B. Robson, E. da Silva, M. Devlin (2017) River plumes of the Great Barrier Reef: freshwater, sediment and optical footprints quantified by the eReefs modelling system. In Syme, G., Hatton MacDonald, D., Fulton, B. and Piantadosi, J. (eds) MODSIM2017, 22nd International Congress on Modelling and Simulation. Modelling and Simulation Society of Australia and New Zealand, December 2017, pp.1892-1898. ISBN: 978-0-9872143-7-9. https://www.mssanz.org.au/modsim2017/L22/baird.pdf.

Baird, M. E., Mongin, M., Rizwi, F., Bay, L. K., Cantin, N. E., Soja-Woźniak, M., Skerratt, J., 2018. A mechanistic model of coral bleaching due to temperature-mediated light-driven reactive oxygen build-up in zooxanthellae. Ecol. Model. 386, 20–37.

Brodie, J., M. Baird, M. Mongin, J. Skerratt, C. Robillot and J. Waterhouse (2017) Pollutant target setting for the Great Barrier Reef: Using the eReefs framework. In Syme, G., Hatton MacDonald, D., Fulton, B. and Piantadosi, J. (eds) MODSIM2017, 22nd International Congress on Modelling and Simulation. Modelling and Simulation Society of Australia and New Zealand, December 2017, pp. 1913-1919. ISBN: 978-0-9872143-7-9. https://www.mssanz.org.au/modsim2017/L22/brodie.pdf

Condie, S. A., Herzfeld, M., Margvelashvili, N., Andrewartha, J. R., 2009. Modeling the physical and biogeochemical response of a marine shelf system to a tropical cyclone. Geophys. Res. Lett. 36 (L22603).

Hadley, S., Wild-Allen, K. A., Johnson, C., Macleod, C., 2015. Modeling macroalgae growth and nutrient dynamics for integrated multi-trophic aquaculture. J. Appl. Phycol. 27, 901–916.

Hadley, S., Wild-Allen, K. A., Johnson, C., Macleod, C., 2015 online. Quantification of the impacts of finfish aquaculture and bioremediation capacity of integrated multi-trophic aquaculture using a 3D estuary model. J. Appl. Phycol. 28, 1875.

Jones, E. M., Baird, M. E., Mongin, M., Parslow, J., Skerratt, J., Lovell, J,. Margvelashvili, N., Matear, R. J., Wild-Allen, K., Robson, B., Rizwi, F., Oke, P., King, E., Schroeder, T., Steven, A., Taylor, J., 2016. Use of remote-sensing reflectance to constrain a data assimilating marine biogeochemical model of the Great Barrier Reef Biogeosciences 13, 6441–6469.

Margvelashvili, N., 2009. Stretched Eulerian coordinate model of coastal sediment transport. Computer Geosciences 35, 1167–1176.

Mongin, M., Baird, M. E., 2014. The interacting effects of photosynthesis, calcification and water circulation on carbon chemistry variability on a coral reef flat: a modelling study. Ecol. Mod. 284, 19–34.

Mongin, M., M. E. Baird, B. Tilbrook, R. J. Matear, A. Lenton, M. Herzfeld, K. A. Wild-Allen, J. Skerratt, N. Margvelashvili, B. J. Robson, C. M. Duarte, M. S. M. Gustafsson, P. J. Ralph, A. D. L. Steven (2016). The exposure of the Great Barrier Reef to ocean acidification. Nature Communications 7, 10732.

Robson, B. J., Baird, M., & Wild-Allen, K. (2013). A physiological model for the marine cyanobacteria, *Trichodesmium*. In MODSIM2013, 20th International Congress on Modelling and Simulation. Modelling and Simulation Society of Australia and New Zealand, ISBN (pp. 978-0).

Robson, B. J., J. Andrewartha, M.E. Baird, M. Herzfeld, E.M. Jones, N. Margvelashvili, M. Mongin, F. Rizwi, J. Skerratt, K. Wild-Allen (2017) Evaluating the eReefs Great Barrier Reef marine model against observed emergent properties. In Syme, G., Hatton MacDonald, D., Fulton, B. and Piantadosi, J. (eds) MODSIM2017, 22nd International Congress on Modelling and Simulation. Modelling and Simulation Society of Australia and New Zealand, December 2017, pp. 1976 ? 1982. ISBN: 978-0-9872143-7-9. https://www.mssanz.org.au/modsim2017/L22/robson.pdf.

Skerratt, J., Wild-Allen, K. A., Rizwi, F., Whitehead, J., Coughanowr, C., 2013. Use of a high resolution 3D fully coupled hydrodynamic, sediment and biogeochemical model to understand estuarine nutrient dynamics under various water quality scenarios. Ocean Coast. Man. 83, 52–66.

Skerratt, J., Mongin, M., Wild-Allen, K. A., Baird, M. E., Robson, B. J., Schaffelke, B., Soja-Woźniak, M., Margvelashvili, N., Davies, C. H., Richardson, A. J., Steven, A. D. L., 2019. Simulated nutrient and plankton dynamics in the Great Barrier Reef (2011-2016). J. Mar. Sys. 192, 51–74.

Wild-Allen, K., Herzfeld, M., Thompson, P. A., Rosebrock, U., Parslow, J., Volkman, J. K., 2010. Applied coastal biogeochemical modelling to quantify the environmental impact of fish farm nutrients and inform managers. J. Mar. Sys. 81, 134–147.

Wild-Allen, K., Skerratt, J., Whitehead, J., Rizwi, F., Parslow, J., 2013. Mechanisms driving estuarine water quality: a 3D biogeochemical model for informed management. Est. Coast. Shelf Sci. 135, 33–45.

Wild-Allen, K. and Andrewartha, J., 2016. Connectivity between estuaries influences nutrient transport, cycling and water quality Mar. Chem. 185, 12-26

Box 1. Comments on the model approach.

Throw up a handful of feathers, and all must fall to the ground according to definite laws; but how simple is this problem compared to the action and reaction of the innumerable plants and animals which have determined, in the course of centuries, the proportional numbers and kinds.
Charles Darwin, The Origin of Species (1859)

Darwin's thoughts while pondering the predictability of river bank flora and fauna says much to our task of aquatic ecological modelling. Firstly, we might expect to do a good job representing the sinking of a handful of different types of plankton! In fact, if an ecological process has a physical limit with a geometric origin that we can parameterise, we might expect to be able to accurately predict the rate of the process. Physical limits that are used in the model include the diffusion of nutrients to the surface of microalgae and macroalgae, the capture of light by microalgae and macrophytes, and the encounter of plankton predators and prey.

Further, it seems reasonable to propose that at the bottom of the food chain, physical limits may be common. Natural selection will refine physiological processes, and even adapt organism anatomy to shapes with favourable physical limits. But paradoxically, the more refined the physiological processes, the more the organism is constrained by the physical limit.

Our greatest uncertainty lies in the physiological limits. Given this uncertainty, keeping the parameterisation of physiological processes simple is an advantage. Thus, physiological limits in the model are often parameterised with just one or two parameters for each organism, typically the maximum growth rate and the mortality / respiration rate. The maximum growth rate captures the organism's growth when all physical limits are faster than the organism's physiology requires. The model has ∼70 parameters that represent physiological and / or chemical processes and ∼30 that represent geometric properties. The model has about ∼60 state variables. Thus for such a complex model, it is relatively well constrained.

Finally, though every effort may be made to constrain the model, there is a time-limit to prediction of model state due to action and reaction (i.e. deterministic, non-linear interactions), that cannot be overcome through refinement of initial conditions and / or perfect model parameterisations (Baird and Suthers, 2010). But like weather and climate modelling, while the instantaneous state may be predictable for only a finite time interval, statistical properties such as the mean and variability of model variables can be predictable over longer periods. Thus, Darwin saw past the problem of instantaneous state prediction of river bank ecology to see that the outcome of such actions and reactions could, over time, explain the origin of species ...

[PS. When referring to falling feathers, Darwin is most likely thinking of George Stokes (of Navier-Stokes fame), who, in 1851, geometrically-derived a law for the terminal velocity of a falling sphere (Eq. 60). They later collaborated on the colours reflected in a peacock's tail!]

10 Acknowledgements

What models can do is make the most of existing scientific knowledge, a major undertaking by any standards.

A Reef in Time: The Great Barrier Reef from Beginning to End (Veron, 2008)

Many scientists and projects have contributed resources and knowhow to the development of this model over 15+ years. For this dedication we are very grateful.

Those who have contributed to the numerical code include (CSIRO unless stated):

Mike Herzfeld, Philip Gillibrand, John Andrewartha, Farhan Rizwi, Jenny Skerratt, Mathieu Mongin, Mark Baird, Karen Wild-Allen, John Parlsow, Emlyn Jones, Nugzar Margvelashvili, Pavel Sakov, Jason Waring, Stephen Walker, Uwe Rosebrock, Brett Wallace, Ian Webster, Barbara Robson, Scott Hadley (University of Tasmania), Malin Gustafsson (University of Technology Sydney, UTS), Matthew Adams (University of Queensland, UQ).

Collaborating scientists include:

Bronte Tilbrook, Andy Steven, Thomas Schroeder, Nagur Cherukuru, Peter Ralph (UTS), Russ Babcock, Kadija Oubelkheir, Bojana Manojlovic (UTS), Stephen Woodcock (UTS), Stuart Phinn (UQ), Chris Roelfsema (UQ), Miles Furnas (AIMS), David McKinnon (AIMS), David Blondeau-Patissier (Charles Darwin University), Michelle Devlin (James Cook University), Eduardo da Silva (JCU), Julie Duchalais, Jerome Brebion, Leonie Geoffroy, Yair Suari, Cloe Viavant, Lesley Clementson (pigment absorption coefficients), Dariusz Stramski (inorganic absorption and scattering coefficients), Erin Kenna, Line Bay (AIMS), Neal Cantin (AIMS) and Luke Morris (AIMS).

Funding bodies: CSIRO Wealth from Oceans Flagship, Gas Industry Social & Environmental Research Alliance (GISERA), CSIRO Coastal Carbon Cluster, Derwent Estuary Program, INFORM2, eReefs, Great Barrier Reef Foundation, Australian Climate Change Science Program, University of Technology Sydney, Department of Energy and Environment, Integrated Marine Observing System (IMOS), National Environment Science Program (NESP TWQ Hub).

References

Alvarez, E., Nogueira, E., Lopez-Urrutia, A., 2017. *In vivo* single-cell fluorescence and size scaling of phytoplankton chlorophyll content. App. Env. Microbiol. 83, e03317–16.

Alvarez-Romero, J. G., Devlin, M., da Silva, E. T., Petus, C., Ban, N. C., Pressey, R. L., Kool, J., Roberts, J. J., Cerdeira-Estrada, S., Wenger, A. S., Brodie, J., 2013. A novel approach to model exposure of coastal-marine ecosystems to riverine flood plumes based on remote sensing techniques. J. Enviro. Manage. 119, 194–207.

Anthony, K. R. N., Kleypas, J. A., Gattuso, J.-P., 2011. Coral reefs modify their seawater carbon chemistry - implications for impacts of ocean acidification. Glob. Change. Biol. 17, 3655–3666.

Atkins, P. W., 1994. Physical Chemistry, 5th Edition. Oxford University Press, Oxford.

Atkinson, M. J., 1992. Productivity of Eniwetak atoll reef predicted from mass-transfer relationships. Cont. Shelf Res. 12, 799–807.

Atkinson, M. J., Bilger, B. W., 1992. Effects of water velocity on phosphate uptake in coral reef-flat communities. Limnol. Oceanogr. 37, 273–279.

Atkinson, M. J., Smith, S. V., 1983. C:N:P ratios of benthic marine plants. Limnol. Oceanogr. 28, 568–574.

Babcock, R. C., Baird, M. E., Pillans, R., Patterson, T., Clementson, L. A., Haywood, M. E., Rochester, W., Morello, E., Kelly, N., Oubelkheir, K., Fry, G., Dunbabin, M., Perkins, S., Forcey, K., Cooper, S., Donovan, A., Kenyon, R., Carlin, G., Limpus, C., 2015. Towards an integrated study of the Gladstone marine system 278 pp ISBN: 978-1-4863-0539-1. Tech. rep., CSIRO Oceans and Atmosphere Flagship, Brisbane.

Baird, M. E., 2003. Numerical approximations of the mean absorption cross-section of a variety of randomly oriented microalgal shapes. J. Math. Biol. 47, 325–336.

Baird, M. E., Adams, M. P., Babcock, R. C., Oubelkheir, K., Mongin, M., Wild-Allen, K. A., Skerratt, J., Robson, B. J., Petrou, K., Ralph, P. J., O'Brien, K. R., Carter, A. B., Jarvis, J. C., Rasheed, M. A., 2016a. A biophysical representation of seagrass growth for application in a complex shallow-water biogeochemical model. Ecol. Model. 325, 13–27.

Baird, M. E., Cherukuru, N., Jones, E., Margvelashvili, N., Mongin, M., Oubelkheir, K., Ralph, P. J., Rizwi, F., Robson, B. J., Schroeder, T., Skerratt, J., Steven, A. D. L., Wild-Allen, K. A., 2016b. Remote-sensing reflectance and true colour produced by a coupled hydrodynamic, optical, sediment, biogeochemical model of the Great Barrier Reef, Australia: comparison with satellite data. Env. Model. Softw. 78, 79–96.

Baird, M. E., Emsley, S. M., 1999. Towards a mechanistic model of plankton population dynamics. J. Plankton Res. 21, 85–126.

Baird, M. E., Emsley, S. M., McGlade, J. M., 2001. Modelling the interacting effects of nutrient uptake, light capture and temperature on phytoplankton growth. J. Plankton Res. 23, 829–840.

Baird, M. E., Middleton, J. H., 2004. On relating physical limits to the carbon: nitrogen ratio of unicellular algae and benthic plants. J. Mar. Sys. 49, 169–175.

Baird, M. E., Mongin, M., Rizwi, F., Bay, L. K., Cantin, N. E., Soja-Woźniak, M., Skerratt, J., 2018. A mechanistic model of coral bleaching due to temperature-mediated light-driven reactive oxygen build-up in zooxanthellae. Ecol. Model. 386, 20–37.

Baird, M. E., Oke, P. R., Suthers, I. M., Middleton, J. H., 2004a. A plankton population model with bio-mechanical descriptions of biological processes in an idealised 2-D ocean basin. J. Mar. Sys. 50, 199–222.

Baird, M. E., Ralph, P. J., Rizwi, F., Wild-Allen, K. A., Steven, A. D. L., 2013. A dynamic model of the cellular carbon to chlorophyll ratio applied to a batch culture and a continental shelf ecosystem. Limnol. Oceanogr. 58, 1215–1226.

Baird, M. E., Roughan, M., Brander, R. W., Middleton, J. H., Nippard, G. J., 2004b. Mass transfer limited nitrate uptake on a coral reef flat, Warraber Island, Torres Strait, Australia. Coral Reefs 23, 386–396.

Baird, M. E., Suthers, I. M., 2010. Increasing model structural complexity inhibits the growth of initial condition errors. Ecol. Comp. 7, 478486.

Baird, M. E., Timko, P. G., Suthers, I. M., Middleton, J. H., 2006. Coupled physical-biological modelling study of the East Australian Current with idealised wind forcing. Part I: Biological model intercomparison. J. Mar. Sys. 59, 249–270.

Baird, M. E., Timko, P. G., Wu, L., 2007. The effect of packaging of chlorophyll within phytoplankton and light scattering in a coupled physical-biological ocean model. Mar. Fresh. Res. 58, 966–981.

Baird, M. E., Walker, S. J., Wallace, B. B., Webster, I. T., Parslow, J. S., 2003. The use of mechanistic descriptions of algal growth and zooplankton grazing in an estuarine eutrophication model. Est., Coastal and Shelf Sci. 56, 685–695.

Beckmann, A., Hense, I., 2004. Torn between extremes: the ups and downs of phytoplankton. Ocean Dynamics 54, 581–592.

Behrenfeld, M. J., Westberry, T. K., Boss, E. S., O'Malley, R. T., Siegel, D. A., Wiggert, J. D., Franz, B. A., McClain, C. R., Feldman, G. C., Doney, S. C., Moore, J. K., Dall'Olmo, G., Milligan, A. J., Lima, I., Mahowald, N., 2009. Satellite-detected fluorescence reveals global physiology of ocean phytoplankton. Biogeosciences 6 (5), 779–794.

Blondeau-Patissier, D., Brando, V. E., Oubelkheir, K., Dekker, A. G., Clementson, L. A., Daniel, P., 2009. Bio-optical variability of the absorption and scattering properties of the Queensland inshore and reef waters, Australia. J. Geophys. Res. (Oceans) 114, C05003.

Bohren, C. F., Huffman, D. R., 1983. Absorption and scattering of light particles by small particles. John Wiley & Sons.

Boudreau, B. P., 1996. A method-of-lines code for carbon and nutrient diagenesis in aquatic sediments. Comp. Geosci. 22, 479–496.

Brando, V. E., Dekker, A. G., Park, Y. J., Schroeder, T., 2012. Adaptive semianalytical inversion of ocean color radiometry in optically complex waters. Applied Optics 51, 2808–2833.

Cambridge, M. L., Lambers, H., 1998. Specific leaf area and functional leaf anatomy in Western Australian seagrasses. In: Lambers, H., Poorter, H., Vuren, M. M. I. V. (Eds.), Inherent variations in plant growth: physiological mechanisms and ecological consequences. Backhuys, Leiden, pp. 88–99.

Carpenter, E., ONeil, J., Dawson, R., Capone, D., Siddiqui, P., Roenneberg, T., Bergman, B., 1993. The tropical diazotrophic phytoplankter *Trichodesmium*: Biological characteristics of two common species. Marine Ecology Progress Series 95, 295–304.

Chartrand, K. M., , Bryant, C. V., Sozou, A., Ralph, P. J., Rasheed, M. A., 2017. Final Report: Deepwater seagrass dynamics: Light requirements, seasonal change and mechanisms of recruitment. Tech. rep., Centre for Tropical Water and Aquatic Ecosystem Research (TropWATER) Publication, James Cook University, Report No 17/16. Cairns, 67 pp.

Chartrand, K. M., Ralph, P. J., Petrou, K., Rasheed, M. A., 2012. Development of a Light-Based Seagrass Management Approach for the Gladstone Western Basin Dredging Program. Tech. rep., DAFF Publication. Fisheries Queensland, Cairns 126 pp.

Clementson, L. A., Wojtasiewicz, B., sub. 9th Jan 2019. Absorption characteristics of phytoplankton pigments. Data in Brief .

Condie, S. A., Herzfeld, M., Margvelashvili, N., Andrewartha, J. R., 2009. Modeling the physical and biogeochemical response of a marine shelf system to a tropical cyclone. Geophys. Res. Lett. 36 (L22603).

Dekker, A. G., Phinn, S. R., Anstee, J., Bissett, P., Brando, V. E., Casey, B., Fearns, P., Hedley, J., Klonowski, W., Lee, Z. P., Lynch, M., Lyons, M., Mobley, C., Roelfsema, C., 2011. Intercomparison of shallow water bathymetry, hydro-optics, and benthos mapping techniques in Australian and Caribbean coastal environments. Limnol. Oceanogr.: Methods 9, 396–425.

Devlin, M., da Silva, E., Petus, C., Wenger, A., Zeh, D., Tracey, D., Alvarez-Romero, J., Brodie, J., 2013. Combining in-situ water quality and remotely sensed data across spatial and temporal scales to measure variability in wet season chlorophyll-a: Great Barrier Reef lagoon (Queensland, Australia). Ecological Processes 2, 31.

Dormand., J. R., Prince, P. J., 1980. A family of embedded Runge-Kutta formulae. J. Comp. App. Math. 6, 19–26.

Duarte, C. M., Chiscano, C. L., 1999. Seagrass biomass and production: a reassessment. Aquat. Bot. 65, 159–174.

Dutkiewicz, S., Hickman, A. E., Jahn, O., Gregg, W. W., Mouw, C. B., Follows, M. J., 2015. Capturing optically important constituents and properties in a marine biogeochemical and ecosystem model. Biogeosciences Discussions 12, 2607–2695.

Duysens, L. N. M., 1956. The flattening of the absorption spectra of suspensions as compared to that of solutions. Biochim. Biophys. Acta 19, 1–12.

Eyre, B. D., Cyronak, T., Drupp, P., Carlo, E. H. D., Sachs, J. P., Andersson, A. J., 2018. Coral reefs will transition to net dissolving before end of century. Science 359, 908–911.

Falkowski, P. G., Raven, J. A., 2007. Aquatic Photosynthesis, 2nd Edition. Blackwell Science.

Falter, J. L., Atkinson, M. J., Merrifield, M. A., 2004. Mass-transfer limitation of nutrient uptake by a wave-dominated reef flat community. Limnol. Oceanogr. 49, 1820–1831.

Fasham, M. J. R., Ducklow, H. W., McKelvie, S. M., 1990. A nitrogen-based model of plankton dynamics in the oceanic mixed layer. J. Mar. Res. 48, 591–639.

Ficek, D., Kaczmarek, S., Stoń-Egiert, J., Woźniak, B., Majchrowski, R., Dera, J., 2004. Spectra of light absorption by phytoplankton pigments in the Baltic; conclusions to be drawn from a Gaussian analysis of empirical data. Oceanologia 46, 533–555.

Finkel, Z. V., 2001. Light absorption and size scaling of light-limited metabolism in marine diatoms. Limnol. Oceanogr. 46, 86–94.

Gentleman, W., 2002. A chronology of plankton dynamics *in silico*: how computer models have been used to study marine ecosystems. Hydrobiologica 480, 69–85.

Gillibrand, P. A., Herzfeld, M., 2016. A mass-conserving advection scheme for offline simulation of tracer transport in coastal ocean models. Env. Model. Soft. 101, 1–16.

Grant, . D., Madsen, O., 1982. Movable bed roughness in unsteady oscillatory flow. J. Geophys. Res. 87(C1), 469–481.

Gras, A. F., Koch, M. S., Madden, C. J., 2003. Phosphorus uptake kinetics of a dominant tropical seagrass *Thalassia testudinum* . Aqu. Bot. 76, 299–315.

Griffies, S. M., Harrison, M. J., Pacanowski, R. C., Rosati, A., March 2004. A technical guide to MOM4 GFDL Ocean Group Technical Report No. 5 Version prepared on March 3, 2004. Tech. rep., NOAA/Geophysical Fluid Dynamics Laboratory.

Gumley, L., Descloitres, J., Shmaltz, J., 2010. Creating reprojected true color MODIS images: A tutorial, Tech. Rep 1.0.2, 17 pp. Tech. rep., Univ. of Wisconsin, Madison.

Gustafsson, M. S. M., Baird, M. E., Ralph, P. J., 2013. The interchangeability of autotrophic and heterotrophic nitrogen sources in scleractinian coral symbiotic relationships: a numerical study. Ecol. Model. 250, 183–194.

Gustafsson, M. S. M., Baird, M. E., Ralph, P. J., 2014. Modelling photoinhibition and bleaching in Scleractinian coral as a function of light, temperature and heterotrophy. Limnol. Oceanogr. 59, 603–622.

Hadley, S., Wild-Allen, K. A., Johnson, C., Macleod, C., 2015a. Modeling macroalgae growth and nutrient dynamics for integrated multi-trophic aquaculture. J. Appl. Phycol. 27, 901–916.

Hadley, S., Wild-Allen, K. A., Johnson, C., Macleod, C., 2015b. Quantification of the impacts of finfish aquaculture and bioremediation capacity of integrated multi-trophic aquaculture using a 3D estuary model. J. Appl. Phycol. 10.1007/s10811-015-0714-2.

Hamilton, L. J., 2001. Cross-shelf colour zonation in northern Great Barrier Reef lagoon surficial sediments. Aust. J. Earth Sci. 48, 193–200.

Hansell, D. A., Carlson, C. A., Repeta, D. J., Schlitzer, R., 2009. Dissolved organic matter in the ocean. Oceanography 22, 202–211.

Hansen, J. W., Udy, J. W., Perry, C. J., Dennison, W. C., Lomstein, B. A., 2000. Effect of the seagrass *Zostera capricorni* on sediment microbial processes. Mar. Ecol. Prog. Ser. 199, 83–96.

Hansen, P. J., Bjornsen, P. K., Hansen, B. W., 1997. Zooplankton grazing and growth: Scaling within the 2-2,000 μm body size range. Limnol. Oceanogr. 42, 687–704.

Herzfeld, M., 2006. An alternative coordinate system for solving finite difference ocean models. Ocean Modelling 14 (3-4), 174 – 196.

Hill, R., Brown, C. M., DeZeeuw, K., Campbell, D. A., Ralph, P. J., 2011. Increased rate of D1 repair in coral symbionts during bleaching is insufficient to counter accelerated photo-inactivation. Limnol. Oceanogr. 56, 139–146.

Hill, R., Whittingham, C. P., 1955. Photosynthesis. Methuen, London.

Hochberg, E. J., Apprill, A. M., Atkinson, M. J., Bidigare, R. R., 2006. Bio-optical modeling of photosynthetic pigments in corals. Coral Reefs 25, 99–109.

Hundsdorfer, W., Verwer, J. G., 2003. Numerical solutions of time-dependent advection-diffusion-reaction equations. Springer.

Huot, Y., Brown, C. A., Cullen, J. J., 2005. New algorithms for MODIS sun-induced chlorophyll fluorescence and a comparison with present data products. Limnol. Oceanogr. Methods 3, 108–130.

Hurd, C. L., 2000. Water motion, marine macroalgal physiology, and production. J. Phycol. 36, 453–472.

Jackson, G. A., 1995. Coagulation of marine algae. In: Huang, C. P., O'Melia, C. R., Morgan, J. J. (Eds.), Aquatic Chemistry: Interfacial and Interspecies Processes. American Chemical Society, Washington, DC, pp. 203–217.

Kaldy, J. E., Brown, C. A., Andersen, C. P., 2013. *In situ* ^{13}C tracer experiments elucidate carbon translocation rates and allocation patterns in eelgrass *Zostera marina* . Mar. Ecol. Prog. Ser. 487, 27–39.

Kemp, W. M., Murray, L., Borum, J., Sand-Jensen, K., 1987. Diel growth in eelgrass *Zostera marina*. Mar. Ecol. Prog. Ser. 41, 79–86.

Kirk, J. T. O., 1975. A theoretical analysis of the contribution of algal cells to the attenuation of light within natural waters. I. General treatment of suspensions of pigmented cells. New Phytol. 75, 11–20.

Kirk, J. T. O., 1991. Volume scattering function, average cosines, and the underwater light field. Limnol. Oceanogr. 36, 455–467.

Kirk, J. T. O., 1994. Light and Photosynthesis in Aquatic Ecosystems, 2nd Edition. Cambridge University Press, Cambridge.

Kooijman, S. A. L. M., 2010. Dynamic Energy Budget theory for metabolic organisation, 3rd Edition. Cambridge University Press.

Lee, K.-S., Dunton, K. H., 1999. Inorganic nitrogen acquisition in the seagrass *Thalassia testudinum* : Development of a whole-plant nitrogen budget. Limnol. Oceanogr. 44, 1204–1215.

Lee, Z., Carder, K. L., Arnone, R. A., 2002. Deriving inherent optical properties from water color: a multiband quasi-analytical algorithm for optically deep waters. Applied Optics 41, 5755–5772.

Lee, Z., Shang, S., Hu, C., Du, K., Weidermann, A., Hou, W., Lin, J., Lin, G., 2015. Secchi disk depth: A new theory and mechanistic model for underwater visibility. Remote sensing of environment 169, 139–149.

Leiper, I., Phinn, S., Dekker, A. G., 2012. Spectral reflectance of coral reef benthos and substrate assemblages on Heron Reef, Australia. Int. J. of Rem. Sens. 33, 3946–3965.

Lilley, R. M., Ralph, P. J., Larkum, A. W. D., 2010. The determination of activity of the enzyme rubisco in cell extracts of the dinoflagellate alga symbiodinium sp. by manganese chemiluminescence and its response to short-term thermal stress of the alga. Plant, Cell & Environment 33 (6), 995–1004.

Liu, G., Heron, S. F., Eakin, C. M., Muller-Karger, F. E., Vega-Rodriguez, M., Guild, L., Cour, J. L. D. L., Geiger, E. F., Skirving, W. J., Burgess, T. F. R., 2014. Reef-scale Thermal Stress Monitoring of Coral Ecosystems: New 5-km Global Products from NOAA Coral Reef Watch. Remote Sens. 6, 11579–11606.

Longstaff, B. J., 2003. Investigations into the light requirements of seagrasses in northeast Australia. Ph.D. thesis, University of Queensland.

LØnborg, C., Álvarez–Salgado, X. A., Duggan, S., Carreira, C., 2017. Organic matter bioavailability in tropical coastal waters: The Great Barrier Reef. Limnol. Oceanogr. in press, .

Macdonald, H. S., Baird, M. E., Middleton, J. H., 2009. The effect of wind on continental shelf carbon fluxes off southeast Australia: a numerical model. J. Geophys. Res. 114, C05016,doi:10.1029/2008JC004946.

Mann, K. H., Lazier, J. R. N., 2006. Dynamics of Marine Ecosystems, 3rd Edition. Blackwell Scientific Publications Inc., Oxford.

Margvelashvili, N., 2009. Stretched Eulerian coordinate model of coastal sediment transport. Computer Geosciences 35, 1167–1176.

McKenzie, L. J., 1994. Seasonal changes in biomass and shoot characteristics of a *Zostera capricorni*Aschers. dominant meadow in Cairns Harbour, northern Queensland. Aust. J. Mar. Freshwater. Res. 45, 1337–52.

Miller, R. L., McKee, B. A., 2004. Using modis terra 250 m imagery to map concentrations of suspended matter in coastal waters. Remote Sens. Environ. 93, 259–266.

Mishchenko, M. I., Travis, L. D., Lacis, A. A., 2002. Scattering, Absorption and Emission of Light by Small Particles. Cambridge University Press.

Mobley, C. D., 1994. Light and Water. Academic Press.

Monbet, P., Brunskill, G. J., Zagorskis, I., Pfitzner, J., 2007. Phosphorus speciation in the sediment and mass balance for the central region of the Great Barrier Reef continental shelf (Australia). Geochimica et Cosmochimica Acta 71, 2762–2779.

Mongin, M., Baird, M. E., 2014. The interacting effects of photosynthesis, calcification and water circulation on carbon chemistry variability on a coral reef flat: a modelling study. Ecol. Mod. 284, 19–34.

Mongin, M., Baird, M. E., Tilbrook, B., Matear, R. J., Lenton, A., Herzfeld, M., Wild-Allen, K. A., Skerratt, J., Margvelashvili, N., Robson, B. J., Duarte, C. M., Gustafsson, M. S. M., Ralph, P. J., Steven, A. D. L., 2016. The exposure of the Great Barrier Reef to ocean acidification. Nature Communications 7, 10732.

Monismith, S. G., Davis, K. A., Shellenbarger, G. G., Hench, J. L., Nidzieko, N. J., Santoro, A. E., Reidenbach, M. A., Rosman, J. H., Holtzman, R., Martens, C. S., Lindquist, N. L., Southwell, M. W., Genin, A., 2010. Flow effects on benthic grazing on phytoplankton by a Caribbean reef. Limnol. Oceanogr. 55, 1881–1892.

Monsen, N., Cloern, J., Lucas, L., Monismith, S. G., 2002. A comment on the use of flushing time, residence time, and age as transport time scales. Limnol. Oceanogr. 47, 1545–1553.

Morel, A., Bricaud, A., 1981. Theoretical results concerning light absorption in a discrete medium, and application to specific absorption of phytoplankton. Deep Sea Res. 28, 1375–1393.

Muller-Parker, G., Cook, C. B., D'Elia, C. F., 1994. Elemental composition of the coral *Pocillopora damicornis* exposed to elevated seawater ammonium. Pac. Sci. 48, 234–246.

Munhoven, G., 2013. Mathematics of the total alkalinity-pH equation pathway - to robust and universal solution algorithms: the SolveSAPHE package v1.0.1. Geosci. Model Dev. 6, 1367–1388.

Najjar, R., Orr, J., 1999. Biotic-howto. internal ocmip report, lsce/cea saclay, gif-sur-yvette, france 15. Tech. rep.

Nielsen, M. V., Sakshaug, E., 1993. Photobiological studies of *Skeletonema costatum* adapted to spectrally different light regimes. Limnol. Oceanogr. 38, 1576–1581.

Pailles, C., Moody, P. W., 1992. Phosphorus sorption-desorption by some sediments of the Johnstone Rivers catchments, northern Queensland. Aust. J. Mar. Freshwater Res. 43, 1535–1545.

Pasciak, W. J., Gavis, J., 1975. Transport limited nutrient uptake rates in *Dictylum brightwellii*. Limnol. Oceanogr. 20 (4), 604–617.

Petrou, K., Jimenez-Denness, I., Chartrand, K., McCormack, C., Rasheed, M., Ralph, P. J., 2013. Seasonal heterogeneity in the photophysiological response to air exposure in two tropical intertidal seagrass species. Mar. Ecol. Prog. Ser. 482, 93–106.

Petus, C., Marieua, V., Novoac, S., Chust, G., Bruneau, N., Froidefond, J.-M., 2014. Monitoring spatio-temporal variability of the Adour River turbid plume (Bay of Biscay, France) with MODIS 250-m imagery. Cont. Shelf Res. 74, 35–49.

Raven, J. A., 1997. Phagotrophy in phototrophs. Limnol. Oceanogr. 42, 198–205.

Redfield, A. C., Ketchum, B. H., Richards, F. A., 1963. The influence of organisms on the composition of sea-water. In: Hill, N. (Ed.), The sea, 2nd Edition. Wiley, pp. 26–77.

Reichstetter, M., Fearns, P. R., Weeks, S. J., McKinna, L. I., Roelfsema, C., Furnas, M., 2015. Bottom reflectance in ocean color satellite remote sensing for coral reef environments. Remote Sens. 7, 15852.

Ribes, M., Atkinson, M. J., 2007. Effects of water velocity on picoplankton uptake by coral reef communities. Coral Reefs 26, 413–421.

Ridgway, K. R., Dunn, J. R., 2003. Mesoscale structure of the mean East Australian Current System and its relationship with topography. Prog. Oceanogr, 56, 189–222.

Roberts, D. G., 1993. Root-hair structure and development in the seagrass *Halophila ovalis* (R. Br.) Hook. f. Aust. J. Mar. Freshw. Res. 44, 85–100.

Robson, B. J., Arhonditsis, G., Baird, M., Brebion, J., Edwards, K., Geoffroy, L., Hbert, M.-P., van Dongen-Vogels, V., Jones, E., Kruk, C., Mongin, M., Shimoda, Y., Skerratt, J., Trevathan-Tackett, S., Wild-Allen, K., Kong, X., Steven, A., 2018. Towards evidence-based parameter values and priors for aquatic ecosystem modelling. Env. Mod. Soft. 100, 74–81.

Robson, B. J., Baird, M. E., Wild-Allen, K. A., 2013. A physiological model for the marine cyanobacteria, *Trichodesmium*. In: Piantadosi, J. R. S. A., Boland, J. (Eds.), MODSIM2013, 20th International Congress on Modelling and Simulation. Modelling and Simulation Society of Australia and New Zealand, ISBN: 978-0-9872143-3-1, www.mssanz.org.au/modsim2013/L5/robson.pdf, pp. 1652–1658.

Roelfsema, C. M., Phinn, S. R., 2012. Spectral reflectance library of selected biotic and abiotic coral reef features in Heron Reef. Tech. rep., Centre for Remote Sensing and Spatial Information Science, School of Geography, Planning and Environmental Management, University of Queensland, Brisbane, Australia, doi:10.1594/PANGAEA.804589.

Sathyendranath, S., Stuart, V., Nair, A., Oke, K., Nakane, T., Bouman, H., Forget, M.-H., Maass, H., Platt, T., 2009. Carbon-to-chlorophyll ratio and growth rate of phytoplankton in the sea. Mar. Ecol. Prog. Ser. 383, 73–84.

Schroeder, T., Devlin, M. J., Brando, V. E., Dekker, A. G., Brodie, J. E., Clementson, L. A., McKinna, L., 2012. Inter-annual variability of wet season freshwater plume extent into the Great Barrier Reef lagoon based on satellite coastal ocean colour observations. Mar. Poll. Bull. 65, 210–223.

Smith, R. C., Baker, K. S., 1981. Optical properties of the clearest natural waters. Applied Optics 20, 177–184.

Soja-Woźniak, M., Baird, M. E., Schroeder, T., Qin, Y., Clementson, L., Baker, B., Boadle, D., Brando, V., Steven, A., submitted. Particulate backscattering ratio as an indicator of changing particle composition in coastal waters: observations from Great Barrier Reef waters. J. Geophys. Res. (Oceans) , .

Straile, D., 1997. Gross growth efficiencies of protozoan and metazoan zooplankton and their dependence on food concentration, predator-prey weight ratio, and taxonomic group. Limnol. Oceanogr. 42, 1375–1385.

Stramski, D., Babin, M., Wozniak, S. B., 2007. Variations in the optical properties of terrigenous mineral-rich particulate matter suspended in seawater. Limnol. Oceanogr. 52, 2418–2433.

Subramaniam, A., Carpenter, E. J., Karentz, D., Falkowski, P. G., 1999. Bio-optical properties of the marine diazotrophic cyanobacteria *Trichodesmium* spp. I. Absorption and photosynthetic action spectra. Limnol. Oceanogr. 44, 608–617.

Suggett, D. J., MacIntyre, H. L., Kana, T. M., Geider, R. J., 2009. Comparing electron transport with gas exchange: parameterising exchange rates between alternative photosynthetic currencies for eukaryotic phytoplankton. Aquat. Microb. Ecol. 56, 147–162.

Suggett, D. J., Warner, M. E., Smith, D. J., Davey, P., Hennige, S., Baker, N. R., 2008. Photosynthesis and production of hydrogen peroxide by *Symbiodinium* (Pyrrhophyta) phylotypes with different thermal tolerances. J. Phycol. 44, 948–956.

Vaillancourt, R. D., Brown, C. W., Guillard, R. R. L., Balch, W. M., 2004. Light backscattering properties of marine phytoplankton: relationship to cell size, chemical composition and taxonomy. J. Plank. Res. 26, 191–212.

Vermaat, J. E., Agawin, N. S. R., Duarte, C. M., Fortes, M. D., Marba, N., Uri, J. S., 1995. Meadow maintenance, growth and productivity of a mixed Philippine seagrass bed. Mar. Ecolo. Prog. Ser. 124, 215–225.

Veron, J. E. N., 2008. A Reef in Time: The Great Barrier Reef from Beginning to End. Harvard University Press.

Wanninkhof, R., 1992. Relationship between wind speed and gas exchange over the ocean. J. Geophys. Res. 97 (C5), 7373–7382.

Wanninkhof, R., McGillis, W. R., 1999. A cubic relationship between air-sea CO_2 exchange and wind speed. Geophys. Res. Letts. 26, 1889–1892.

Weeks, S., Werdell, P. J., Schaffelke, B., Canto, M., Lee, Z., Wilding, J. G., Feldman, G. C., 2012. Satellite-derived photic depth on the Great Barrier Reef: spatio-temporal patterns of water clarity. Remote Sens. 4, 3781–3795.

Weiss, R., 1970. The solubility of nitrogen, oxygen and argon in water and seawater. Deep Sea Res. 17, 721–735.

Wild-Allen, K., Herzfeld, M., Thompson, P. A., Rosebrock, U., Parslow, J., Volkman, J. K., 2010. Applied coastal biogeochemical modelling to quantify the environmental impact of fish farm nutrients and inform managers. J. Mar. Sys. 81, 134–147.

Wojtasiewicz, B., Stoń-Egiert, J., 2016. Bio-optical characterization of selected cyanobacteria strains present in marine and freshwater ecosystems. Journal of Applied Phycology 28, 22992314.

Wright, S., Thomas, D., Marchant, H., Higgins, H., Mackey, M., Mackey, D., 1996. Analysis of Phytoplankton of the Australian Sector of the Southern Ocean:comparisons of Microscopy and Size Frequency Data with Interpretations of Pigment HPLC Data Using the CHEMTAX Matrix Factorisation Program. Marine Ecology Progress Series 144, 285–98.

Wyatt, A. S. J., Lowe, R. J., Humphries, S., Waite, A. M., 2010. Particulate nutrient fluxes over a fringing coral reef: relevant scales of phytoplankton production and mechanisms of supply. Mar. Ecol. Prog. Ser. 405, 113–130.

Yonge, C. M., 1930. A year on the Great Barrier Reef. Putham, London.

Zeebe, R. E., Wolf-Gladrow, D., 2001. CO_2 in seawater: equilibrium, kinetics isotopes. Elsevier.

Zhang, Z., Lowe, R., Falter, J., Ivey, G., 2011. A numerical model of wave- and current-driven nutrient uptake by coral reef communities. Ecol. Mod. 222, 1456–1470.

A State (prognostic) variables

The below tables list the ecologically-relevant physical variables (Table 44), 10 dissolved (Table 45), 20 microalgal (Table 46), 2 zooplankton (Table 47), 7 non-living inorganic particulate (Table 48), 7 non-living organic particulate (Table 49) and 7 epibenthic plant (Table 50) and 5 coral polyp (Table 51) and 4 reaction centre (Table 52) state variables. All state variables that exist in the water column layers have an equivalent in the sediment layers (and are specified by `<variable name>_sed`). The dissolved tracers are given as a concentration in the porewater, while the particulate tracers are given as a concentration per unit volume (see Sec. 8.5.2).

Name	Symbol	Units	Description
Temperature (temp)	T	°C	Water temperature
Salinity (salt)	S	PSU	Water salinity
Sea level elevation (eta)	η	m	Sea level elevation relative to mean sea level
Porosity (porosity)	ϕ	-	Fraction of the volume made up of water
Bottom shear stress (ustrcw_skin)	τ	N m^{-2}	Shear stress due to currents and waves
Sand ripple height (PHYSRIPH)	-	m	Physical dimension used for estimating bottom roughness due to ripples according to Grant and Madsen (1982)
Solar zenith (Zenith)	θ_{air}	radians	Solar zenith angle is the angle between the zenith and the centre of the Sun's disc, taking a value of zero with the sun directly above, and $\pi/2$ when at, or below, the horizon.

Table 44: Long name (and variable name) in model output files, symbol and units used in this document, and a description of ecologically-relevant physical state and diagnostic variables.

Name	Symbol	Units	Description
Total alkalinity (alk)	A_T	mol kg^{-1}	Concentration of ions that can be converted to uncharged species by a strong acid. The model assumes A_T =[HCO_3^-] + [CO_3^{2-}], often referred to as carbonate alkalinity. Alkalinity and DIC together quantify the equilibrium state of the seawater carbon chemistry.
Nitrate (NO3)	[NO_3^-]	mg N m^{-3}	Concentration of nitrate. In the absence of nitrite [NO_2^-] in the model, nitrate represents [NO_3^-] + [NO_2^-].
Ammonia (NH4)	[NH_4^-]	mg N m^{-3}	Concentration of ammonia.
Dissolved Inorganic Phosphorus (DIP)	P	mg P m^{-3}	Concentration of dissolved inorganic phosphorus, also referred to as orthophosphate or soluble reactive phosphorus, SRP, composed chiefly of HPO_4^{2-} ions, with a small percentage present as PO_4^{3-}.
Dissolved inorganic carbon (DIC)	DIC	mg C m^{-3}	Concentration of dissolved inorganic carbon, composed chiefly at seawater pH of HCO_3^-, with a small percentage present as CO_3^{2-}.
Dissolved oxygen (Oxygen)	[O_2]	mg O m^{-3}	Concentration of oxygen.
Chemical Oxygen Demand (COD)	COD	mg O m^{-3}	Concentration of products of anoxic respiration in oxygen units. This represents products such as hydrogen sulfide, H_2S, that are produced during anoxic respiration and which, upon reoxidation of the water, will consume oxygen.
Dissolved Organic Carbon (DOR_C)	O_C	mg C m^{-3}	The concentration of carbon in dissolved organic compounds.
Dissolved Organic Nitrogen (DOR_N)	O_N	mg N m^{-3}	The concentration of nitrogen in dissolved organic compounds.
Dissolved Organic Phosphorus (DOR_P)	O_P	mg P m^{-3}	The concentration of phosphorus in dissolved organic compounds.

Table 45: Long name (and variable name) in model output files, symbol and units used in this document, and a description of all dissolved state variables. When the concentration of an ion is given, the chemical formulae appears in [ ] brackets.

Name	Symbol & Units	Description
Phytoplankton N (*_N)	B [mg N m^{-3}]	Total structural biomass of nitrogen of the phytoplankton population. All microalgae have a C:N:P ratio of the structural material of 106:16:1. Thus the mass of phosphorus in the structural material of a population with a biomass B is given by: $\frac{1}{16}\frac{31}{14}B$ and the mass of carbon by: $\frac{106}{16}\frac{12}{14}$ B. The number of cells is given by B/m_N.
Phytoplankton N reserves (*_NR)	BR_N^* [mg N m^{-3}]	Total non-structural biomass of nitrogen of the phytoplankton population. Phytoplankton N reserves divided by Phytoplankton N is a number between 0 and 1 and represents the factor by which phytoplankton growth is inhibited due to the internal reserves of nitrogen.
Phytoplankton P reserves (*_PR)	$\frac{1}{16}\frac{31}{14}BR_P^*$ [mg P m^{-3}]	Total non-structural biomass of phosphorus of the phytoplankton population. Phytoplankton P reserves divided by (Phytoplankton N $\times\frac{1}{16}\frac{31}{14}$) is a number between 0 and 1 and represent the factor by which phytoplankton growth is inhibited due to the internal reserves of phosphorus.
Phytoplankton I reserves (*_I)	$\frac{1060}{16}\frac{1}{14}BR_I^*$ [mmol photon m^{-3}]	Total non-structural biomass of fixed carbon of the phytoplankton population, quantified in photons. Phytoplankton I reserves divided by (Phytoplankton N $\times\frac{1060}{16}\frac{1}{14}$) is a number between 0 and 1 and represent the factor by which phytoplankton growth is inhibited due to the internal reserves of energy (or fixed carbon).
Phytoplankton chlorophyll (*_Chl)	nc_iV [mg m^{-3}]	Concentration of the chlorophyll a pigment of the population. The four phytoplankton classes have two pigments, a chlorophyll a-based pigment and an accessory pigment. As the pigment concentration adjusts to optimise photosynthesis, including the presence of the accessory pigment, the intracellular content, c_iV, represents only the chlorophyll a-based pigment. As the model does not distinguish between monovinyl and di-vinyl forms of chlorophyll, this c_i represents either form, depending on the phytoplankton type.

Table 46: Long name (and variable name) in model output files, symbol and units used in this document, and description of all microalgae state variables in the model. The model contains four categories of phytoplankton (category shown as * in left column, and given in brackets in following list): small (PhyS), $r < 2$ μm phytoplankton; large (PhyL): $r > 2$ μm phytoplankton; *Trichodesmium* (Tricho): nitrogen fixing phytoplankton; and benthic microalgae (MPB): fast-sinking diatoms that are suspended primarily in the top layer of sediment porewaters. The elemental ratio of phytoplankton including both structural material and reserves is given by: C:N:P $= 106(1 + R_C^*) : 16(1 + R_N^*) : (1 + R_P^*)$. In the model description (this document) we have more correctly described fixed carbon as carbon reserves, while in the model outputs they are represented quantified as energy reserves. The relationship is 1 mg C of carbon reserves is equal to (1060/106)/12.01 mmol photons of energy reserves.

Name		Symbol	Units		Description
Zooplankton (ZooS_N, ZooL_N)	N	Z	[mg m^{-3}]	N	Total biomass of nitrogen in animals. With only small and large zooplankton categories resolved, small zooplankton represents the biomass of unicellular fast growing animals (protozoans) and large zooplankton represents the biomass of all other animals (metazoans). All zooplankton have a C:N:P ratio of 106:16:1. Thus the mass of phosphorus of a population with a biomass Z is given by: $\frac{1}{16}\frac{31}{14}Z$ and the mass of carbon by: $\frac{106}{16}\frac{12}{14}$ Z.

Table 47: Long name (and variable name) in model output files, symbol, unit used in this document, and description of zooplankton state variables in the model.

Name	Symbol	Units	Description
Fine Sediment (FineSed)	$FineSed$	[kg m^{-3}]	Identical to Mud-mineral, except that it is initialised to zero in the model domain, and enters only from the catchments.
Dust (Dust)	$Dust$	[kg m^{-3}]	Very small sized, re-suspending particles with a sinking velocity of 1 m d^{-1} and mass-specific optical properties based on observations in Gladstone Harbour.
Mud-mineral (Mud-mineral)	$Mud_{\mathrm{non-CaCO_3}}$	[kg m^{-3}]	Small sized, re-suspending particles with a sinking velocity of 17 m d^{-1}, and mass-specific optical properties based on observations in Gladstone Harbour.
Mud-carbonate (Mud-carbonate)	$Mud_{\mathrm{CaCO_3}}$	[kg m^{-3}]	Small sized, re-suspending particles with a sinking velocity of 17 m d^{-1}, and mass-specific optical properties based on observations of suspended carbonates at Lucinda Jetty.
Sand-mineral (Sand-mineral)	$Sand_{\mathrm{non-CaCO_3}}$	[kg m^{-3}]	Medium sized, re-suspending particles with a sinking velocity of 173 m d^{-1} and mass-specific optical properties based on observations in Gladstone Harbour.
Sand-carbonate (Sand-carbonate)	$Sand_{\mathrm{CaCO_3}}$	[kg m^{-3}]	Medium sized, re-suspending particles with a sinking velocity of 173 m d^{-1} and mass-specific optical properties based on observations of suspended carbonates at Lucinda Jetty.
Gravel-mineral (Gravel-mineral)	$Gravel_{\mathrm{non-CaCO_3}}$	[kg m^{-3}]	Large, non-resuspending particles.
Gravel-carbonate (Gravel-carbonate)	$Gravel_{\mathrm{CaCO_3}}$	[kg m^{-3}]	Large, non-resuspending particles.

Table 48: Long name (and variable name) in model output files, symbol, unit used in this document, and description of all inorganic particulate state variables in the model.

Name	Symbol	Units	Description
Particulate Inorganic Phosphorus (PIP)	PIP	[mg P m^{-3}]	Phosphorus ions that are absorbed onto particles. It is considered a particulate with the same properties as Mud.
Immobilised Particulate Inorganic Phosphorus (PIPI)	$PIPI$	[mg P m^{-3}]	Phosphorus that is permanently removed from the system through burial of PIP.
Labile Detritus Nitrogen Plank (DetPL_N)	D_{Red}	[mg N m^{-3}]	Concentration of N in labile (quickly broken down) organic matter with a C:N:P ratio of 106:16:1 derived from living microalgae, zooplankton, coral host tissue and zooxanthellae with the same C:N:P ratio. Thus the mass of phosphorus in D_{Red} is given by: $\frac{1}{16}\frac{31}{14}D_{Red}$ and the mass of carbon by: $\frac{106}{16}\frac{12}{14}D_{Red}$.
Labile Detritus Nitrogen Benthic (DetBL_N)	D_{Atk}	[mg N m^{-3}]	Concentration of N in labile (quickly broken down) organic matter with a C:N:P ratio of 550:30:1 derived from living seagrass and macroalgae with the same C:N:P ratio. Thus the mass of phosphorus in D_{Atk} is given by: $\frac{1}{30}\frac{31}{14}D_{Atk}$ and the mass of carbon by: $\frac{550}{30}\frac{12}{14}D_{Atk}$.
Refractory Detritus Carbon (DetR_C)	D_C	[mg C m^{-3}]	Concentration of carbon as particulate refractory (slowly breaking down) material. It is sourced only from the breakdown of labile detritus, and from rivers.
Refractory Detritus Nitrogen (DetR_N)	D_N	[mg N m^{-3}]	Concentration of nitrogen as particulate refractory (slowly breaking down) material. It is sourced only from the breakdown of labile detritus, and from rivers.
Refractory Detritus Phosphorus (DetR_P)	D_P	[mg P m^{-3}]	Concentration of phosphorus as particulate refractory (slowly breaking down) material. It is sourced only from the breakdown of labile detritus, and from rivers.

Table 49: Long name (and variable name) in model output files, symbol, unit used in this document, and description of all particulate detrital state variables in the model.

Name	Symbol	Description
Macroalgae (MA)	MA [g N m^{-2}]	Concentration of nitrogen biomass per m^2 of macrolagae. Macroalgae (or seaweed) grows above all other benthic plants (corals, seagrasses, benthic microalgae). It is parameterised as a non-calcifying leafy algae, with a C:N:P ratio of 550:30:1, and a formulation for calculating the percentage of the bottom covered as $1-\exp(-\Omega_{MA}MA)$. In the model, in the absence of both calcifying macroalgae (particularly *Halimeda*) and unicellular epiphytes, macroalgae represents the biomass of all seaweeds and epiphytes.
Seagrass (SG)	SG [g N m^{-2}]	Concentration of nitrogen biomass per m^2 of a seagrass form parameterised to be similar to *Zostera*. This form captures light after it has passed through macroalgae and before it passes through *Halophila*. This form is better adapted to high light, low nutrient conditions than *Halophila* as a result of a deeper root structure and being able to shade it. See macroalgae for elemental ratio and bottom cover.
Halophila (SGH)	SGH [g N m^{-2}]	Concentration of nitrogen biomass per m^2 of a seagrass form parameterised to be similar to *Halophila ovalis*. This form captures light after it has passed through the *Zostera* seagrass form. The *Halophila ovalis* form is batter adapted to low light conditions than *Zostera*, having a faster growth rate and lower minimum light requirement. See macroalgae for elemental ratio and bottom cover.
Deep seagrass (SGD)	SGD [g N m^{-2}]	Concentration of nitrogen biomass per m^2 of a seagrass form parameterised to be similar to *Halophila deciphens*. This form captures light after it has passed through the *Zostera* and *Halophila ovalis* seagrass form.
*root N	$*ROOT\_N$ [g N m^{-2}]	Concentration of nitrogen biomass per m^2 in the roots of seagrass type * (SG, SGH or SGD). While this biomass in reality exists in multiple depths in the sediments, and in the model accesses multiple layers for nutrient uptake, it is quantified in the epibenthic compartment.

Table 50: Long name (and variable name) in model output files, units, symbol used in this document, and description of macroalgae and seagrass state variables in the model. The order in the above table corresponds to their vertical position, and therefore the order in which they access light. Benthic microalage, being suspended in porewaters, is consider as a particulate in Table 48.

Name	Symbol	Description
Coral host N (CH_N)	CH [g N m^{-2}]	Concentration of nitrogen biomass per m^2 of coral host tissue in the entire grid cell. Unlike other epibenthic variables, corals area is assumed to exist in communities that are potentially smaller than the grid size. The fraction of the grid cell covered by corals is given by A_{CH}. Thus the biomass in the occupied region is given by CH/A_{CH}. The percent coverage of the coral of the bottom for the whole cell is given by $A_{CH}\,(1 - \exp(-\Omega_{CH}\ CH/A_{CH}))$. With only one type of coral resolved, CH represents the biomass of all symbiotic corals. Since the model contains no other benthic filter-feeders, CH best represent the sum of the biomass of all symbiotic filter-feeding organisms such as corals, sponges, clams etc. C:N:P is 106:16:1.
Coral symbiont N (CS_N)	CS [mg N m^{-2}]	Concentration of nitrogen biomass per m^2 of coral symbiont cells, or zooxanthellae. To determine the density of cells, use $n = CS/m_N$. The percentage of the bottom covered is given by $\frac{\pi}{2\sqrt{3}} n\pi r_{zoo}^2$ where πr^2 is the projected area of the cell, n is the number of cells, and $\pi/(2\sqrt{3}) \sim 0.9069$ accounts for the maximum packaging of spheres. C:N:P is 106:16:1.
Coral symbiont chl (CS_Chl)	nc_iV [mg chl m^{-2}]	Concentration of chlorophyll biomass per m^2 of coral symbiont cells.
Coral symbiont diadinoxanthin (CS_Xp)	nx_pV [mg pig m^{-2}]	Concentration of the photosynthetic xanthophyll cycle pigment per m^2 of coral symbiont cells.
Coral symbiont diatoxanthin (CS_Xh)	nx_hV [mg pig m^{-2}]	Concentration of heat dissipating xanthophyll cycle pigment biomass per m^2 of coral symbiont cells.

Table 51: Long name (and variable name) in model output files, units, symbol used in this document, and description of coral state variables in the model.

Name	Symbol	Description
Symbiont oxidised RC (CS_Qox)	Q_{ox} [mg N m^{-2}]	Concentration of symbiont reaction centres in an oxidised state per m^2, residing in the symbiont, of in the entire grid cell.
Symbiont reduced RC (CS_Qred)	Q_{red} [mg N m^{-2}]	Concentration of symbiont reaction centres in a reduced state per m^2, residing in the symbiont, of in the entire grid cell.
Symbiont inhibited RC (CS_Qin)	Q_{in} [mg N m^{-2}]	Concentration of symbiont reaction centres in an inhibited state per m^2, residing in the symbiont, of in the entire grid cell.
Symbiont reactive oxygen (CS_RO)	$[ROS]$ [mg N m^{-2}]	Concentration of reactive oxygen per m^2, residing in the symbiont, of in the entire grid cell.

Table 52: Long name (and variable name) in model output files, units, symbol used in this document, and description of coral reaction state variables in the model.

B Diagnostic outputs

Name	Units	Description
Absorption at 440 nm (at_440)	m^{-1}	Total absorption due to clear water, CDOM, microalgae and suspended sediments at 440 nm.
Scattering at 550 nm (bt_550)	m^{-1}	Total scattering due to clear water, microalgae and suspended sediments at 550 nm.
Vertical attenuation at 490 nm (Kd_490)	m^{-1}	Vertical attenuation (along z axis not along zenith angle) of light at 490 nm.
Average PAR in layer (PAR)	mol photon m^{-2} s^{-1}	Mean scalar photosynthetically available radiation (400 - 700 nm) within the layer.
Downwelling PAR (PAR_z)	mol photon m^{-2} s^{-1}	Mean downwelling photosynthetically available radiation (400 - 700 nm) at the top of each layer (i.e. on z_grid not z_centre)
Light intensity above seagrass (EpiPAR_sg)	mol photon m^{-2} d^{-1}	Mean downwelling photosynthetically available radiation (400 - 700 nm) above seagrass canopy.
Light intensity above sediment layer (EpiPAR)	mol photon m^{-2} d^{-1}	Mean downwelling photosynthetically available radiation (400 - 700 nm) at the sediment-water interface.
Vertical attenuation of heat (K_heat)	m^{-1}	Vertical attenuation (along z axis not along zenith angle) of heat energy.
Remote-sensing reflectance (R_X)	sr^{-1}	Remote-sensing reflectance at wavelength XXX nm, $R_{rs,X}$. R_{rs} is the ratio of water-leaving radiance (i.e. per solid angle) to the incoming solar irradiance (i.e. from all directions).
Satellite chlorophyll (OC*)	mg m^{-3}	Output of band ratio cholorophyll algorithms (OC3M, OC3V)

Table 53: Long name (and variable name) in model output files, units, and description of optical diagnostic variables. Unless otherwise stated quantities are cell centred vertical averages.

Name	Units	Description
Bicarbonate (HCO3)	mmol m^{-3}	Concentration of bicarbonate ions [HCO_3^-] calculated from carbon chemistry equlibra at water column values of T, S, DIC and A_T.
Carbonate (CO3)	mmol m^{-3}	Concentration of carbonate ions [CO_3^{2-}] calculated from carbon chemistry equlibra at water column values of T, S, DIC and A_T.
Aragonite saturation state (omega_ar)	-	Aragonite saturation state (Ω_a) calculated from DIC, A_T, T and S assuming the carbonate system is at equilibrium.
Oxygen % saturation (Oxy_sat)	%	Dissolved oxygen concentration as a percentage of the saturation concentration at atmospheric pressure and local T and S.
pH (PH)	$\log_{10}$ mol m^{-3}	pH based on [H^+] calculated from carbon chemistry equlibra at water column values of T, S, DIC and A_T.
Sea-air CO_2 flux (CO2_flux)	mg C m^{-2} s^{-1}	Flux of carbon from sea to air (positive from sea to air). The value is given in the layer in which it was deposited (must be thicker than 20 cm), but still represents an areal flux.
Sea-air O_2 flux (O2_flux)	mg O m^{-2} s^{-1}	Flux of oxygen from sea to air (positive from sea to air). The value is given in the layer in which it was deposited (must be thicker than 20 cm), but still represents an areal flux.
Delta pCO_2 (dco2star)	ppmv	Partial pressure of CO_2 in the ocean minus that of the atmosphere (396 ppmv).
Oceanic pCO_2 (pco2surf)	ppmv	Partial pressure of CO_2 in the ocean.

Table 54: Long name (and variable name) in model output files, units, and description of gas diagnostic variables. Unless otherwise stated quantities are cell centred vertical averages.

Name	Units	Description
Total C, N, P (TC, TN, TP)	mg m^{-3}	Sum of dissolved and particulate C, N, and P.
Total chlorophyll a (Chl_a_sum)	mg m^{-3}	Sum of chlorophyll concentration of the four microalgae types ($\sum nc_i V_i$).
Ecology Fine Inorganics (EFI)	kg m^{-3}	Sum of inorganic components (see `ecology_setup.txt` for those specified in the code) used for TSS-dependent calculations such as phosphorus absorption.
Ecology Particulate Organics (EPO)	kg m^{-3}	Weight of carbon in microalgae, zooplankton, and particulate detritus.
Large phytoplankton net production (PhyL_N_pr)	mg C m^{-3} d^{-1}	Rate of large phytoplankton organic matter synthesis from inorganic constituents.
Small phytoplankton net production (PhyS_N_pr)	mg C m^{-3} d^{-1}	Rate of small phytoplankton organic matter synthesis from inorganic constituents.
Trichodesmium net production (Tricho_N_pr)	mg C m^{-3} d^{-1}	Rate of *Trichodesmium* organic matter synthesis from inorganic constituents.
Microphytobenthos net production (MPB_N_pr)	mg C m^{-3} d^{-1}	Rate of microphytobenthos organic matter synthesis from inorganic constituents.
Total phytoplankton net production (P_prod)	mg C m^{-3} d^{-1}	Rate of total phytoplankton organic matter synthesis from inorganic constituents.
Large zooplankton removal rate from small zooplankton	mg C m^{-3} d^{-1}	Rate of carnivory of large zooplankton on small zooplankton.
Small zooplankton removal rate from small phytoplankton	mg C m^{-3} d^{-1}	Secondary production of small zooplankton.
Large zooplankton removal rate from large phytoplankton	mg C m^{-3} d^{-1}	Secondary production of large zooplankton.
Zooplankton total grazing (Z_grazing)	mg C m^{-3} d^{-1}	Total secondary pelagic production - feeding of both zooplankton classes on phytoplankton.
N_2 fixation (Nfix)	mg N m^{-3} s^{-1}	Nitrogen fixation by *Trichodesmium*.
Trichodesmium settling velocity (Tricho_sv)	m s^{-1}	Vertical sinking rate of *Trichodesmium*.

Table 55: Long name (and variable name) in model output files, units, and description of pelagic diagnostic variables.

Name	Units	Description
Total epibenthic C, N, P (EpiTC, EpiTN, EpiTP)	mg m^{-2}	Sum of C, N, and P in epibenthic plants and corals.
Halophila production (SGH_N_pr)	g N m^{-2} d^{-1}	Gross production of nitrogen in *Halophila*, where N fluxes are not accounted for in respiration.
Halophila growth rate (SGH_N_gr)	s^{-1}	Turnover time of above-ground *Halophila* biomass.
Seagrass growth rate (SG_N_gr)	s^{-1}	Turnover time of above-ground *Zostera* biomass.
Seagrass production (SG_N_pr)	g N m^{-2} d^{-1}	Gross production of nitrogen in *Zostera*, where N fluxes are not accounted for in respiration.
Seagrass shear mort. (SG_shear_mort)	d^{-1}	Loss rate of seagrass due to shear stress mortality.
Deep SG shear mort. (SGD_shear_mort)	d^{-1}	Loss rate of deep seagrass due to shear stress mortality.
Halophila shear mort. (SGH_shear_mort)	d^{-1}	Loss rate of *Halophila* due to shear stress mortality.
Deep seagrass growth rate (SGD_N_gr)	s^{-1}	Turnover time of above-ground deep seagrass biomass.
Deep seagrass production (SGD_N_pr)	g N m^{-2} d^{-1}	Gross production of nitrogen in deep seagrass, where N fluxes are not accounted for in respiration.
Macroalgae growth rate (MA_N_gr)	s^{-1}	Turnover time of macroalgae biomass.
Macroalgae production (MA_N_pr)	g N m^{-2} d^{-1}	Gross production of nitrogen in macroalgae, where N fluxes are not accounted for in respiration.

Table 56: Long name (and variable name) in model output files, units and description of benthic diagnostic variables.

Name	Units	Description
Coral inorganic supply (Coral_IN_up)	mg N m^{-2} s^{-1}	Flux of dissolved inorganic nitrogen into coral polyps from the water column, absorbed by zooxanthellae. Note that the flux is averaged over the whole grid cell, while the fraction of the bottom that is responsible for this uptake is given by A_{eff} (Eq. 159)
Coral organic supply (Coral_ON_up)	mg N m^{-2} s^{-1}	Flux of particulate organic nitrogen into coral polyps from the water column, consumed by the coral host. See coral organic supply.
Net calcification (Gnet)	mg C m^{-2} s^{-1}	Net calcification (calcification minus dissolution) at the sediment-water column interface leading to a change in the water column properties.
Rubisco activity, $a^*_{Q_{ox}}$ (CS_tempfunc)	-	Activity of the Ribulose-1,5-bisphosphate carboxylase/oxygenase (RuBisCO) enzyme based on the seabed temperature anomaly from a spatially-varying maximum summer temperature. It takes a value of 1 below the summer time maximum, and 0 at 2°C above (Eq. 173).
Coral bleaching rate (CS_bleach)	d^{-1}	Loss rate of zooxanthellae due to reactive oxygen stress.
Coral mucus release (mucus)	mg N m^{-2} s^{-1}	Release rate of organic matter (at the Redfield ratio) due to polyp and symbiont moratlity terms, excluding those due to reactive oxygen stress driven expulsion.

Table 57: Long name (and variable name) in model output files, units and description of coral diagnostic variables.

Name	Units	Description
Porosity (porosity_sed, ϕ)	-	Fraction of a layer by volume that is occupied by water. Calculated from the the sum of the mass divided by Sediment density of each of the particulate components, compared to that of water.
Sea-water sed * flux (*_sedflux)	mg m^{-2}	The sea-water (+ve into water) flux of diffused tracer * calculated by the ecological process `diffusion_epi`. This diffusion rate, typically much quicker than the sediment model, accounts for the fast diffusion between the top sediment layer and the bottom
Sea-water sed * flux (*_fluxsedi_inst)	mg m^{-2}	The sea-water (+ve into water) flux of diffused tracer * calculated by the sediment model. This calculation includes, entrainment of porewaters during sediment deposition, loss of porewater during erosion, and a slow diffusion rate.
Denitrfication flux (Den_fl)	mg N m^{-2} d^{-1} $layer^{-1}$	Denitrification rate, specified per layer per m^2 (rather than per m^3) so that the depth-integrated denitrification rate can be calculated by summing each layer without knowing the thickness of each layer (that varies with time).

Table 58: Long name (and variable name) in model output files, units and description of sediment model diagnostic variables.

B.1 Diagnostic age tracer

Tracer 'age' is a diagnostic tracer (Monsen et al., 2002; Macdonald et al., 2009) use to quantify the spatially-resolved residence time of water in different regions. The age tracer, τ, is advected and diffused by the hydrodynamic model using the same numerical schemes as other tracers such as salinity. When inside the region of interest, the age increases at the rate of 1 d d^{-1}. When the age tracer is outside the region of interest, its age decays (or anti-ages) at the rate of Φ d^{-1}. Thus, the local rate of change over the whole domain is given by:

$$\frac{\partial \tau}{\partial t} = 1 \tag{320}$$

$$\frac{\partial \tau}{\partial t} = -\Phi\tau \qquad \text{outside ageing region} \tag{321}$$

$$\tag{322}$$

In some applications the age is held to zero outside the region to represent time since water moved within the area of interested (such as the surface mixed layer (Baird et al., 2006)). For more information see Mongin et al. (2016).

B.2 Simulated true colour

True color images are often used in the geophysical sciences to provide a broad spatial view of a phenomenon such as cyclones, droughts or river plumes. Their strength lies in the human experience of natural colors that allows three 'layers' of information, and the interaction of these information streams, to be contained within one image. Spectacular true color images of, for example, the Great Barrier Reef (GBR), simultaneously depict reef, sand and mud substrates, sediment-laden river plumes and phytoplankton blooms. Further, the advection of spatially-variable suspended coloured constituents reveals highly-resolved flow patterns.

For these reasons and more, true color imagery has become a valued communication tool within both the geosciences and wider community. Here we demonstrate that the power of true colour images can be harnessed for interpreting geophysical models if the model output includes remote-sensing reflectance, or normalised water leaving radiance, at the red, green and blue wavelengths.

In order to interpret simulated true colour images, a palette of true colours from the model optical relationships has been painted (Fig. 19), for varying values of water column CDOM, NAP and chlorophyll concentration. The green hues produced for varying IOPs are quite similar, demonstrating the difficulty in ocean colour analysis. The most obvious trend in the image is that Chl produces a greener hue than NAP (top panels vs bottom panels). The difference between increasing

CDOM and chlorophyll (right panels vs left panels) is more subtle, which is a significant challenge in remote sensing of chlorophyll in high CDOM coastal waters (Schroeder et al., 2012).

The important role of scattering can be seen in Fig. 19. At low chl and / or NAP, the colour becomes dark at moderately low CDOM concentration. In reality CDOM is usually associated with either chlorophyll or NAP, hence natural waters rarely appear black.

As the model calculates remote-sensing reflectance at any wavelength, it is possible to reproduce simulated true colour images using the same algorithms as the MODIS processing (Fig. 20). The comparison of observed and modelled true colour images is particular insightful because the impact of multiple spectrally-distinct events (such as a sediment plume and a phytoplankton bloom) can be viewed on one image (Fig. 21). Furthermore, the colour match-up provides an intuitive and challenging test for parameterisation of the spectrally-resolved optical coefficients.

True colour images use intensity in the red, green and blue wavebands. We use the centre wavelengths of MODIS bands 1 (645 nm), 2 (555 nm) and 4 (470 nm). Simulated true colour image brightness is adjusted using the MODIS approach by linearly scaling the above surface remote-sensing reflectance at each wavelength so that the brightest band has an intensity of approximately 1. This requires multiplication of between 20 to 30. The scaled intensity is intensified in the darker bands by scaling [0 30 60 120 190 255]/255 onto [0 110 160 210 240 255]/255. The final image is rendered in MATLAB.

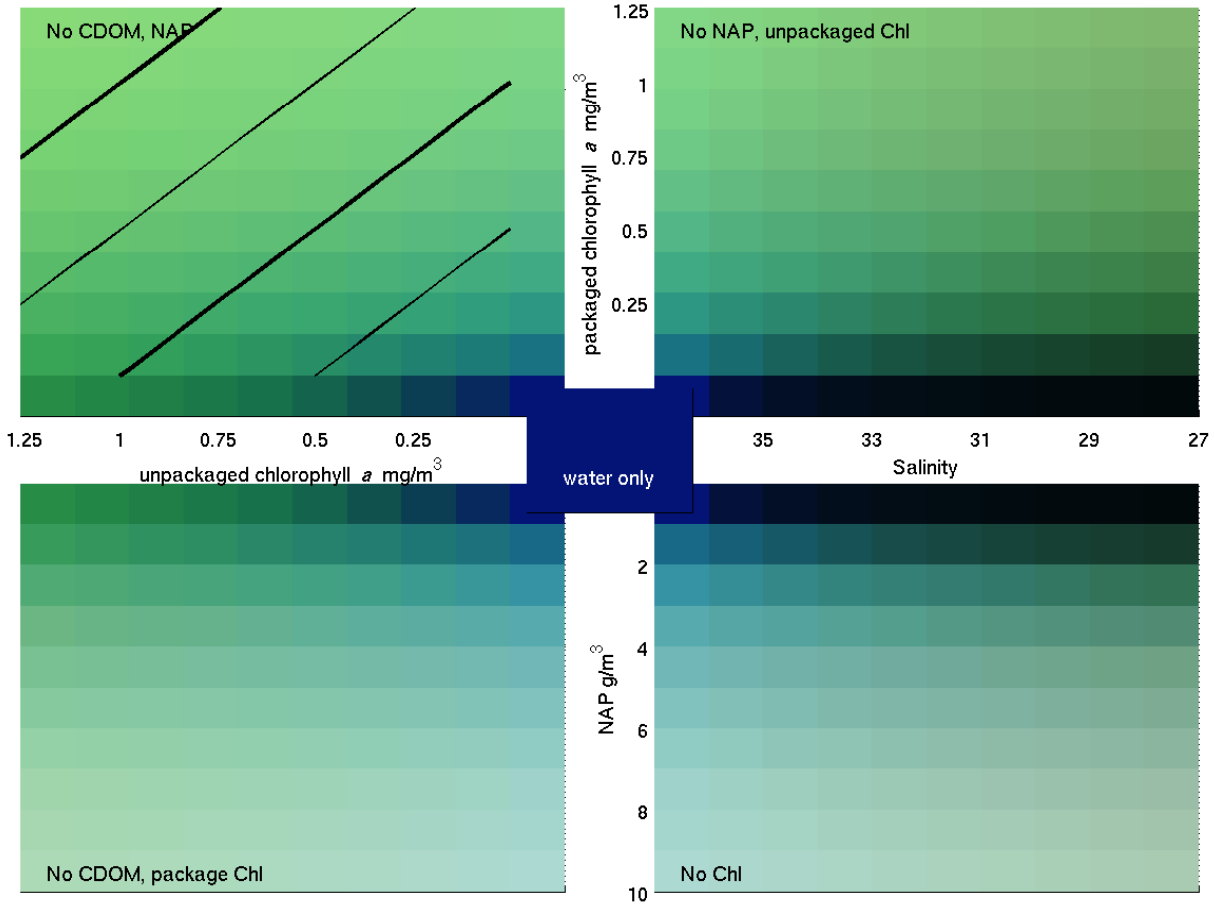

Figure 19: Palette of true colours from IOP relationships. The true colours are produced from the MODIS algorithm (Sec. B.2), and IOP relationships in Sec. 4.2.1. The centre box is the colour produced by clear water absorption and scattering alone. From the centre, moving right is increasing CDOM (as quantified by salinity), down is increasing NAP, and left and up are increasing chlorophyll in cells package by 0.35 and 0.73 respectively. The line contours in the top left panel are 0.5, 1, 1.5 and 2 mg Chl m^{-3}. Note that packaged chlorophyll is not plotted with NAP and unpackaged is not plotted with CDOM.

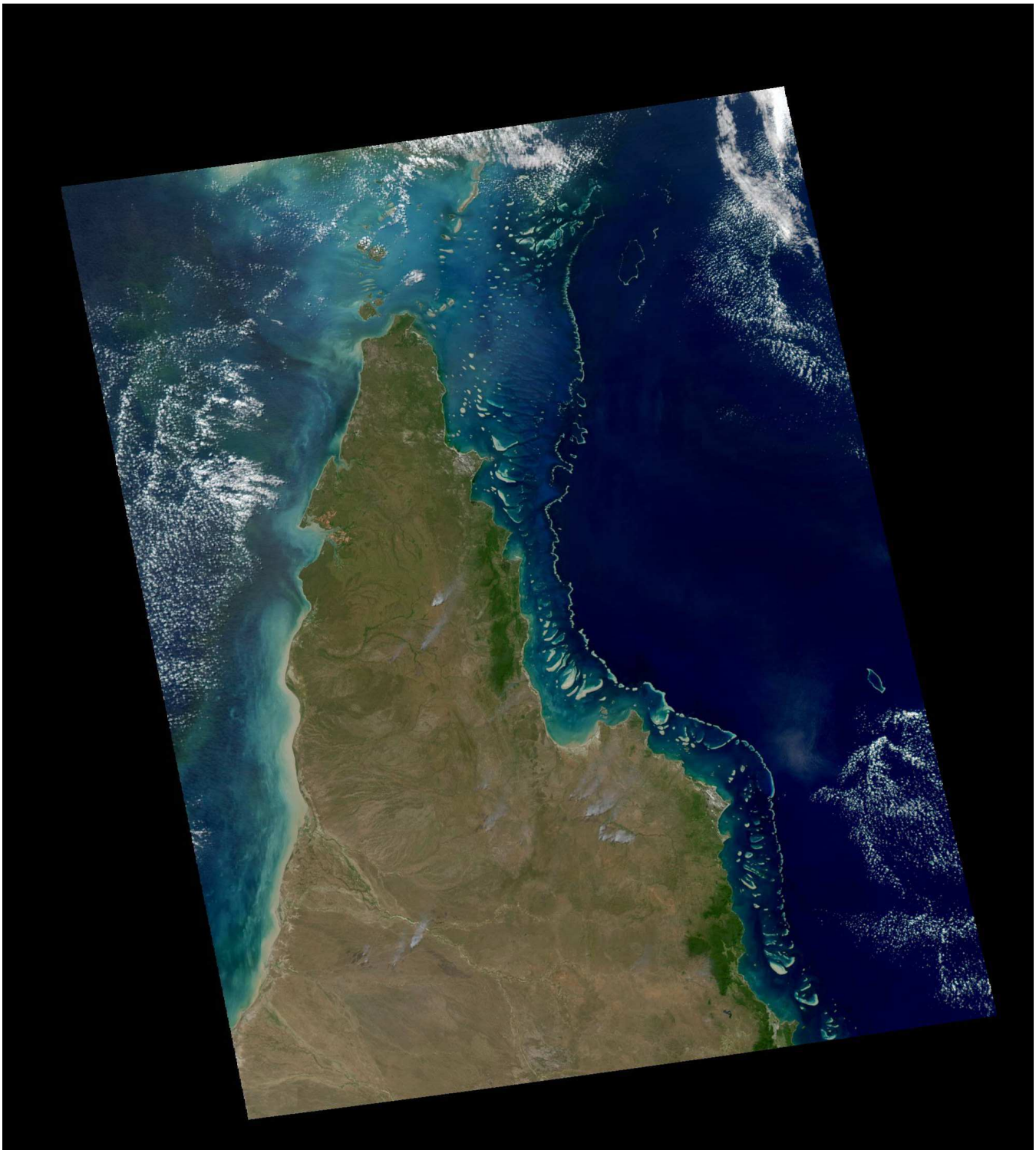

Figure 20: Observed true colour from MODIS using reflectance at 670, 555 and 470 nm.

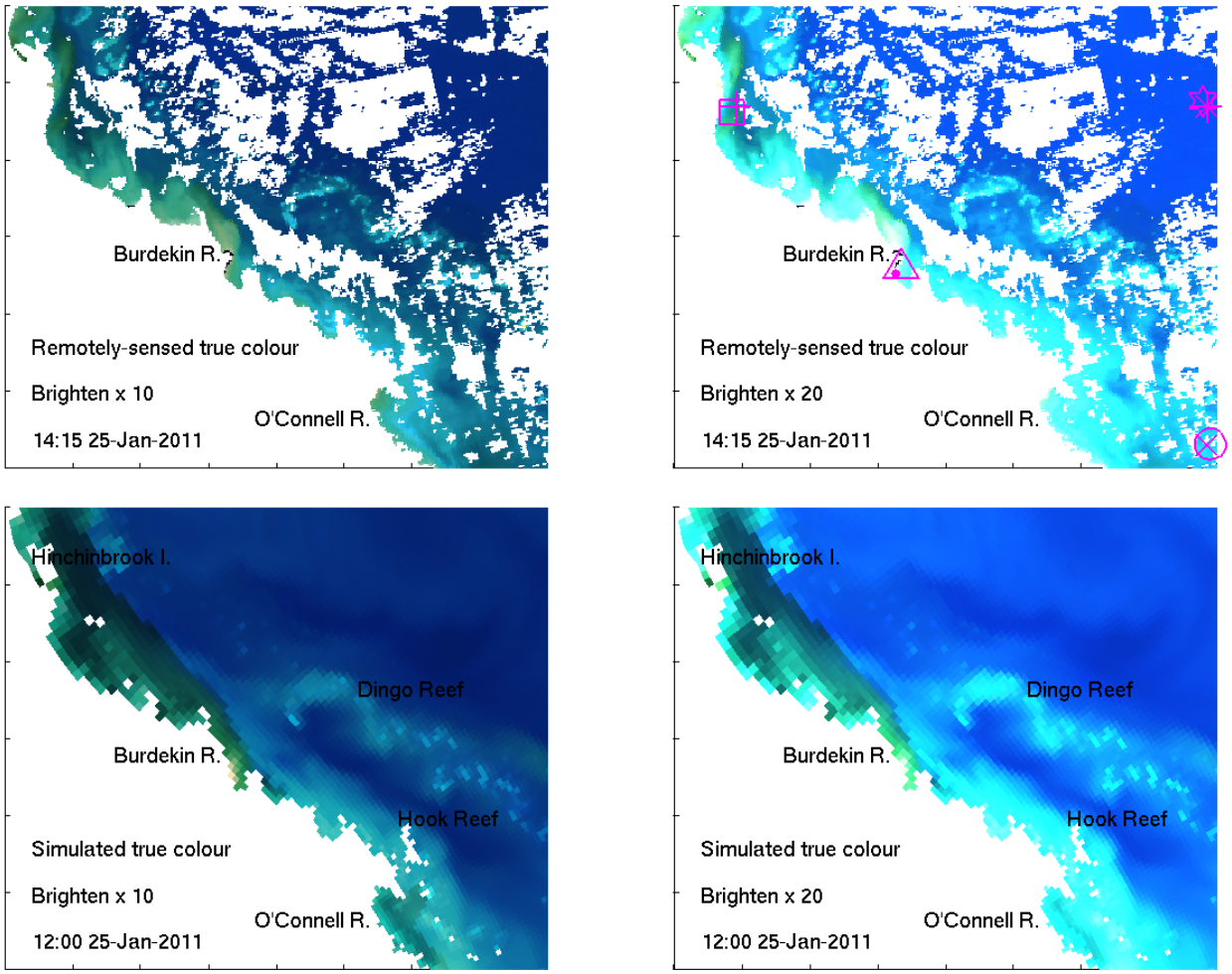

Figure 21: Observed (top) and simulated (bottom) true colour from simulated remote-sensing reflectance at 670, 555 and 470 nm in the GBR4 model configuration in the region of the Burdekin River. A brightening of 10 (left) and 20 (right) was applied for comparison.

B.3 Estimates of chlorophyll using the OC3 algorithm

The ratio of above-surface remote-sensing reflectance as a combination of three wavelengths, R', is given by:

$$R' = \log_{10}\left(\max\left[R_{rs,443}, R_{rs,488}\right]/R_{rs,551}\right) \tag{323}$$

The ratio R' is used in the MODIS OC3 algorithm to estimate surface chlorophyll, Chl_{OC3}, with coefficients from the 18 March 2010 reprocessing:

$$\mathrm{Chl}_{OC3} = 10^{0.283+R'(-2.753+R'(1.457+R'(0.659-1.403R')))} \tag{324}$$

obtained from `http://oceancolor.gsfc.nasa.gov/REPROCESSING/R2009/ocv6/`.

B.4 Estimates of vertical attenuation using the $K_{d,490}$ algorithm

The ratio of above-surface remote-sensing reflectance as a combination of two wavelengths, R', is given by:

$$R' = \log_{10}\left(R_{rs,488}/R_{rs,547}\right) \tag{325}$$

The ratio R' is used in the MODIS algorithm to estimate vertical attenuation at 490 nm, $K_{d,490}$, with coefficients from the 18 March 2010 reprocessing:

$$K_{d,490} = 10^{-0.8813+R'(-2.0584+R'(2.5878+R'(-3.4885-1.5061R')))} \tag{326}$$

obtained from `http://oceancolor.gsfc.nasa.gov/REPROCESSING/R2009/ocv6/`.

B.5 Estimates of particulate organic carbon using the POC algorithm

The ratio of above-surface remote-sensing reflectance as a combination of two wavelengths, R', is given by:

$$R' = \log_{10}\left(R_{rs,488}/R_{rs,555}\right) \tag{327}$$

The ratio R' is used in the MODIS algorithm to estimate concentration of particulate organic carbon, POC, with coefficients from the 18 March 2010 reprocessing:

$$POC = 308.3R'^{-1.639} \tag{328}$$

obtained from `http://oceancolor.gsfc.nasa.gov/REPROCESSING/R2009/ocv6/`.

B.6 Simulated turbidity from $b_{b,595}$

Turbidity is a measure of water clarity. The units of turbidity from a calibrated nephelometer are called Nephelometric Turbidity Units (NTU). Turbidity is often directly related to total suspended solids. However, as turbidity is measured optically (in the case of the three-wavelength Wetlabs sensor the scattering at 700 nm at a measured angle of 124°), it is better to produce a simulated turbidity - a calculation of what the optical model predicts an optical turbidity sensor would measure. Simulated turbidity, like simulated remote-sensing reflectance, is an example of "taking the model to the observations".

Thus, simulated turbidity (NTU) is given by:

$$\mathcal{T} = 47.02\,(b_{b,595} - 0.5 b_{b,clear,595}) + 0.13 \tag{329}$$

where $b_{b,595}$ is the backscattering coefficient at 595 nm, and the linear coefficient and offset were obtained from comparison of a BB9 backscattering sensor and a Wetlabs NTU at Lucinda Jetty, north Queensland. The coefficients are an empirical fit to the factory calibration of NTU standards. The clear water backscatter is removed because it was also removed in the output of the BB9. In practice

B.7 Estimates of total suspended matter using 645 nm

We use a local relationship between the remote-sensing reflectance at 645 nm, $R_{rs,645}$ [sr^{-1}], and total suspended matter, TSM (Petus et al., 2014):

$$TSM = \left(12450 R_{rs,645}^2 + 666 R_{rs,645} + 0.48\right)/1000 \tag{330}$$

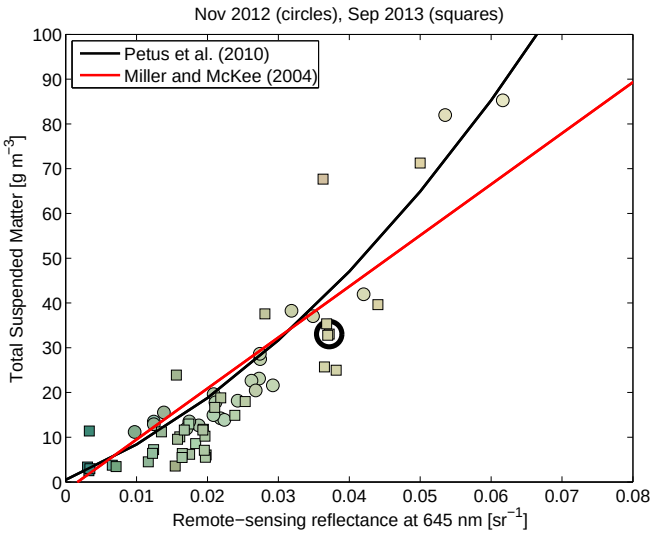

Figure 22: Relationship between the remote-sensing reflectance at 645 nm, $R_{rs,645}$, [sr^{-1}], and total suspended matter, TSM, in the samples taken during November 2012 (circles) and September 2013 (squares), compared to the empirical relationship of Petus et al. (2014) for the Bay of Biscay and Miller and McKee (2004) for the Mississippi. The symbols are coloured by true color, showing browner sites with higher TSM and remote-sensing reflectance. The black circle represents the site used for the model parameterisation of TSM optical properties.

B.8 Simulated fluorescence

The chlorophyll a molecule absorbs light at a range of wavelengths, and can, under certain circumstances, fluoresce strongly (Falkowski and Raven, 2007; Huot et al., 2005). As a result, active fluorescence is commonly used as a measure of chlorophyll a concentration. For this measurement, the stimulus for fluorescence comes from the sensor. For example, the Wetlabs ECOPuck emits light at 470 nm, and detects excitation at 695 nm. The fraction of the light that is returned depends primarily on the concentration of chlorophyll, but can also be affected by the size of the phytoplankton, through the packaging of pigments, and on the physiological state of the cells (Alvarez et al., 2017; Baird et al., 2013). As the model calculates spatially- and temporally- resolved measures of pigment packaging and cell physiology for each phytoplankton type, it is possible to calculate a new diagnostic, simulated fluorescence, that represents florescence that would be measured by a fluorometer exciting at 470 nm, measuring at 695 nm, and sampling a phytoplankton community with the properties (number, cell size, physiological state) of the community in the model.

Simulated fluorescence uses the model predicted cell number, cell size, chlorophyll content, and the pigment-specific absorption coefficient at the excitation wavelength (470 nm, $\gamma = 0.03$ m^2 mg^{-1}) to calculate a simulated fluorescence. Specifically, the per unit of pigment absorption effectiveness, a^*, of a spherical cell r, pigment-specific absorption coefficient, γ, and intracellular pigment concentration c_i is given by:

$$a^* = \pi r^2 \left(1 - \frac{2(1-(1+2\rho)e^{-2\rho})}{4\rho^2}\right) / (n\gamma_{470} c_i V) \tag{331}$$

where $\rho = \gamma_{470} c_i r$, n is the concentration of cells and V is the cell volume ($4/3\pi r^3$). Because we are using the above equation to calculate the packaging effect, we sum the product $\gamma_{470} c_i$ for all pigments, recognising that the presence of any pigment can shade the chlorophyll a molecule.

Cell physiology also affects fluorescence. The photosystem II (PSII) fluorescences when light is absorbed by the cell, but not used for either photosynthesis or dissipated as heat by photoprotective pigments (called non-photochemical quenching, NPQ; see coral zooxanthellae photosystem model in (Baird et al., 2018)). To capture reduced fluorescence due to NPQ, we use the normalised carbon reserves of the cell, R^*_C.

The simulated fluorescence from all phytoplankton is given:

$$FL = CF \frac{3}{4} \sum_{p=1}^{P} a^*_p c_p \left(1 - 0.5 R^*_{C,p}\right) \tag{332}$$

where the sum is applied across all P cell types (small and large phytoplankton, *Trichodesmium*, microphytobenthos and dinoflagellates), c_p is the water column concentration of chlorophyll-a from each cell type, and CF is a calibration factor and depends on the initial factory calibration, which is

usually undertaken using a monoculture of a large diatom. The factor of 3/4 has been pulled out of CF to compare absorption cross-sections and volume specific attenuation (see Baird et al. (2013)). The term $(1 - 0.5R^*_C)$, accounts for the heat dissipation by the xanthophyll cycle, and takes a value of 1 when the carbon reserves are deplete (i.e. at depth in low light), and a value of 0.5 when the cells are carbon replete. The factor 0.5 accounts for the absorption of photosynthetic pigments even when the cell is energy replete, and can be thought of as the ratio of photoabsorbing pigments to xanthophyll pigments.

B.9 Simulated normalised fluorescence line height (nFLH)

In complex coastal waters, absorption in the blue is often dominated by CDOM, so band ratio algorithms like OC3M do not correlate well with *in situ* chlorophyll (Schroeder et al., 2012). An alternate remotely-sensed product is normalised fluorescence line height (nFLH, Behrenfeld et al. (2009)). nFLH is a measure of the light emitted by fluorescence at a red wavelength (678 nm for MODIS), as a result of solar radiation absorbed by photosynthetic pigments throughout the spectrum. Thus while simulated fluorescence described above (Sec. B.8) is a measure of active fluorescence, nFLH is due to passive fluorescence. The passive fluorescence, PF (measured in photons), at 678 nm due to absorption by P phytoplankton types is given by:

$$PF = \sum_{p=1}^{P} n_p \left(1 - 0.5R^*_{C,p}\right) R^*_C \frac{(10^9 hc)^{-1}}{A_V} \int \alpha E_{o,\lambda} \lambda d\lambda \tag{333}$$

where the term $\left(1 - 0.5R^*_{C,p}\right)$ is discussed in Sec. B.8, the multiplication by R^*_C removes the component of absorption that is used for photosynthesis (that was not applied in Sec. B.8 for simulated fluorescence due to the saturating pulse of the active fluorometer), and $E_{o,\lambda}$ is the scalar irradiance at wavelength λ [W m^{-2}], n_p is the concentration of cell type p, and h, c and A_v are the Planck constant, speed of light in a vacuum and Avagadro number respectively.

The passive fluorescence is assumed to be emitted isotropically (equal in all directions), while for the purposes of calculating the impact on remote-sensing reflectance, we need to consider only the upwelling component. Further, to obtain remote-sensing reflectance we need to compare the upwelling component to downwelling irradiance at 678 nm, also in photons. Thus the ratio of passive fluorescence at 678 nm to incoming radiation at 678 nm is:

$$u^+ = \frac{1}{4\pi} PF / \left(\frac{(10^9 hc)^{-1}}{A_V} 678 E_{o,678} \right) \tag{334}$$

This ratio of upwelling PF to downwelling solar radiation can then be added to u, the ratio of backscattering to absorption plus backscattering, at 678 nm (Eq. 24). The revised u then results in an updated $R_{rs,678}$, with the depth weighting based on the vertical attenuation coefficient. Finally,

nFLH is determined from the normalised water leaving irradiance (nLw) at the fluorescing band, and the bands either side of it. The term nLw is normalised to the sun zenith, $F_o = 148.097$ mW cm^{-2} μm^{-1},

$$nFLH = \frac{F_o}{\pi}\left(R_{rs,678} - \frac{70}{81}R_{rs,667} - \frac{11}{81}R_{rs,748}\right) \tag{335}$$

where π has units of sr^{-1} to convert between planar flux of nLw to a solid angle of remote-sensing reflectance (R_{rs}).

Note that passive fluorescence will contributes to the underwater light field in all directions, but because it is at 678 nm where there is strong absorption by clear water we have assumed that it does not lead to photosynthesis. Thus we have only considered the effect of passive fluorescence on $R_{rs,678}$ and therefore nFLH.

B.10 Secchi depth

Secchi depth is often calculated using:

$$Z_{SD} = 1.7/K_d \tag{336}$$

where K_d is a vertical attenuation of light, typically energy-weighted PAR. At a particular wavelength the constant varies from 1.7. In a recent study (Lee et al., 2015), it was shown that the constant has a value of approximately 1.0 when the colour of human perception of the disk surface is used as the wavelength. This varies in different waters, from 486 to 475 nm, as the water clarity improves. Even though this value is slightly bluer than 490 nm, we found a good match with observations for:

$$Z_{SD,490} = 1/K_{d,490} \tag{337}$$

The light level at the Secchi depth is $E_{SD,490} = E_{0,490}\exp(-Z_{SD,490}K_{d,490})$. Substituting Eq. 337, $E_{SD,490}/E_{0,490} = \exp(-1)$.

Depth-varying vertical attenuation. If $K_{d,490}$ varies with depth (as it does in the simulations), then the Secchi depth is found by looking for the layer in which $E_{SD,490}/E_{0,490}$ drops below $\exp(-1)$. The top of this layer has a depth Z_{top}. Given a light level at the top of this layer of E_{top}, and an attenuation within the layer of $K_{d,490}$, the Secchi depth is given by:

$$Z_{SD,490} = Z_{top} + \log\left(\frac{\exp(-1)/E_{top}}{-K_{d,490}}\right) \tag{338}$$

Over 5000 measurements of Secchi depth have been undertaken in the GBR and used to develop a satellite algorithm for Secchi depth (Weeks et al., 2012). We adopt this approach to define a

simulated remotely-sensed Secchi depth, Z_{SD}:

$$Z_{SD,sim,rs} = 10^{\left(\log_{10}\left(2.303/K_{d,490}\right)-0.529\right)/0.816} \tag{339}$$

where $2.303/K_{d,490}$ gives the 10 percent light depth and the empirical constants come from Weeks et al. (2012).

Finally these can be compared to the observed in situ Secchi depth, $Z_{SD,obs}$, and the remotely-sensed Secchi depth, $Z_{SD,rs}$.

B.11 Optical plume classification

Optical properties have been used to classify the extend of plumes (Devlin et al., 2013; Alvarez-Romero et al., 2013). Here we use a similar approach on simulated plumes. First we determine from observations the spectra of 6 standard plume classes (Fig. 23), as adopted by Alvarez-Romero et al. (2013). Using these standard plume classifications, we determine the dissimilarity between an observed or simulated spectra and the spectra of each standard class. The cosine dissimilarity between standard class c and the observed or simulated spectra, $S(c)$, is determined by:

$$S(c) = \cos^{-1}\left(\frac{\sum_{\lambda=1}^{W} R_{rs,c,\lambda} R_{rs,sim,\lambda}}{\sqrt{\sum_{\lambda=1}^{W} R_{rs,c,\lambda}^2}\sqrt{\sum_{\lambda=1}^{W} R_{rs,sim,\lambda}^2}}\right) \tag{340}$$

where $R_{rs,c,\lambda}$ is the remote-sensing reflectance of class c at wavelength λ, $R_{rs,sim,\lambda}$ is the remote-sensing reflectance of the simulation at wavelength λ and W is the number of wavelengths considered. The observed or simulated spectra is then assigned to the standard class c with the minimum dissimilarity, S, between the standard class and the observed or simulated spectra.

A simpler spectra matching scheme using the rms difference between the spectra is also employed.

Using this classification technique we can compare the extent of plumes in an observed scene (Fig. 24 left), and a simulated scene (Fig. 24 right) of the same day. The areal extent of the observed and simulated plume classes can also be calculated, noting that the observed area is less due to clouds.

As a metric of the recent history of plume exposure, we propose a metric the plume exposure, $\mathcal{P}$, which is given by:

$$\mathcal{P} = \int_{t-t_{c<6}}^{t} (1/c)\, dt \tag{341}$$

where c is the plume class determined from Eq. 340. The plume exposure is calculated for each model grid cell. The metric is calculated from the most recent time that c for a grid cell was less

than 6 (i.e. impacted by a plume class 1, 2, 3, 4 or 5). The metric is a weighted-running mean, such that exposure to plume class 1 for 10 days would give a value of 10, plume class 2 for 10 days 5, plume class 3 for 10 days would give 10/3 etc.

An additional concept is the annual plume extent, or the mean plume area over the year.

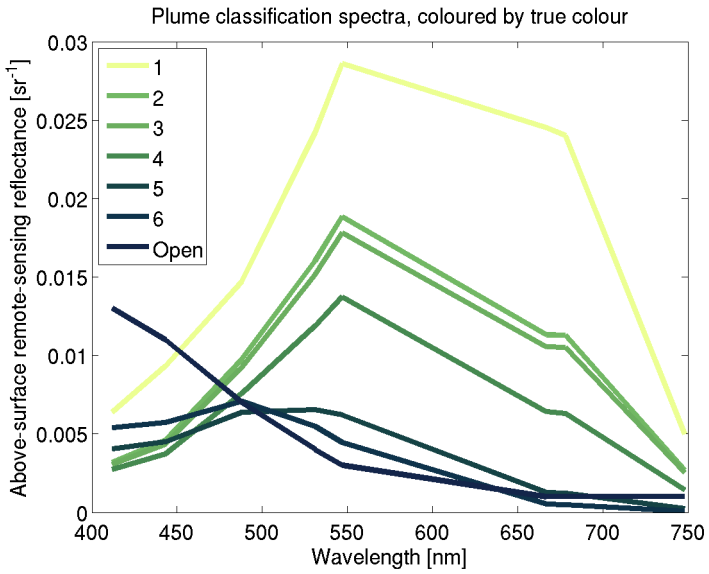

Figure 23: Spectra of each of the optical plume classifications (1-6) and the open ocean. The area in km^2 for each plume class within the region plotted is given on the left for both the observed and simulated classes.

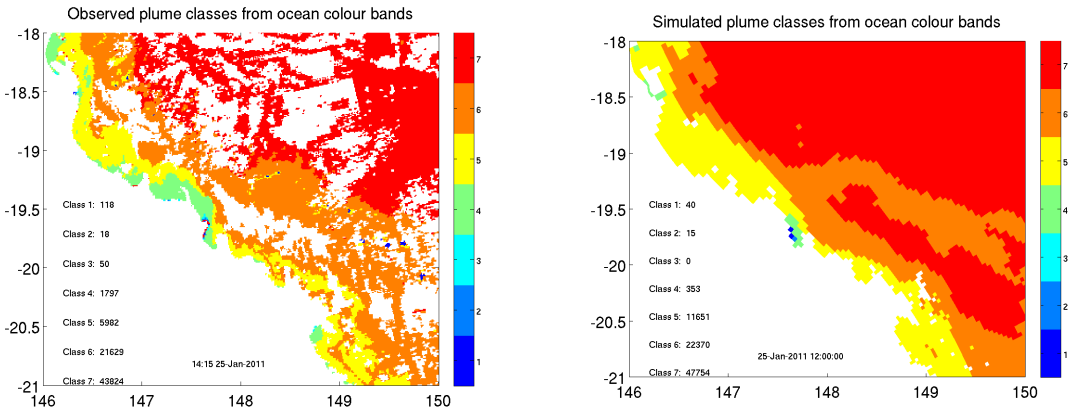

Figure 24: Observed and simulated optical plume classification on the 25 Jan 2011 in the Burdekin River region. See Fig. 23 for spectra of individual classes.

Description	Calculation	Application
Monthly bottom light (eqival. to daily dose]	1 hourly running-mean $\frac{1}{\tau}\int_0^t E_{d,\lambda,t}\exp(-(t-t')/\tau)dt'$ [mol m^{-2} d^{-1}]	seagrass viability
Aragonite dissolution exposure	$\int_{t-t_{\Omega<3}}^{t}(3-\Omega)\,dt'$ reset time 1 day, [unit days]	acidification stress
Monthly net calcification rate	1 hourly running-mean $\frac{1}{\tau}\int_0^t g_{net,t}\exp(-(t-t')/\tau)dt'$	calcification index coral accretion
Temperature exposure (degree heating weeks)	$\int_{t-t_{T>T_{clim}}}^{t}(T-T_{clim})\,dt'$ rest time 7 day, [°C weeks]	thermal coral bleaching
Weekly inorganic N uptake by corals	1 hourly running-mean $\frac{1}{\tau}\int_0^t G_t\exp(-(t-t')/\tau)dt'$	oxidative stress
Salinity exposure	$\int_{t-t_{S<28}}^{t}(28-S)\,dt'$ reset time 1 day, [PSU days]	freshwater coral bleaching
Weekly net deposition rate (sinking / resuspension / diffusion)	1 hourly running-mean $\frac{1}{\tau}\int_0^t D_t\exp(-(t-t')/\tau)dt'$ [cm d^{-1}]	coral smothering
Hypoxic exposure	$\int_{t-t_{[O_2]<2000}}^{t}(2000-[O_2])\,dt$ rest time 1 hour, [mg O m^{-3} d^{-1}]	low oxygen stress
Weekly bottom light attenuation (approx. from 490 nm)	1 hourly running-mean $\frac{1}{\tau}\int_0^t K_{d,490,t}\exp(-(t-t')/\tau)dt'$ [m^{-1}]	predator visibility prey behaviour
Remote-sensing reflectance R_{rs}	see Section 4.2.2 412, 443, 488, 531, 547, 648, 667, 748 nm	comparison with ocean colour products
MODIS algorithms - Kd, OC3, TSS, POC - Kd, OC3, TSS, POC	empirical algorithms using remote-sensing reflectance	comparison with ocean colour products
Simulated true colour	RGB additive colour model using remote-sensing reflectance	water quality non-expert communication
Plume classification (1-6) + clear water	categorical from spectra matching using RMS errors on OC bands 1-7	plume extent

Table 59: Diagnostic variables. In addition to 60+ state variables, derived diagnostic variables have been developed in consultation with researchers and managers that provide metrics for improve understanding and application. For those metrics with a time scale, τ, the coefficient represents an exponential decay time - thus for a weekly running average, the impact of the value 1 week earlier on the running average is $100 \times \exp(-1)$, or 37 % of the impact of the present value. Or 63.2 % of the value is based on the last week, 86.5 % on the last two weeks etc.

C Parameter values used in eReefs biogeochemical model (B3p0).

The below five tables of parameters are specified for each run, and can be automatically generated by the EMS software after a simulation from the parameter file. At model initialisation the model produces a file `ecology_setup.txt` that contains a list of all the parameter values used, both those specified in the parameter file, and those using model defaults.

For a more information see Robson et al. (2018).

Description	Name in code	Symbol	Value	Units
Reference temperature	Tref	T_{ref}	2.000000e+01	Deg C
Temperature coefficient for rate parameters	Q10	$Q10$	2.000000e+00	none
Nominal rate of TKE dissipation in water column	TKEeps	ϵ	1.000000e-06	$m^2\ s^{-3}$
Atmospheric CO2	xco2_in_air	pCO_2	3.964800e+02	ppmv
Concentration of dissolved N2	N2	$[N_2]_{gas}$	2.000000e+03	mg N m^{-3}
DOC-specific absorption of CDOM 443 nm	acdom443star	$k_{CDOM,443}$	1.300000e-04	m^2 mg C^{-1}

Table 60: Environmental parameters in eReefs biogeochemical model (B3p0).

Description	Name in code	Symbol	Value	Units
Chl-specific scattering coef. for microalgae	bphy	b_{phy}	2.000000e-01	m^{-1}(mg Chla $m^{-3})^{-1}$
Nominal N:Chl a ratio in phytoplankton by weight	NtoCHL	$R_{N:Chl}$	7.000000e+00	g N(g Chla)$^{-1}$
Maximum growth rate of PL at Tref	PLumax	μ_{PL}^{max}	1.400000e+00	d^{-1}
Radius of the large phytoplankton cells	PLrad	r_{PL}	4.000000e-06	m
Natural (linear) mortality rate, large phytoplankton	PhyL_mL	$m_{L,PL}$	1.000000e-01	d^{-1}
Natural (linear) mortality rate in sed., large phyto.	PhyL_mL_sed	$m_{L,PL,sed}$	1.000000e+01	d^{-1}
Maximum growth rate of PS at Tref	PSumax	μ_{PL}^{max}	1.600000e+00	d^{-1}
Radius of the small phytoplankton cells	PSrad	r_{PS}	1.000000e-06	m
Natural (linear) mortality rate, small phyto.	PhyS_mL	$m_{L,PS}$	1.000000e-01	d^{-1}
Natural (linear) mortality rate in sed., small phyto.	PhyS_mL_sed	$m_{L,PS,sed}$	1.000000e+00	d^{-1}
Maximum growth rate of MB at Tref	MBumax	μ_{MPB}^{max}	8.390000e-01	d^{-1}
Radius of the MPB cells	MBrad	r_{MPB}	1.000000e-05	m
Natural (quadratic) mortality rate, MPB (in sed)	MPB_mQ	$m_{Q,MPB}$	1.000000e-04	d^{-1}(mg N $m^{-3})^{-1}$
Ratio of xanthophyll to chl a of PS	PSxan2chl	$\Theta_{xan2chl,PS}$	5.100000e-01	mg mg $^{-1}$
Ratio of xanthophyll to chl a of PL	PLxan2chl	$\Theta_{xan2chl,PL}$	8.100000e-01	mg mg $^{-1}$
Ratio of xanthophyll to chl a of MPB	MBxan2chl	$\Theta_{xan2chl,MPB}$	8.100000e-01	mg mg $^{-1}$
Maximum growth rate of Trichodesmium at Tref	Tricho_umax	μ_{MPB}^{max}	2.000000e-01	d^{-1}
Radius of Trichodesmium colonies	Tricho_rad	r_{MPB}	5.000000e-06	m
Sherwood number for the Tricho dimensionless	Tricho_Sh	Sh_{Tricho}	1.000000e+00	none
Linear mortality for Tricho in sediment	Tricho_mL	$m_{L,Tricho}$	1.000000e-01	d^{-1}
Quadratic mortality for Tricho due to phages in wc	Tricho_mQ	$m_{Q,Tricho}$	1.000000e-01	d^{-1}(mg N $m^{-3})^{-1}$
Critical Tricho above which quadratic mortality applies	Tricho_crit		2.000000e-04	mg N m^{-3}
Minimum density of Trichodesmium	p_min	$\rho_{min,Tricho}$	9.000000e+02	kg m^{-3}
Maximum density of Trichodesmium	p_max	$\rho_{max,Tricho}$	1.050000e+03	kg m^{-3}
DIN conc below which Tricho N fixes	DINcrit	DIN_{crit}	1.000000e+01	mg N m^{-3}
Ratio of xanthophyll to chl a of Trichodesmium	Trichoxan2chl	$\Theta_{xan2chl,Tricho}$	5.000000e-01	mg mg $^{-1}$
Minimum carbon to chlorophyll a ratio	C2Chlmin	θ_{min}	2.000000e+01	wt/wt

Table 61: Phytoplankton parameters in eReefs biogeochemical model (B3p0).

Description	Name in code	Symbol	Value	Units
Maximum growth rate of ZS at Tref	ZSumax	μ_{max}^{ZS}	4.000000e+00	d^{-1}
Radius of the small zooplankton cells	ZSrad	r_{ZS}	5.000000e-06	m
Swimming velocity for small zooplankton	ZSswim	U_{ZS}	2.000000e-04	m s^{-1}
Grazing technique of small zooplankton	ZSmeth		rect	none
Maximum growth rate of ZL at Tref	ZLumax	μ_{max}^{ZL}	1.330000e+00	d^{-1}
Radius of the large zooplankton cells	ZLrad	r_{ZL}	3.200000e-04	m
Swimming velocity for large zooplankton	ZLswim	U_{ZL}	3.000000e-03	m s^{-1}
Grazing technique of large zooplankton	ZLmeth		rect	none
Growth efficiency, large zooplankton	ZL_E	E_{ZL}	4.260000e-01	none
Growth efficiency, small zooplankton	ZS_E	E_{ZS}	4.620000e-01	none
Natural (quadratic) mortality rate, large zooplankton	ZL_mQ	$m_{Q,ZL}$	1.200000e-02	d^{-1}(mg N m^{-3})$^{-1}$
Natural (quadratic) mortality rate, small zooplankton	ZS_mQ	$m_{Q,ZS}$	2.000000e-02	d^{-1}(mg N m^{-3})$^{-1}$
Fraction of growth inefficiency lost to detritus, large zoo.	ZL_FDG	γ_{ZL}	5.000000e-01	none
Fraction of mortality lost to detritus, large zoo.	ZL_FDM	N/A	1.000000e+00	none
Fraction of growth inefficiency lost to detritus, small zoo.	ZS_FDG	γ_{ZS}	5.000000e-01	none
Fraction of mortality lost to detritus, small zooplankton	ZS_FDM	N/A	1.000000e+00	none

Table 62: Zooplankton parameters in eReefs biogeochemical model (B3p0).

Description	Name in code	Symbol	Value	Units
Fraction of labile detritus converted to refractory detritus	F_LD_RD	ζ_{Red}	1.900000e-01	none
Fraction of labile detritus converted to DOM	F_LD_DOM	ϑ_{Red}	1.000000e-01	none
fraction of refractory detritus that breaks down to DOM	F_RD_DOM	ϑ_{Ref}	5.000000e-02	none
Breakdown rate of labile detritus at 106:16:1	r_DetPL	r_{Red}	4.000000e-02	d^{-1}
Breakdown rate of labile detritus at 550:30:1	r_DetBL	r_{Atk}	1.000000e-03	d^{-1}
Breakdown rate of refractory detritus	r_RD	r_R	1.000000e-03	d^{-1}
Breakdown rate of dissolved organic matter	r_DOM	r_O	1.000000e-04	d^{-1}
Respiration as a fraction of umax	Plank_resp	ϕ	2.500000e-02	none
Oxygen half-saturation for aerobic respiration	KO_aer	K_{OA}	2.560000e+02	mg O m^{-3}
Maximum nitrification rate in water column	r_nit_wc	$\tau_{nit,wc}$	1.000000e-01	d^{-1}
Maximum nitrification rate in water sediment	r_nit_sed	$\tau_{nit,sed}$	2.000000e+01	d^{-1}
Oxygen half-saturation for nitrification	KO_nit	$K_{O_2,nit}$	5.000000e+02	mg O m^{-3}
Rate at which P reaches adsorbed/desorbed equilibrium	Pads_r	τ_{Pabs}	4.000000e-02	d^{-1}
Freundlich Isothermic Const P adsorption to TSS in wc	Pads_Kwc	$k_{Pads,wc}$	3.000000e+01	mg P kg TSS^{-1}
Freundlich Isothermic Const P adsorption to TSS in sed	Pads_Ksed	$k_{Pads,sed}$	7.400000e+01	mg P kg TSS^{-1}
Oxygen half-saturation for P adsorption	Pads_KO	$K_{O_2,abs}$	2.000000e+03	mg O m^{-3}
Exponent for Freundlich Isotherm	Pads_exp	N/A	1.000000e+00	none
Maximum denitrification rate	r_den	τ_{denit}	8.000000e-01	d^{-1}
Oxygen half-saturation constant for denitrification	KO_den	$K_{O_2,denit}$	1.000000e+04	mg O m^{-3}
Rate of conversion of PIP to immobilised PIP	r_immob_PIP	τ_{Pimm}	1.200000e-03	d^{-1}

Table 63: Detritus parameters in eReefs biogeochemical model (B3p0).

Description	Name in code	Symbol	Value	Units
Sediment-water diffusion coefficient	EpiDiffCoeff	D	3.000000e-07	$m^2\ s^{-1}$
Thickness of diffusive layer	EpiDiffDz	h	6.500000e-03	m
Maximum growth rate of MA at Tref	MAumax	μ_{MA}^{max}	1.000000e+00	d^{-1}
Natural (linear) mortality rate, macroalgae	MA_mL	ζ_{MA}	1.000000e-02	d^{-1}
Nitrogen-specific leaf area of macroalgae	MAleafden	Ω_{MA}	1.000000e+00	$m^2\ g\ N^{-1}$
Respiration as a fraction of umax	Benth_resp	ϕ	2.500000e-02	none
net dissolution rate of sediment without coral	dissCaCO3_sed	d_{sand}	1.000000e-03	$mmol\ C\ m^{-2}\ s^{-1}$
Grid scale to reef scale ratio	CHarea	A_{CH}	1.000000e-01	$m^2\ m^{-2}$
Nitrogen-specific host area of coral polyp	CHpolypden	Ω_{CH}	2.000000e+00	$m^2\ g\ N^{-1}$
Max. growth rate of Coral at Tref	CHumax	μ_{CH}^{max}	5.000000e-02	d^{-1}
Max. growth rate of zooxanthellae at Tref	CSumax	μ_{CS}^{max}	4.000000e-01	d^{-1}
Radius of the zooxanthellae	CSrad	r_{CS}	5.000000e-06	m
Quadratic mortality rate of coral polyp	CHmort	ζ_{CH}	1.000000e-02	$(g\ N\ m^{-2})^{-1}\ d^{-1}$
Linear mortality rate of zooxanthellae	CSmort	ζ_{CS}	4.000000e-02	d^{-1}
Fraction of coral host death translocated.	CHremin	f_{remin}	5.000000e-01	-
Rate coefficent for particle uptake by corals	Splank	S_{part}	3.000000e+00	$m\ d^{-1}$
Maximum daytime coral calcification	k_day_coral	k_{day}	1.320000e-02	$mmol\ C\ m^{-2}\ s^{-1}$
Maximum nightime coral calcification	k_night_coral	k_{night}	6.900000e-03	$mmol\ C\ m^{-2}\ s^{-1}$
Carbonate sediment dissolution rate on shelf	dissCaCO3_shelf	d_{shelf}	1.000000e-04	$mmol\ C\ m^{-2}\ s^{-1}$
Age tracer growth rate per day	ageing_decay	n/a	1.000000e+00	$d\ d^{-1}$
Age tracer decay rate per day outside source	anti_ageing_decay	Φ	1.000000e-01	d^{-1}
Bleaching ROS threshold	ROSthreshold	ϕ_{ROS}	5.000000e-04	$mg\ O\ cell^{-1}$
Xanthophyll switching rate coefficient	Xanth_tau	τ_{xan}	8.333333e-04	s^{-1}
Ratio of RCII to Chlorophyll a	chla2rcii	A_{RCII}	2.238413e-06	$mol\ RCII\ g\ Chl^{-1}$
Stoichiometric ratio of RCII units to photons	photon2rcii	m_{RCII}	1.000000e-07	$mol\ RCII\ mol\ photon^{-1}$
Maximium zooxanthellae expulsion rate	ROSmaxrate	γ	1.000000e+00	d^{-1}
Scaling of DetP to DOP, relative to N	r_RD_NtoP	r_{RD_NtoP}	2.000000e+00	-
Scaling of DOM to DIP, relative to N	r_DOM_NtoP	r_{DOM_NtoP}	1.500000e+00	-
Radius of Trichodesmium colonies	Tricho_colrad	$r_{Trichocolony}$	5.000000e-06	m

Table 64: Benthic parameters in eReefs biogeochemical model (B3p0), excluding seagrass

Description	Name in code	Symbol	Value	Units
Maximum growth rate of SG at Tref	SGumax	μ_{SG}^{max}	4.000000e-01	d^{-1}
Half-saturation of SG N uptake in SED	SG_KN	$K_{SG,N}$	4.200000e+02	mg N m^{-3}
Half-saturation of SG P uptake in SED	SG_KP	$K_{SG,P}$	9.600000e+01	mg P m^{-3}
Natural (linear) mortality rate aboveground seagrass	SG_mL	ζ_{SG_A}	3.000000e-02	d^{-1}
Natural (linear) mortality rate belowground seagrass	SGROOT_mL	ζ_{SG_B}	4.000000e-03	d^{-1}
Fraction (target) of SG biomass below-ground	SGfrac	$f_{below,SG}$	7.500000e-01	-
Time scale for seagrass translocation	SGtransrate	$\tau_{tran,SG}$	3.330000e-02	d^{-1}
Nitrogen-specific leaf area of seagrass	SGleafden	Ω_{SG}	1.500000e+00	m^2 g N^{-1}
Seagrass seed biomass as fraction of 63 % cover	SGseedfrac	$f_{seed,SG}$	1.000000e-02	-
Sine of nadir Zostera canopy bending angle	SGorient	$\sin\beta_{blade,SG}$	5.000000e-01	-
Compensation irradiance for Zostera	SGmlr	$E_{comp,SG}$	4.500000e+00	mol m^{-2}
Maximum depth for Zostera roots	SGrootdepth	$z_{root,SG}$	-1.500000e-01	m
Critical shear stress for SG loss	SG_tau_critical	$\tau_{SG,shear}$	1.000000e+00	N m^{-2}
Time-scale for critical shear stress for SG loss	SG_tau_time	$\tau_{SG,time}$	4.320000e+04	s
Maximum growth rate of SGH at Tref	SGHumax	μ_{SGH}^{max}	4.000000e-01	d^{-1}
Half-saturation of SGH N uptake in SED	SGH_KN	$K_{SGH,N}$	4.200000e+02	mg N m^{-3}
Half-saturation of SGH P uptake in SED	SGH_KP	$K_{SGH,P}$	9.600000e+01	mg P m^{-3}
Nitrogen-specific leaf area of SGH	SGHleafden	Ω_{SGH}	1.900000e+00	m^2 g N^{-1}
Natural (linear) mortality rate, aboveground SGH	SGH_mL	ζ_{SGH_A}	6.000000e-02	d^{-1}
Natural (linear) mortality rate, belowground SGH	SGHROOT_mL	ζ_{SGH_B}	4.000000e-03	d^{-1}
Fraction (target) of SGH biomass below-ground	SGHfrac	$f_{below,SGH}$	5.000000e-01	-
Time scale for Halophila translocation	SGHtransrate	$\tau_{tran,SGH}$	3.330000e-02	d^{-1}
Halophila seed biomass as fraction of 63 % cover	SGHseedfrac	$f_{seed,SGH}$	1.000000e-02	-
Sine of nadir Halophila canopy bending angle	SGHorient	$\sin\beta_{blade,SGH}$	1.000000e+00	-
Compensation irradiance for Halophila	SGHmlr	$E_{comp,SGH}$	2.000000e+00	mol m^{-2}
Maximum depth for Halophila roots	SGHrootdepth	$z_{root,SGH}$	-8.000000e-02	m
Critical shear stress for SGH loss	SGH_tau_critical	$\tau_{SGH,shear}$	1.000000e+00	N m^{-2}
Time-scale for critical shear stress for SGH loss	SGH_tau_time	$\tau_{SGH,time}$	4.320000e+04	s

Table 65: Seagrass parameters in eReefs biogeochemical model (B3p0).

Description	Name in code	Symbol	Value	Units
Maximum growth rate of SGD at Tref	SGDumax	μ_{SGD}^{max}	4.000000e-01	d^{-1}
Half-saturation of SGD N uptake in SED	SGD_KN	$K_{SGD,N}$	4.200000e+02	mg N m^{-3}
Half-saturation of SGD P uptake in SED	SGD_KP	$K_{SGD,P}$	9.600000e+01	mg P m^{-3}
Nitrogen-specific leaf area of SGD	SGDleafden	Ω_{SGD}	1.900000e+00	m^2 g N^{-1}
Natural (linear) mortality rate, aboveground SGD	SGD_mL	ζ_{SGD_A}	6.000000e-02	d^{-1}
Natural (linear) mortality rate, belowground SGD	SGDROOT_mL	ζ_{SGD_B}	4.000000e-03	d^{-1}
Fraction (target) of SGD biomass below-ground	SGDfrac	$f_{below,SGD}$	2.500000e-01	-
Time scale for deep SG translocation	SGDtransrate	$\tau_{tran,SGD}$	3.330000e-02	d^{-1}
Deep SG seed biomass as fraction of 63 % cover	SGDseedfrac	$f_{seed,SGD}$	1.000000e-02	-
Sine of nadir deep SG canopy bending angle	SGDorient	$\sin\beta_{blade,SGD}$	1.000000e+00	-
Compensation irradiance for deep SG	SGDmlr	$E_{comp,SGD}$	1.500000e+00	mol m^{-2}
Maximum depth for deep SG roots	SGDrootdepth	$z_{root,SGD}$	-5.000000e-02	m
Critical shear stress for deep SG loss	SGD_tau_critical	$\tau_{SGD,shear}$	1.000000e+00	N m^{-2}
Time-scale for shear stress for deep SG loss	SGD_tau_time	$\tau_{SGD,time}$	4.320000e+04	s

Table 66: Deep seagrass parameters in eReefs biogeochemical model (B3p0).